ABSTRACT

Title of Thesis: Cooperative Detection and Network Coding in Wireless Networks

Mohammed W. Baidas, Master of Science, 2009

Thesis directed by: Professor K. J. Ray Liu
Department of Electrical and Computer Engineering

In cooperative communication systems, multiple terminals in wireless networks share their antennas and resources for information exchange and processing. Recently, cooperative communications have been shown to achieve significant performance improvements in terms of transmission reliability, coverage area extension, and network throughput, with respect to existing classical communication systems. This thesis is focused on two important applications of cooperative communications, namely: (i) cooperative distributed detection in wireless sensor networks, and (ii) many-to-many communications via cooperative space-time network coding.

The first application of cooperative communications presented in this thesis is concerned with the analysis and modeling of the deployment of cooperative relay nodes in wireless sensor networks. Particularly, in dense wireless sensor networks, sensor nodes continuously observe and collect measurements of a physical phenomenon. Such observations can be highly correlated, depending on the spatial separation between the sensor nodes as well as how the physical properties of the phenomenon are evolving over time. This unique characteristic of wireless sensor networks can be ef-

fectively exploited with cooperative communications and relays deployment such that the distributed detection performance is significantly improved as well as the energy efficiency. In particular, this thesis studies the Amplify-and-Forward (AF) relays deployment as a function of the correlation of the observations and analyzes the achievable spatial diversity gains as compared with the classical wireless sensor networks. Moreover, it is demonstrated that the gains of cooperation can be further leveraged to alleviate bandwidth utilization inefficiencies in current sensor networks. Specifically, the deployment of cognitive AF cooperative relays to exploit empty/under-utilized time-slots and the resulting energy savings are studied, quantified and compared.

The multiple terminal communication and information exchange form the second application of cooperative communications in this thesis. Specifically, the novel concept of Space-Time-Network Coding (STNC) that is concerned with formulation of the many-to-many cooperative communications over Decode-and-Forward (DF) nodes is studied and analyzed. Moreover, the exact theoretical analysis as well as upper-bounds on the network symbol error rate performance are derived. In addition, the tradeoff between the number of communicating nodes and the timing synchronization errors is analyzed and provided as a network design guideline. With STNC, it is illustrated that cooperative diversity gains are fully exploited per node and significant performance improvements are achieved. It is concluded that the STNC scheme serves as a potential many-to-many cooperative communications scheme and that its scope goes much further beyond the generic source-relay-destination communications.

Cooperative Detection and Network Coding in Wireless Networks

by
Mohammed W. Baidas

Thesis submitted to the Faculty of the Graduate School of the
University of Maryland, College Park in partial fulfillment
of the requirements for the degree of
Master of Science
2009

Advisory Committee:

Professor K. J. Ray Liu, Chairman

Professor Min Wu

Professor Adrian Papamarcou

Dedication

To my family.

Acknowledgments

Praise be to God "Allah", the most gracious and the most merciful. Without his blessing and guidance, my accomplishments would never have been possible.

I would like to thank my thesis advisor Prof. K. J. Ray Liu for agreeing to supervise this work and for giving me the opportunity to be part of his research group over the past two years. These two years were a time of dramatic change in my life and have greatly influenced me, both personally and academically.

I am also grateful for my colleagues in the Signals and Information Group at the University of Maryland for all the times we shared in our group discussions and activities. Heartfelt thanks go to my good friends Dr. Karim G. Seddik, Dr. Ahmed S. Ibrahim and Dr. Amr A. El-Sherif for their numerous stimulating discussions, fruitful suggestions and continuous guidance. I would also like to say thanks to Mohammed Al-Yaqoub and Mohammed Safar for their brotherhood and friendship.

I would also like to express my gratitude to Professor Min Wu and Professor Adrian Papamarcou for agreeing to be in my thesis committee and for devoting their invaluable time to review the thesis.

I would particularly like to anonymously acknowledge many people at the University of Maryland who have always helped and supported me over the past two years. You have done so much for me, so thank you!

I am deeply indebted to my family for their continuous support, commitment, motivation, encouragement and all their prayers. In addition, I gratefully acknowledge the financial support of Kuwait University. Lastly, special thanks go to Dr. Ali Al-Mutairi for his availability, advice and guidance.

Table of Contents

List of Tables

List of Figures

List of Abbreviations

AF	Amplify-and-Forward
AWGN	Additive White Gaussian Noise
BP	Broadcasting Phase
CFNC	Complex Field Network Coding
CP	Cooperation Phase
CSI	Channel State Information
DF	Decode-and-Forward
ECS	Equally-Correlated Scenario
LRT	Likelihood Ratio Test
M-PSK	M-ary Phase Shift Keying
MAC	Medium Access Control
MFB	Matched Filter Bank
MIS	Mutually-Independent Scenario
ML	Maximum Likelihood
MRC	Maximum Ratio Combining
QPSK	Quadrature Phase Shift Keying
SER	Symbol Error Rate
SNR	Signal-to-Noise Ratio
STNC	Space-Time Network Coding
TDMA	Time Division Multiple Access
WSN	Wireless Sensor Network

Chapter 1

Introduction

In recent years, the wireless communications and networking field has rapidly advanced and significantly evolved, leading to a wide spectrum of wireless mobile and multimedia applications covering video, voice and data. The growing demand for mobility and reliable high data rate communications has pushed researchers to further explore this field with the aim of efficiently utilizing the scarcity of the two fundamental resources in communications, namely, energy and bandwidth. Moreover, transmitted signals in wireless communication systems experience multipath fading, shadowing and path-loss. Furthermore, surrounding wireless devices introduce interference to wireless systems of interest which has a dramatic limiting effect on the overall system performance. Therefore, there is an urgent need for wireless communication systems that can counteract and mitigate the adverse effects of interference and channel fading for a more robust and improved overall system performance.

Cooperative communications have recently attracted much attention in the wireless research literature due to their achievable capacity, extended coverage area, enhanced transmission reliability and improved network throughput [1]. In this chapter, a literature review on the concept of relay channels is introduced which is then followed by an overview of the basic principles of cooperative diversity in wireless communication systems that are related to the problems studied in this thesis.

A motivating example is also provided to highlight the two potential cooperative protocols studied throughput the thesis. This is then followed by an outline of the thesis chapters and their main contributions.

1.1 Literature Review

Cooperative communications build significantly on the work on relay channels and their multi-terminal extensions within the information theory community. In particular, the classical relay channel modeling a three terminal communication channel was first introduced by Van der Meulen in [2]. The author proposed a relay channel in which a terminal called a "relay" was used to listen to the information-bearing signal transmitted from a source node and then re-transmit it the destination after processing it, with the aim of improving the system performance. In [3], Cover and El Gamal derived lower and upper bounds on the channel capacity for specific non-faded relay channel models via random coding and converse arguments. In general, the lower and upper bounds do not coincide, except in particular cases such as the degraded relay channel [3]. Later works considered parallel relay channels and multiple-access channels with relaying. Specifically, the parallel relay channel model was introduced by Schein and Gallager in [4] to make the classical relay channel symmetric. The capacity theorems of multiple-access relay channels and transmitter-receiver cooperation were studied in [5], and [6], respectively. Further significant extensions of the existing results for multiple relays also appeared in the works of Gupta, Gastpar [7, 8] and many others. These studies have laid the foundation for analyzing multiple terminal communications and led to the notion of cooperative diversity in wireless networks.

1.2 Cooperative Diversity

It has been established that channel fading can be mitigated by exploiting diversity which can be defined as any technique by which multiple copies of the signal are delivered to the receiver through independently faded channels. The intuition behind diversity is that the probability of having all the channels in deep fade is much lower than that of any individual channel. The diversity order of a wireless system can be loosely defined in terms of the number of independent channels over which the signal is transmitted. However, in [9], the diversity order was rigorously defined as the rate of decay of the probability of error P_e with the Signal-to-Noise Ratio (SNR) when using $\log - \log$ scale which can be mathematically expressed as

$$\text{Diversity Order} = -\lim_{SNR\to\infty} \frac{\log P_e}{\log SNR}. \tag{1.1}$$

Diversity can be exploited in three physical domains in which independent fading channels can be generated, namely, time, frequency and space [9]. Time diversity can be achieved by interleaving the transmitted signal across independently faded time-slots. However, for delay-sensitive applications over slowly fading environments, time diversity may not be suitable. Frequency diversity is particularly attractive for frequency-selective wideband systems and it can be exploited for example, by coding independently faded subcarriers in orthogonal frequency division multiplexing (OFDM) systems. However, exploiting frequency diversity could result in bandwidth inefficiencies and thus is not suited for narrowband systems.

Spatial diversity can be achieved by using multiple antennas at the transmitter and/or at the receiver with the aim of enhancing signal quality and achieving

bandwidth efficiency. Thus, multiple-input multiple-output (MIMO) communication systems have been introduced in the past decade to exploit spatial diversity and to allow more degrees of freedom over the conventional single antenna systems [10][11]. However, in practical wireless networks, it may not be feasible to implement multiple antennas at the mobile terminals due to cost, size, weight and power limitations [12]. Furthermore, the required separation among antennas of about half of wavelength, makes MIMO systems unsuitable for low transmit frequencies. To alleviate such limitations, *cooperative diversity* was introduced [13, 14, 15, 16]. In cooperative communication systems, a number of relay nodes in the network share their transmission antennas and processing resources to help in exchanging information between a source and its destination and hence forming a virtual antenna array without the need to use multiple antennas at the source node, and hence mimic a distributed MIMO system.

User-cooperation was first introduced and studied in the two-part paper [13, 14]. Specifically, the cooperation system description was developed for code-division-multiple-access (CDMA) systems in which each pair of users are coupled to help each other. Moreover, the two users employ orthogonal codes to eliminate multiple-access interference. It was demonstrated that with the knowledge of the channel phases at the transmitter sides, increased data rates can be achieved.

The term cooperative diversity was introduced in [15] where several cooperation protocols were studied and their outage capacity behavior was analyzed with the assumption of half-duplex transmission. In particular, the authors proposed two main categories of cooperative diversity protocols: fixed relaying and adaptive relaying.

In fixed relaying, channel resources are divided between the source and the relay in a fixed (predetermined) manner and the cooperation is performed over two phases. In Phase I, the source node transmits its message and both the relay and destination nodes receive it. In Phase II, the relay node transmits a processed version of its received message to the destination nodes. After that, the destination combines both signals received during the two phases and then detects the message. The Amplify-and-Forward (AF) and Decode-and-Forward (DF) relaying protocols are examples of fixed relaying and are presented in the motivating example demonstrated in the following section. Fixed relaying has the advantage of easy implementation; however, lacks bandwidth efficiency. This is because the transmission is split into two phases and thus the overall rate is reduced to $1/2$ symbols per channel use. For this purpose, adaptive relaying protocols were proposed, which comprise two main classes, selective and incremental relaying.

In selective relaying, the channel fading between the source and the relay nodes are assumed to be known to both of them. Thus, if the signal-to-noise ratio of the signal received at the relay exceeds a certain threshold, the relay node decodes-and-forwards the received message; otherwise, the relay remains idle. Furthermore, channel is assumed to be reciprocal, thus, the source node is aware when the relay is idle and hence transmits a copy of its signal to the destination instead. The operation of the selective relaying is very similar to that of the decode-and-forward as the signal-to-noise ratio threshold can be utilized to overcome the inherent problem of correct decoding at the relay. Furthermore, it was shown in [15] that selective relaying achieves diversity order two.

In incremental relaying, a feedback channel exists between the destination and the relay, through which the destination sends an acknowledgement to the relay if it has correctly decoded the source's message in the first phase and thus the relay does not have to re-transmit the message. The incremental relaying has been shown to achieve a diversity order of two as well as achieving the best spectral efficiency among the existing relaying protocols since the second phase becomes opportunistic, depending on the channel fading between the source and the destination [15].

The distributed space-time coding was proposed in [16], where in the first phase, multiple relays receive the source's transmitted message and then each relay decodes-and-forwards the message using an assigned unique codeword which represents a column from a space-time code. In the second phase, the destination combines the received signals from the relays' synchronized transmissions which was shown to provide full diversity gain equal to the number of cooperating relay nodes.

In order to illustrate the merits of cooperative communications, a motivating example of a single-relay cooperative network is presented in the following section along with a basic performance comparison.

1.3 Motivating Example

In this section, an introductory motivating example of a single-node cooperative network (shown in Fig. 1.1) is presented for M-PSK systems. In the traditional relay networks, the communication between the source and destination nodes is performed over two phases. In Phase I, the source transmits its data symbol x to the destination and due to the broadcast nature of wireless channels, that data symbol is also received

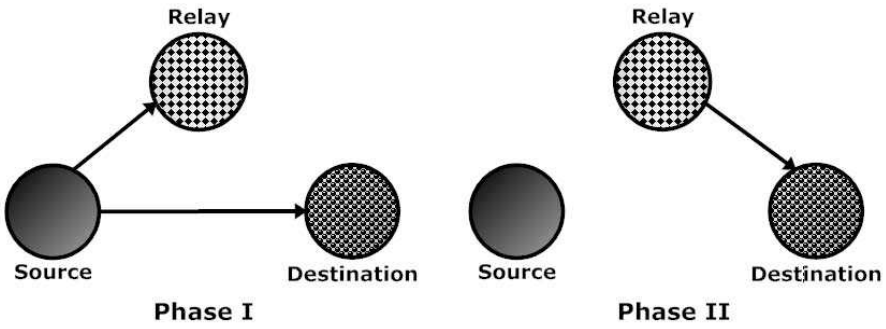

Figure 1.1: Single-Relay Cooperative Network Model and Operation

by the mediating cooperative relay node. Thus the received signals at the destination and relay nodes can be expressed as

$$y_{s,d} = \sqrt{P_s} h_{s,d} x + n_{s,d}, \text{ and } y_{s,r} = \sqrt{P_s} h_{s,r} x + n_{s,r}, \tag{1.2}$$

respectively, where P_s is the source transmitter power, x is the transmitted unit energy data symbol and $n_{s,d}$ and $n_{s,r}$ are the additive noise terms. Moreover, $h_{s,d}$ and $h_{s,r}$ are the statistically independent source-destination and source-relay channel fading coefficients, respectively.

In the sequel, the operation of the single-relay wireless network employing the two commonly used cooperative relaying protocols, namely the amplify-and-forward and decode-and-forward is described.

1.3.1 Amplify-and-Forward (AF) Cooperative Protocol

In Phase II of the AF cooperation protocol, the relay scales the received signal during Phase I and then transmits/forwards a scaled version of it to the destination with a transmitter power of P_r. The received signal at the destination node can thus

be written as

$$y_{r,d}^{AF} = \sqrt{\frac{P_r}{P_s|h_{s,r}|^2 + N_0}} h_{r,d} y_{s,r} + n_{r,d}, \tag{1.3}$$

where $h_{r,d}$ is the relay-destination channel coefficient. The destination node then performs a maximum ratio combining (MRC) operation on the received signals from the source and the relay. The output of the MRC is expressed as

$$y^{AF} = \alpha_{s,d} y_{s,d} + \alpha_{r,d} y_{r,d}^{AF}, \tag{1.4}$$

where

$$\alpha_{s,d} = \sqrt{\frac{P_s h_{s,d}^*}{N_0}}, \text{ and } \alpha_{r,d} = \frac{\sqrt{\frac{P_s P_r}{P_s|h_{s,r}|^2+N_0}}}{\left(\frac{P_r|h_{r,d}|^2}{P_2|h_{s,r}|^2+N_0} + 1\right) N_0}. \tag{1.5}$$

It should be noted that the channel coefficients are $h_{s,d}$, $h_{s,r}$ and $h_{r,d}$ are modeled as zero-mean complex Gaussian random variables with variances $\sigma_{s,d}^2$, $\sigma_{s,r}^2$ and $\sigma_{r,d}^2$, respectively. Furthermore, the additive noise terms $n_{s,d}$, $n_{s,r}$ and $n_{r,d}$ are modeled as zero-mean independent complex Gaussian random variables with variance N_0.

1.3.2 Decode-and-Forward (DF) Cooperative Protocol

For the DF cooperation protocol, the relay node decodes the received symbol, and if it is decoded correctly, it then forwards it to the destination during Phase II; otherwise, the relay node remains idle. It is assumed that the relay node perfectly determine whether the symbol is decoded correctly or not and this can be practically achieved through a signal-to-noise ratio (SNR) threshold on the received signal. Therefore, the received symbol at the destination from the relay node can be written as

$$y_{s,d}^{DF} = \sqrt{\tilde{P}_r} h_{r,d} x + n_{r,d}, \tag{1.6}$$

where

$$\tilde{P}_r = \begin{cases} P_r, & \text{if the relay node decodes } x \text{ correctly} \\ 0, & \text{otherwise} \end{cases}. \tag{1.7}$$

As before, the output of the MRC can be expressed as

$$y^{DF} = \alpha_{s,d} y_{s,d} + \tilde{\alpha}_{r,d} y_{r,d}^{DF}, \tag{1.8}$$

where $\alpha_{s,d}$ is defined as in (1.5) and $\tilde{\alpha}_{r,d} = \sqrt{\tilde{P}_r} h_{r,d}^* / N_0$. It should be noted that the total network power P under both the AF and DF protocols is distributed between the source and relay nodes as $P = P_s + P_r$.

1.3.3 Cooperative Diversity Gain

The cooperative diversity order can be verified by analyzing the SER expression as high enough SNR as follows

$$P_{SER} \lesssim (SNR \cdot \Delta)^{-d}, \tag{1.9}$$

where exponent d is the diversity order, Δ is the coding gain and $SNR \triangleq P/N_0$. It was shown in [17] that the SER for both the AF and DF can be written as

$$P_{SER} \lesssim \begin{cases} \left(\frac{P}{N_0} \cdot \frac{b_{PSK} \sigma_{s,d} \sigma_{s,r} \sigma_{r,d}}{\sqrt{B\left((1/\mu^2)\sigma_{r,d}^2 + (1/\mu(1-\mu))\sigma_{s,r}^2\right)}} \right)^{-2}, & \text{for amplify-and-forward protocol} \\ \left(\frac{P}{N_0} \cdot \frac{b_{PSK} \sigma_{s,d} \sigma_{s,r} \sigma_{r,d}}{\sqrt{(A^2/\mu^2)\sigma_{r,d}^2 + (B/\mu(1-\mu))\sigma_{s,r}^2}} \right)^{-2}, & \text{for decode-and-forward protocol} \end{cases}. \tag{1.10}$$

where $b_{PSK} = \sin^2(\pi/M)$, $A = \frac{1}{\pi} \int_0^{(M-1)\pi/M} \sin^2\theta \, d\theta$, $B = \frac{1}{\pi} \int_0^{(M-1)\pi/M} \sin^4\theta \, d\theta$ and $\mu = P_S/P$; while $1 - \mu = P_r/P$. Therefore, it can be easily seen from (1.10) that both the AF and DF protocols achieve a full cooperative diversity order of two. This can also be verified using (1.1) as $d = -\lim_{SNR \to \infty} \log(P_{SER}) / \log(SNR) = 2$.

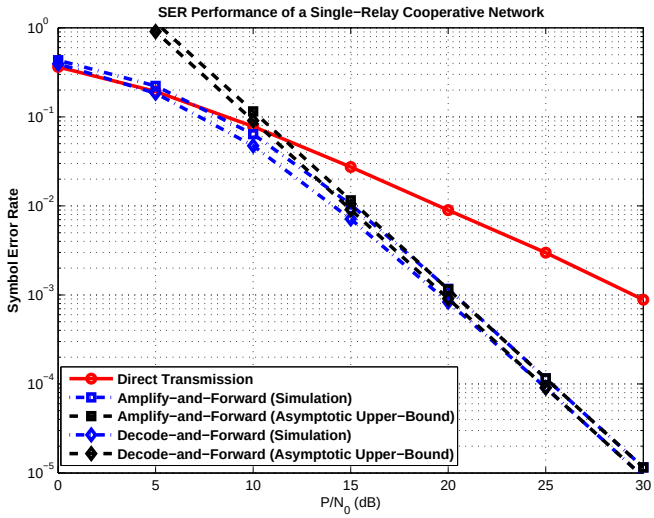

Figure 1.2: QPSK SER Performance of the AF and DF Cooperative Protocols

1.3.4 Performance Comparison

In Fig. 1.2, the symbol error rate (SER) performance for the AF and DF cooperative protocols is evaluated for QPSK systems and is also compared with that of the direct transmission. In the simulations, for the direction transmission, the source is allocated the total network power P; while under the cooperative network, the total network power P is equally distributed between the source and relay nodes (i.e. $P_s = P_r = P/2$). In addition, the channel coefficients are assumed to have unity variances (i.e. $\sigma^2_{s,d} = \sigma^2_{s,r} = \sigma^2_{r,d} = 1$). It can be seen that the performance of the cooperative protocols significantly outperform that of the direct transmission. In addition, the upper-bounds asymptotically agree with the simulated SER performance. This in turn confirms that both the AF and DF protocols achieve a full diversity order of two while clearly, the direct transmission only achieves a diversity order of one.

Another important observation is that the DF protocol slightly outperforms that of the AF protocol. This is due to the fact that the AF results in a noise ampli-

fication which is translated into a slight performance degradation. Over multiple-hop and multi-node relay networks, the noise propagation problem becomes severe [1]. However, the AF is less complex than the DF and thus is more suited for applications with analog transmission such as wireless sensor networks [18] [35]. However, the DF protocol is more suited for applications involving network coding and error-correction schemes [19] [20].

An extensive analysis of the symbol error rate performance for Rayleigh flat fading single-relay channels for both the amplify-and-forward and decode-and-forward protocol can be found in [1] [17]. For both cooperative protocols, exact symbol error rate and upper-bound expressions were derived in [17] along with optimal power allocations between the source and relay nodes.

1.4 Thesis Organization and Contributions

In this thesis, two important applications of cooperative communications in wireless networks are studied and analyzed. The ultimate goal of this research work is to apply the amplify-and-forward and decode-and-forward relaying protocols in two different practical applications and illustrate the achievable performance gains. In the sequel, an overview of each chapter and their main contributions are presented.

1.4.1 Correlation-Based Cooperation for Distributed Detection (Chapter 2)

In this chapter, the first main application of cooperative communications is considered, namely the distributed detection in wireless sensor networks. Sensor nodes

observe and collect measurements of a physical phenomenon and such measurements could be highly correlated depending on node density and their spatial separations. Thus, in this chapter, the deployment of relay nodes to cooperatively relay measurements from sensor nodes is considered. In particular, the natural tradeoffs between the number of sensor/relay nodes, communication reliability and their impact on the power-constrained sensor network detection performance is analyzed. It is shown that with cooperative distributed detection and spatial diversity exploitation, significant detection performance gains can be achieved as well as a reduction in the total number of sensor nodes required for optimal detection.

1.4.2 Energy Efficiency of Cognitive Cooperative Distributed Detection (Chapter 3)

The main focus of Chapter 2 is on understanding and analyzing the relays deployment as a function of the correlation between the sensor nodes in the network and also the total number of sensor/relay nodes under strict network power constraint. In Chapter 3, the deployment of cognitive-cooperative relay nodes is considered in order to exploit the empty/under-utilized time-slots to achieve energy-efficiency and optimal detection. A closed form expression for energy consumption calculation under conventional sensor networks with sensor nodes only is derived. Also, a closed form expression for the energy consumption of the cognitive cooperative relays deployment in sensor networks is also derived and quantified. A simple scenario of two sensor nodes paired with a cooperative relay node is considered. It is shown that by cognitively utilizing empty time-slots with cognitive-cooperative relays, significant

detection performance gains are achieved as well as energy savings with bandwidth losses alleviated.

1.4.3 Many-to-Many Communications via Space-Time Network Coding (Chapter 4)

In Chapter 4, the novel concept of Space-Time Network Coding (STNC) that allows N nodes to exchange their data symbols in a total of $2N$ time-slots is presented and analyzed. In particular, the theoretical Symbol Error Rate (SER) performance of decode-and-forward cooperative communication nodes under the STNC scheme is derived. A theoretical performance upper-bound is also derived and is compared for symmetric and asymmetric networks, which is then shown to be consistent with the simulated performance results. Furthermore, the full cooperative diversity order of $N-1$ per node is also verified and proved.

Timing synchronization errors arise in distributed space-time cooperative schemes when the cooperatively communicating nodes are simultaneously transmitting their data symbols over the same channel. Also, it is well-known that the effects of the timing synchronization errors become much more severe with the increase in the number of communicating nodes. Therefore, in this Chapter, the effect of the timing synchronization errors are also analytically studied. Theoretical exact and lower-bound expressions on the symbol error rate performance for an arbitrary number of communicating nodes as a function of the timing errors are also derived and provided as a network design guideline.

1.4.4 Conclusions and Future Work (Chapter 5)

The conclusions and a summary of the findings of this thesis along with the potential future research directions are given in Chapter 5.

Chapter 2

Correlation-Based Cooperation for Distributed Detection

2.1 Overview

As discussed in Chapter 1, cooperative communications have attracted much attention in the wireless research literature due to their ability to combat fading effects through spatial diversity and improve communication reliability [1]. Motivated by applications in wireless sensor networks (WSNs), the cooperative amplify-and-forward relays deployment is particularly attractive for efficient power consumption and bandwidth utilization, and also for accurate distributed detection [21].

In this chapter, a binary hypothesis distributed detection problem in correlated wireless sensor networks consisting of a set of sensor nodes communicating their measurements to the fusion center is considered. As some sensor nodes are likely to provide correlated measurements to the fusion center, it would be advantageous to utilize some of the sensor nodes as cooperative relay nodes to reliably forward measurements. Thus, this chapter considers the deployment of a set of relay nodes to cooperatively relay measurements from a set of sensor nodes and analyzes the effect of correlation between sensor nodes in both Additive White Gaussian Noise (AWGN) and Rayleigh flat fading channels, in order to explore the natural tradeoffs between the number of sensor/relay nodes, the reliability of communication and their impact

on the detection error performance in the network. In particular, two transmission protocols are compared; in Protocol I, each sensor node communicates its observation directly to the fusion center while in Protocol II, a set of Amplify-and-Forward (AF) cooperative relays are deployed and paired with a set of sensor nodes. Based on the theoretical analysis and simulations for a simple two-nodes network, the spatial region over which Protocol II outperforms Protocol I is characterized and the analysis is then extended to a network with arbitrary N number of sensor/relay nodes. It is revealed that under strict total network power constraint, the detection performance of a network with a fewer number of sensor nodes paired with cooperative relay nodes can significantly outperform that of a network with a larger number of sensor nodes only. It is concluded that with cooperative distributed detection and exploitation of spatial diversity, significant detection error performance gains are achievable as well as a reduction in the required number of sensor nodes for optimal detection performance.

2.2 Introduction, Motivation and Prior Work

In wireless sensor networks, sensor nodes are limited in power, memory and processing capabilities [22]. Moreover, the densely distributed sensor nodes over the wireless network area are characterized by spatially correlated measurements, and sending all the local observations from the sensor nodes to the fusion center can be inefficient in terms of network resources utilization. This in turn suggests that the correlation among sensors can be exploited such that correlated sensors can cooperate and share transmission channels via cooperative relays deployment [23][24].

In the research literature, several variants of the distributed detection prob-

lem of correlated observations have been studied. For instance, in [25], the optimal constellation size and number of MIMO cooperating nodes have been analytically quantified with respect to the correlation coefficient where it was shown that optimal constellation size is an increasing function of the correlation coefficient while the optimal number of MIMO cooperating nodes is a decreasing function of the correlation coefficient. The authors in [26] considered the problem of determining whether it is better to use a few high-cost, high power nodes or to use many low-cost, lower power nodes in a system, where the correlated observations are obtained from a set of sensor nodes distributed uniformly on a straight line. In [27], it was shown that the distributed detection of deterministic signals in additive Gaussian noise with a set of identical binary sensors is asymptotically optimal as the number of observations per sensor approaches infinity. The work in [28] analyzes the performance of the MAC layer by taking into account the spatio-temporally correlated phenomena when evaluating the distortion level with minimum energy expenditure. The authors in [29] derived the outage statistics and investigated the effects of the spatio-temporal correlation of collaborative processing on the probability, average duration and rate of outage events.

In conventional wireless sensor networks, every sensor node transmits all its measurements directly to the fusion center for data gathering and detection. While most of the previously published works assume independent observations, this assumption is likely to fail in dense wireless sensor networks; since that sensor nodes with close vicinity of each other in a finite area would observe highly correlated data. Therefore, separate direct transmissions of each sensor's correlated data introduces

redundancy but not necessarily reliability, which results in an unnecessary waste of network resources. This in turn suggests the use of relay nodes to improve the reliability of measurements rather than redundancy, under stringent sensor network power constraint.

Our interest in this chapter is to study the impact of correlation on the detection error performance in a wireless sensor network with relays deployment. In particular, the main question to be addressed is: under strict network power constraint, is it better to employ many spatially correlated sensors or to have a fewer number of correlated sensors paired with cooperating relays? An answer to this question can be obtained by comparing two network transmission protocols, namely Protocol I and Protocol II. In Protocol I, each node directly transmits its measurements to the fusion center; while in Protocol II, the measurements of each sensor node are amplified-and-forwarded through a cooperating relay node. The performance of the two protocols in terms of the probability of detection error will be compared in both the Additive White Gaussian Noise (AWGN) and Rayleigh flat fading channels. Due to the fact that increasing the number of sensor nodes in a finite wireless sensor network area results in increasingly correlated measurements, it would be expected that employing a fewer number of sensor nodes cooperatively paired with relay nodes, would improve transmission reliability and detection performance. Thus, it is essential to explore the natural tradeoffs between the total number of sensor/relay nodes, degree of correlation and detection error performance.

In this work, a simple yet effective model suitable for the analysis of wireless sensor networks with correlated observations, along with the effect of path-loss and

inter-sensor separation on the detection error performance is proposed. Based on the assumption model, the effect of correlation on the detection performance is analyzed and characterized for a simple two-nodes network in order to determine the spatial region over which Protocol II outperforms Protocol I. The analysis is then extended and generalized for a network with arbitrary number N of sensor/relay nodes where it will be shown that using fewer sensor nodes with cooperative relay nodes can improve the network's detection performance significantly depending on the spatial separation/correlation, and also reduces the number of sensor nodes required for optimal detection performance under strict network power constraint.

In the remainder of this chapter, the system model is presented in Section 2.3. In Section 2.4, the network transmission protocols and model are presented; while in Section 2.5, the probability of detection error performance for each network protocol in both AWGN and Rayleigh flat fading channels is derived. Sections 2.6, and 2.7 present a theoretical analysis of the performance of the network transmission protocols under the AWGN and the Rayleigh fading channels, respectively. Simulation results and performance evaluation of the network protocols are presented in Section 2.8. Finally, the summary and conclusions are drawn in Section 2.9.

2.3 System Model

In this section, the distributed detection with correlated observations problem is described. A wireless sensor network with N sensor nodes are used to sense a particular phenomenon after which their observations are communicated to the fusion center for decision-making. In this work, dumb sensor nodes are assumed (i.e. they

do not perform any local decisions due to their limited capabilities). In addition, the specific case of correlated spatial data $\mathbf{x}$ gathering is modeled using the *Gaussian Random Field* model [30] where the measurement observed at the i^{th} sensor node is a Gaussian random variable, given by

$$x_i = m_i + w_i, \qquad i = 1, \ldots, N, \tag{2.1}$$

where m_i represents a deterministic value. Moreover, w_i is the measurement noise at the i^{th} sensor node and is distributed as a zero-mean Gaussian random variable with variance σ^2. The *N-dimensional* multivariate normally distributed gaussian random vector is expressed as

$$f(\mathbf{x}) = \frac{1}{(2\pi)^{N/2}|\mathbf{\Phi}_N|^{1/2}} \exp\left(-\frac{1}{2}(\mathbf{x}-\mathbf{m})^H \mathbf{\Phi}_N^{-1}(\mathbf{x}-\mathbf{m})\right), \tag{2.2}$$

where $\mathbf{m} \equiv E[\mathbf{x}]$ is the means vector and $\mathbf{\Phi}_N \triangleq E[(\mathbf{x}-\mathbf{m})(\mathbf{x}-\mathbf{m})^H]$ is the covariance matrix of $\mathbf{x}$. The diagonal elements of $\mathbf{\Phi}_N$ (symmetric and positive-definite) are the measurement noise variances of each sensor node $[\mathbf{\Phi}_N]_{i,i} = \sigma^2$. The rest of the coefficients in $\mathbf{\Phi}_N$ (for $i \neq j$) are expressed as $[\mathbf{\Phi}_N]_{i,j} = \sigma^2 \rho_{i,j}$, where $\rho_{i,j} = \exp(-\lambda d_{s_{i,j}}^2)$ is the inter-sensor distance $d_{s_{i,j}}$ dependent correlation coefficient, and λ is a medium-dependent correlation decay factor [28].

The distributed detection problem is formulated as a binary hypothesis testing where the measured data from the sensor nodes are based on two hypotheses, namely $\mathcal{H}_1$ and $\mathcal{H}_0$. The $\mathcal{H}_1$ hypothesis indicates the presence of the phenomenon within the sensor network while $\mathcal{H}_0$ indicates its absence. Thus, the vector of measured data $\mathbf{x}$ under each hypotheses is given by

$$\begin{aligned} \mathcal{H}_0 &: \mathbf{x} \sim \mathcal{CN}(\mathbf{0}, \mathbf{\Phi}_N) \\ \mathcal{H}_1 &: \mathbf{x} \sim \mathcal{CN}(\mathbf{m}, \mathbf{\Phi}_N), \end{aligned} \tag{2.3}$$

where $\mathbf{x} \triangleq \mathcal{CN}(\mathbf{m}, \mathbf{\Phi}_N)$ denotes the complex *correlated* Gaussian random variables.

2.4 Network Protocols and Model

In this section, the network transmission protocols and the wireless sensor network model are presented. In Protocol I, each sensor transmits its sensed observation directly to the fusion center without employing any intermediate relay nodes; while in Protocol II, sensor nodes are paired with amplify-and-forward (AF) relay nodes deployed closer to the fusion center. The network protocols assume a simple geometric path-loss that is proportional to $d^{-\alpha}$ where α is the path-loss exponent and d is the distance between the sensor/relay nodes and the fusion center.

2.4.1 Protocol I: Sensing Without Cooperation

In Protocol I, each sensor directly transmits its observations to the fusion center where uncoded transmission at each sensor node is assumed (as shown in Fig. 2.1a). The received signals at the fusion center transmitted from two different sensors S_i and S_j through TDMA orthogonal channels [15] are expressed as

$$y_{s_i,f} = \sqrt{P_{s_i} d_{s_i,f}^{-\alpha}} h_{s_i,f} x_i + n_{s_i,f}, \tag{2.4}$$

and

$$y_{s_j,f} = \sqrt{P_{s_j} d_{s_j,f}^{-\alpha}} h_{s_j,f} x_j + n_{s_j,f}, \tag{2.5}$$

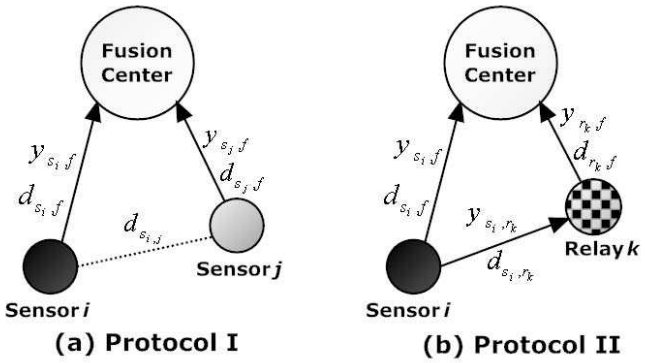

Figure 2.1: Network protocols

respectively; where $h_{s_i,f}$ and $h_{s_j,f}$ are the channel coefficients from the S_i and S_j sensor nodes to the fusion center and are modeled as zero-mean complex Gaussian random variables with variance 1/2 per dimension. In addition, $d_{s_i,f}$ and $d_{s_j,f}$ are the distances from sensor nodes S_i and S_j to the fusion center, respectively. It is assumed that sensor node S_j is closer to the fusion center than sensor node S_i (i.e. $d_{s_j,f} < d_{s_i,f}$). Furthermore, P_{s_i} and P_{s_j} are the transmission power assigned to sensors S_i and S_j respectively and are selected to satisfy a total power constraint P_T while $n_{s_i,f}$ and $n_{s_i,f}$ are the additive white Gaussian noise at the fusion center. In this protocol, all the N nodes are utilized as sensors for the transmission of observations (i.e. $|\mathcal{S}| = N$) (where $\mathcal{S}$ is the set of all the sensor nodes in the network).

2.4.2 Protocol II: Sensing With Cooperation

In Protocol II, the farther sensor node S_i is paired with a known neighboring cooperative relay node R_k located at $d_{r_k,f}$ from the fusion center, as shown in Fig. 2.1b. In the amplify-and-forward (AF) relaying, signal transmissions are separated into two phases through TDMA orthogonal channels [15]. In Phase 1, sensor node

S_i transmits its observation x_i with power P_{s_i} and the received signals at the fusion center $y_{s_i,F}$ and at the relay node y_{s_i,r_k} are

$$y_{s_i,f} = \sqrt{P_{s_i} d_{s_i,f}^{-\alpha}} h_{s_i,f} x_i + n_{s_i,f}, \tag{2.6}$$

and

$$y_{s_i,r_k} = \sqrt{P_{s_i} d_{s_i,r_k}^{-\alpha}} h_{s_i,r_k} x_i + n_{s_i,r_k}, \tag{2.7}$$

respectively; where $h_{s_i,f}$ and h_{s_i,f_k} are the fading channel coefficients from sensor S_i to the fusion center and to the R_k relay node, respectively; whereas, $d_{s_i,f}$ and d_{s_i,r_k} are the distances from S_i to the fusion center and to R_k relay node, respectively and $n_{s_i,f}$ and n_{s_i,r_k} are the white Gaussian noises. In Phase 2, the relay node amplifies the received signal and forwards it to the destination with transmit power P_{r_k}. The received signal at the fusion center can be written as

$$\begin{aligned} y_{r_k,f} &= \sqrt{\tilde{P_{r_k}} d_{r_k,f}^{-\alpha}} h_{r_k,f} y_{s_i,r_k} + n_{r_k,f} \\ &= \sqrt{\tilde{P_{r_k}} P_{s_i} d_{s_i,r_k}^{-\alpha} d_{r_k,f}^{-\alpha}} h_{r_k,f} h_{s_i,r_k} x_j + \tilde{n}_{r_k,f}, \end{aligned} \tag{2.8}$$

where $\tilde{n}_{r_k,f} = \sqrt{\tilde{P_{r_k}} d_{r_k,f}^{-\alpha}} h_{r_k,f} n_{s_i,r_k} + n_{r_k,f}$. In addition, $\tilde{P_{r_k}}$ represents the normalized transmit power and is chosen to ensure a transmit power at the relay node of P_{r_k} and thus is specified as $\tilde{P_{r_k}} = P_{r_k}/(P_{s_i} d_{s_i,r_k}^{-\alpha} |h_{s_i,r_k}|^2 \sigma^2 + N_o)$. Furthermore, $d_{r_k,f}$ is the distance from the relay to the fusion center, $h_{r_k,f}$ is the channel coefficient between the k^{th} relay node to the fusion center and $n_{r_k,f}$ is the additive Gaussian noise. It should be noted that the noise $n_{s_i,f}$, n_{s_i,r_k} and $n_{r_k,f}$ are modeled as independent complex Gaussian random variables with zero means and variance N_o. In this protocol the N nodes in the network are split into two sets $\mathcal{S}$ and $\mathcal{R}$ representing sensor and relay

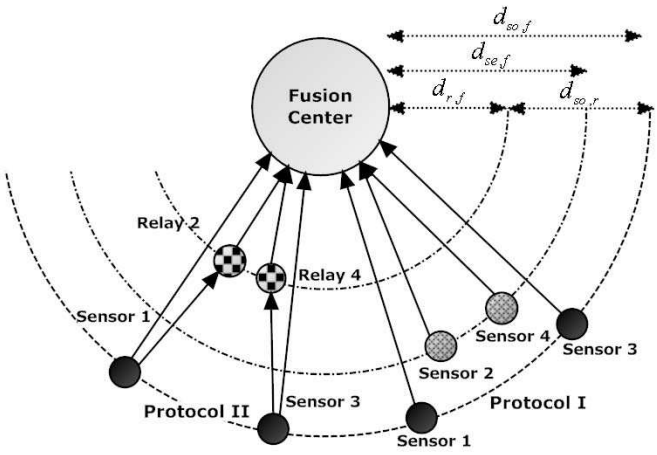

Figure 2.2: Wireless sensor network model

nodes respectively with equal cardinality (i.e. $|\mathcal{S}| = |\mathcal{R}| = N/2$) since each sensor node is paired with a cooperating relay node.

2.4.3 Wireless Sensor Network Model

In this subsection, a wireless sensor network model suitable for correlation analysis amongst sensor nodes is presented. Specifically, the model considers the scenario where the sensor/relay nodes are distributed over a circular area with three concentric circles with the fusion center at the center, as illustrated in Fig. 2.2 for $N = 4$ for both transmission protocols. The two larger circles of radii $d_{so,f}$ and $d_{se,f}$ contain two sets ($\mathcal{S}_{\mathcal{O}}$ and $\mathcal{S}_{\mathcal{E}}$) of uniformly distributed *o*dd-numbered $(S_1, S_3, ..., S_{N-1})$ and *e*ven-numbered $(S_2, S_4, ..., S_N)$ sensor nodes respectively. On the other hand, the smallest circle contains the set of relay nodes $\mathcal{R}$ with radius of $d_{r,f}$ and uniformly deployed $(R_2, R_4, ..., R_N)$ with even-numbered indices such that $(d_{so,f} > d_{se,f} > d_{r,f})$. That is, the relays are deployed closer to the fusion center than the two sets of sensor nodes.

Also, every sensor (in the outer circle - set $\mathcal{S}_{\mathcal{O}}$) is separated from its cooperating node by a distance $d_{so,r}$. This circular model as will be seen in later sections simplifies the analysis greatly as all the nodes in $\mathcal{S}_{\mathcal{O}}$ are of equal distance $d_{so,f}$ from the fusion center and so are the nodes in $\mathcal{S}_{\mathcal{E}}$ and $\mathcal{R}$ with distances $d_{se,f}$ and $d_{r,f}$ respectively. The proposed model also introduces symmetry that allows matrix decompositions of covariance matrices and makes the analysis of a network of N nodes mathematically tractable. This model also has the advantage that it lends itself to feasible practical implementation with relays deployment.

In this model, it is assumed that the sensors, relays and the fusion center are stationary and that the fusion center knows the relative distances/locations of the sensor/relay nodes (on the concentric circles). In addition, the sensor nodes in each of the sets $\mathcal{S}_{\mathcal{O}}$ and $\mathcal{S}_{\mathcal{E}}$ are allocated a total power of $P_{\mathcal{O}}$ and $P_{\mathcal{E}}$, respectively under Protocol I such that $P_T = P_{\mathcal{O}} + P_{\mathcal{E}}$. In Protocol II, the relay nodes in the set $\mathcal{R}$ are allocated a total power of $P_{\mathcal{R}}$ such that the network power constraint is $P_T = P_{\mathcal{O}} + P_{\mathcal{R}}$. This total network power constraint P_T implies that the power decreases linearly with the increase in the number of sensor/relay nodes over a wireless network area $\mathcal{A}$.

2.5 Performance Analysis

In this section, the probability of detection error P_e expressions of the two network protocols in AWGN and Rayleigh flat-fading channels are derived, which are then compared as function of the correlation coefficient between the sensor nodes to determine when Protocol I or Protocol II should be used. To simplify notation and the analysis, it is assumed (without loss of generality) for both protocols, that all the

nodes in each set have equal power, i.e. $P_{so} = P_{so_i}$, $\forall i \in \mathcal{S}_{\mathcal{O}}$, $P_{se} = P_{se_j}$, $\forall j \in \mathcal{S}_{\mathcal{E}}$ and $P_r = P_{r_k}$, $\forall k \in \mathcal{R}$. Also, let $d_{so,f} = d_{so_i,f}$, $d_{se,f} = d_{se_j,f}$ and $d_{r,f} = d_{r_k,f}$ in each set. Furthermore, it is assumed that all the measured data have the same mean (i.e. under $\mathcal{H}_1$ all sensor nodes measure the same phenomenon with the same *real* mean $m_i = m$ for $i = 1, ..., N$, within an area $\mathcal{A}$).

Let $\pi_0 = \Pr\{\mathcal{H} = \mathcal{H}_o\}$ and $\pi_1 = \Pr\{\mathcal{H} = \mathcal{H}_1\}$ denote the prior probabilities for hypotheses $\mathcal{H}_0$ and $\mathcal{H}_1$, respectively where it is assumed for simplicity that $\pi_0 = \pi_1 = 1/2$. The hypothesis-dependent average power consumption of a sensor/relay node is equal to a power constraint P and is given by [26][35]

$$P = \pi_0 \bar{P}\sigma^2 + \pi_1 \bar{P}(\sigma^2 + m^2) = \bar{P}\left(\sigma^2 + \frac{1}{2}m^2\right), \tag{2.9}$$

which in turn can be written as

$$\bar{P} = \frac{P}{\left(\sigma^2 + \frac{1}{2}m^2\right)}, \tag{2.10}$$

where, $\bar{P} = P_{so}$ for sensor nodes in the set $\mathcal{S}_{\mathcal{O}}$ and $\bar{P} = P_{se}$ for the sensor nodes in the set $\mathcal{S}_{\mathcal{E}}$, respectively. Also $\bar{P} = P_r$ for the relay nodes in the set $\mathcal{R}$. For simplicity, in this model, it is assumed that the total network power is distributed equally between the sensor nodes in the two sensor node sets under Protocol I (i.e. $P_{\mathcal{O}} = P_{\mathcal{E}} = P_T/2$). Similarly, under Protocol II, the total network power is distributed equally between the set of sensor nodes $\mathcal{S}_{\mathcal{O}}$ and $\mathcal{R}$ (i.e. $P_{\mathcal{O}} = P_{\mathcal{R}} = P_T/2$). However, it should be noted that optimal power allocation among the set of sensor/relay nodes is also possible; however is beyond the scope of this chapter as it would deviate from the main thrust of the analysis and modeling presented in this work.

Given the foregoing system model and protocols, the optimal likelihood decision

rule at fusion center of the received observations over AWGN and Rayleigh fading channels is derived as follows. The *N-dimensional* received observations vector $\mathbf{y}_N$ under each hypothesis is given by

$$\begin{aligned} \mathcal{H}_0 &: \mathbf{y}_N \sim \mathcal{CN}(\mathbf{0}, \mathbf{\Sigma}_N) \\ \mathcal{H}_1 &: \mathbf{y}_N \sim \mathcal{CN}(\mu_N, \mathbf{\Sigma}_N), \end{aligned} \tag{2.11}$$

where $\mathbf{0}$ is the all zeros vector, $\mu_N \triangleq E[\mathbf{y}_N]$ is the means vector and $\mathbf{\Sigma}_N \triangleq E[(\mathbf{y}_N - \mu_N)(\mathbf{y}_N - \mu_N)^H]$ is the covariance matrix of $\mathbf{y}_N$. The optimal test for minimizing the probability of detection error is the likelihood ratio test (LRT) given by [31]

$$\frac{\frac{1}{(2\pi)^{N/2}|\mathbf{\Sigma}_N|^{1/2}} \exp\{-\frac{1}{2}(\mathbf{y}_N - \mu_N)^H \mathbf{\Sigma}_N^{-1}(\mathbf{y}_N - \mu_N)\}}{\frac{1}{(2\pi)^{N/2}|\mathbf{\Sigma}_N|^{1/2}} \exp\{-\frac{1}{2}\mathbf{y}_N^H \mathbf{\Sigma}_N^{-1}\mathbf{y}_N\}} \gtrless_{\mathcal{H}_0}^{\mathcal{H}_1} 1. \tag{2.12}$$

The decision rule can be further simplified and expressed in terms of the sufficient statistic to $T(\mathbf{y}_N) = \frac{1}{2}\mu_N^H \mathbf{\Sigma}_N^{-1}\mathbf{y}_N + \frac{1}{2}\mathbf{y}_N^H \mathbf{\Sigma}_N^{-1}\mu_N \gtrless_{\mathcal{H}_0}^{\mathcal{H}_1} \frac{1}{2}\mu_N^H \mathbf{\Sigma}_N^{-1}\mu_N$ where it should be noted that $T(\mathbf{y}_N)$ is linear transformation of the Gaussian random vector $\mathbf{y}_N$ and it characterizes its distributions under $\mathcal{H}_0$ and $\mathcal{H}_1$ by finding its means and variances under each hypothesis as $P_{\mathcal{H}_0}(T) \sim \mathcal{CN}(\mathbf{0}, \mu_N^H \mathbf{\Sigma}_N^{-1}\mu_N)$ and $P_{\mathcal{H}_1}(T) \sim \mathcal{CN}(\mu_N^H \mathbf{\Sigma}_N^{-1}\mu_N, \mu_N^H \mathbf{\Sigma}_N^{-1}\mu_N)$ [32]. By defining probabilities of detection error conditioned on hypotheses $\mathcal{H}_0$ and $\mathcal{H}_1$ in terms of the the probability of false alarm P_{FA} and the probability of miss P_M, respectively; the probability of detection error $P_e = \Pr\{\hat{\mathcal{H}} \neq \mathcal{H}\}$ is expressed as $P_e = \pi_0 P_{FA} + \pi_1 P_M$. Under the AWGN channel, the channel coefficients in (2.4 - 2.8) are set to 1 (i.e. $h_{s_i,f} = h_{s_j,f} = h_{r_k,f} = 1$ for all i, j and k). Therefore, the probability of detection error can be straightforwardly shown to be

$$P_e^{AWGN} = Q\left(\frac{1}{2}\sqrt{\mu_N^H \mathbf{\Sigma}_N^{-1}\mu_N}\right), \tag{2.13}$$

where $Q(u) \triangleq \frac{1}{\sqrt{2\pi}} \int_u^\infty \exp\left(-\frac{t^2}{2}\right) dt$ is the Gaussian Q-function. On the other hand, the conditional probability of detection error under the Rayleigh fading channel (assuming perfect channel state information (CSI) at the fusion center) is given by

$$P_e^{Ray} = E\left\{Q\left(\frac{1}{2}\sqrt{\mu_N^H \mathbf{\Sigma}_N^{-1} \mu_N}\right)\right\}, \tag{2.14}$$

where the expectation is taken with respect to the channel statistics. It should be noted that finding a closed-form expression for the expectation in (2.14) is in general very difficult; thus, it will be numerically evaluated in the performance evaluation section.

2.6 Theoretical Analysis: AWGN Channels

In the following sections, the theoretical detection error performance analysis of Protocols I and II under the AWGN channel will be derived.

2.6.1 Protocol I - A Two Sensors Network over AWGN Channels

In this section, the probability of error detection of the $N = 2$ sensors network (as shown in Fig. 2.1a) in AWGN channels under Protocol I is analyzed. Let the received data vector be defined as $\mathbf{y}_{I,2}^A = [y_{s_1,f} \quad y_{s_2,f}]^T$ (using (2.4) and (2.5)) which is employed by the fusion center to decide between the two hypotheses. In addition, the data model under hypothesis $\mathcal{H}_0$ is written as $\mathbf{y}_{I,2}^A = \mathcal{N}(\mathbf{0}, \mathbf{\Sigma}_{I,2}^A)$; while under $\mathcal{H}_1$ is given by $\mathbf{y}_{I,2}^A = \mathcal{N}(\mu_{I,2}^A, \mathbf{\Sigma}_{I,2}^A)$. The vector of means $\mu_{I,2}^A$ can be shown to be

$$\mu_{I,2}^A = \left[\sqrt{P_{so} d_{so,f}^{-\alpha}} m \quad \sqrt{P_{se} d_{se,f}^{-\alpha}} m\right]^T, \tag{2.15}$$

while the covariance matrix $\mathbf{\Sigma}_{I,2}^A$ of the received observations vector is expressed as

$$\mathbf{\Sigma}_{I,2}^{A} = \begin{pmatrix} P_{so}d_{so,f}^{-\alpha}\sigma^2 + N_o & \sqrt{P_{so}P_{se}d_{so,f}^{-\alpha}d_{se,f}^{-\alpha}}\sigma^2\rho_{1,2} \\ \sqrt{P_{so}P_{se}d_{so,f}^{-\alpha}d_{se,f}^{-\alpha}}\sigma^2\rho_{1,2} & P_{se}d_{se,f}^{-\alpha}\sigma^2 + N_o \end{pmatrix}, \tag{2.16}$$

which can also be written in the matrix form as $\mathbf{\Sigma}_{I,2}^{A} = (\mathbf{\Gamma}_2^A)^T\mathbf{\Omega}_2\mathbf{\Gamma}_2^A + N_o\mathbf{I}$, where $(\cdot)^T$ is the transpose of the parameter matrix, $\mathbf{I}$ is the identity matrix of appropriate dimensions. The matrices $\mathbf{\Gamma}_2^A$ and $\mathbf{\Omega}_2$ are defined as

$$\mathbf{\Gamma}_2^A = \begin{pmatrix} \sqrt{P_{so}d_{so,f}^{-\alpha}\sigma^2} & 0 \\ 0 & \sqrt{P_{se}d_{se,f}^{-\alpha}\sigma^2} \end{pmatrix}, \tag{2.17}$$

and

$$\mathbf{\Omega}_2 = \begin{pmatrix} 1 & \rho_{1,2} \\ \rho_{1,2} & 1 \end{pmatrix}, \tag{2.18}$$

respectively. Thus, the probability of detection error can be obtained using

$$P_{e,I}^{AWGN} = Q\left(\frac{1}{2}\sqrt{(\mu_{I,2}^A)^T(\mathbf{\Sigma}_{I,2}^A)^{-1}\mu_{I,2}^A}\right), \tag{2.19}$$

which upon substitution and some manipulation can be written as

$$P_{e,I}^{AWGN} = Q\left(\frac{1}{2}\sqrt{\frac{2P_{so}P_{se}(d_{so,f}^{-\alpha}d_{se,f}^{-\alpha})m^2\sigma^2(1-\rho_{1,2}) + N_om^2(P_{so}d_{so,f}^{-\alpha} + P_{se}d_{se,f}^{-\alpha})}{P_{so}P_{se}(d_{so,f}^{-\alpha}d_{se,f}^{-\alpha})\sigma^4(1-\rho_{1,2}^2) + N_o\sigma^2(P_{so}d_{so,f}^{-\alpha} + P_{se}d_{se,f}^{-\alpha}) + N_o^2}}\right). \tag{2.20}$$

For the case where sensor nodes S_1 and S_2 have independent observations (i.e. $\rho_{1,2} = 0$), the probability of detection error can be expressed as

$$P_{e,I}^{AWGN} = Q\left(\frac{1}{2}\sqrt{\frac{P_{so}d_{so,f}^{-\alpha}m^2}{P_{so}d_{so,f}^{-\alpha}\sigma^2 + N_o} + \frac{P_{se}d_{se,f}^{-\alpha}m^2}{P_{se}d_{se,f}^{-\alpha}\sigma^2 + N_o}}\right). \tag{2.21}$$

2.6.2 Protocol I - N Sensors Network over AWGN Channels

The analysis is extended to the case of arbitrary N number of sensors in the network (where N is even). The N nodes are split into two sets $\mathcal{S}_{\mathcal{O}}$ and $\mathcal{S}_{\mathcal{E}}$ of

equal cardinality. The $N-$*dimensional* vector of received observations is $\mathbf{y}_{I,N}^{A} = \begin{bmatrix} y_{s_1,f} & y_{s_2,f} & \cdots & y_{s_{N-1},f} & y_{s_N,f} \end{bmatrix}^T$ for which the data model under hypothesis $\mathcal{H}_0$ is expressed as $\mathbf{y}_{I,N}^{A} = \mathcal{N}(\mathbf{0}, \mathbf{\Sigma}_{I,N}^{A})$; while under hypothesis $\mathcal{H}_1$ is written as $\mathbf{y}_{I,N}^{A} = \mathcal{N}(\mu_{I,N}^{A}, \mathbf{\Sigma}_{I,N}^{A})$. As before, the covariance matrix $\mathbf{\Sigma}_{I,N}^{A}$ can be expressed as $\mathbf{\Sigma}_{I,N}^{A} = (\mathbf{\Gamma}_{I,N}^{A})^T \mathbf{\Omega}_N \mathbf{\Gamma}_{I,N}^{A} + N_o \mathbf{I}$ and the matrix $\mathbf{\Omega}_N$ is given by

$$\mathbf{\Omega}_N = \begin{pmatrix} 1 & \rho_{1,2} & \cdots & \rho_{1,N} \\ \rho_{1,2} & 1 & \cdots & \rho_{2,N} \\ \vdots & \vdots & \ddots & \vdots \\ \rho_{1,N} & \rho_{2,N} & \cdots & 1 \end{pmatrix}, \tag{2.22}$$

and due to the symmetry of the model, the $\mathbf{\Gamma}_N^A$ matrix has the recursive form for $N \geq 4$

$$\mathbf{\Gamma}_N^A = \begin{pmatrix} \mathbf{\Gamma}_{N/2}^A & \mathbf{0}_{(N/2)\times(N/2)} \\ \mathbf{0}_{(N/2)\times(N/2)} & \mathbf{\Gamma}_{N/2}^A \end{pmatrix}, \tag{2.23}$$

where $\mathbf{0}_{(N/2)\times(N/2)}$ is the all-zeros matrix of dimension $(N/2) \times (N/2)$ and $\mathbf{\Gamma}_2^A$ is the unit matrix, as defined in (2.17). Furthermore, the vector of means $\mu_{I,N}^A$ for $N \geq 4$ has the recursive form

$$\mu_{I,N}^A = \begin{bmatrix} \mu_{I,(N/2)}^A & \mu_{I,(N/2)}^A \end{bmatrix}^T, \tag{2.24}$$

and $\mu_{I,2}^A$ is the unit vector, given in (2.15). Thus, the probability of detection error is obtained as

$$P_{e,I}^{AWGN} = Q\left(\frac{1}{2}\sqrt{(\mu_{I,N}^A)^T (\mathbf{\Sigma}_{I,N}^A)^{-1} \mu_{I,N}^A}\right). \tag{2.25}$$

Since it is difficult to specify an arbitrary correlation matrix $\mathbf{\Omega}_N$ that allows fair comparison between the protocols and due to the fact that the aim of this investigation is to characterize the effect "degree" of correlation and the optimum error performance;

two *extreme* scenarios are considered, namely the Equally-Correlated Scenario (ECS) and the Mutually-Independent Scenario (MIS) [33].

In the Equally-Correlated Scenario, it is assumed that the N sensors are distributed in the wireless network such that every pair of sensor nodes are *equi-correlated* (i.e. $\rho_{i,j} = \rho$ for $i \neq j$). Therefore, the matrix $\mathbf{\Omega}_N$ has all its nondiagonal elements equal to ρ and all the diagonal elements equal to one. Under this scenario, the probability of detection error is evaluated using (2.25).

In the Mutually-Independent Scenario, the N sensors in the two sets $\mathcal{S}_{\mathcal{E}}$ and $\mathcal{S}_{\mathcal{O}}$ are spatially separated far enough from each other such that $\rho_{i,j} \approx 0$ for $i \neq j$. Therefore, due to the symmetry of the model, it can be easily shown that the probability of detection error is expressed as

$$P_{e,I}^{AWGN} = Q\left(\frac{1}{2}\sqrt{\frac{N}{2}\left(\frac{P_{so}d_{so,f}^{-\alpha}m^2}{P_{so}d_{so,f}^{-\alpha}\sigma^2 + N_o} + \frac{P_{se}d_{se,f}^{-\alpha}m^2}{P_{se}d_{se,f}^{-\alpha}\sigma^2 + N_o}\right)}\right). \tag{2.26}$$

It should also be noted that under MIS, the optimal *lower bound* error performance is achieved.

2.6.3 Protocol II - A Sensor with a Relay Network over AWGN Channels

The probability of detection error of Protocol II (shown in Fig. 2.1b) is analyzed in this section. It is noteworthy that in this case, there is no correlation between the sensor and the relay nodes since the former node takes measurements of the phenomenon while the latter node only amplifies and forwards the received signals from the source sensor node (see (2.6) - (2.8)). Under Protocol II, the received signal

vector $\mathbf{y}_{II,2}^{A} = [y_{s_1,f} \quad y_{r_2,f}]^T$ and the data model under hypotheses $\mathcal{H}_0$ and $\mathcal{H}_1$ are given by $\mathbf{y}_{II,2}^{A} = \mathcal{CN}(\mathbf{0}, \mathbf{\Sigma}_{II,2}^{A})$ and $\mathbf{y}_{II,2}^{A} = \mathcal{CN}(\mu_{II}^{A}, \mathbf{\Sigma}_{II,2}^{A})$, respectively. The covariance matrix $\mathbf{\Sigma}_{II,2}^{A}$ is shown to be

$$\mathbf{\Sigma}_{II,2}^{A} = \begin{pmatrix} P_{so}d_{so,f}^{-\alpha}\sigma^2 + N_o & \sqrt{\tilde{P}P_{so}P_r d_{so,f}^{-\alpha}d_{r,f}^{-\alpha}}\sigma^2 \\ \sqrt{\tilde{P}P_{so}P_r d_{so,f}^{-\alpha}d_{r,f}^{-\alpha}}\sigma^2 & P_r d_{r,f}^{-\alpha} + N_o \end{pmatrix}, \tag{2.27}$$

which can be expressed in matrix form as $\mathbf{\Sigma}_{II,2}^{A} = (\mathbf{\Upsilon}_2^{A})^T \mathbf{\Psi}_2^{A} \mathbf{\Upsilon}_2^{A} + N_o\mathbf{I}$; where

$$\mathbf{\Upsilon}_2^{A} = \begin{pmatrix} \sqrt{P_{so}d_{so,f}^{-\alpha}\sigma^2} & 0 \\ 0 & \sqrt{P_r d_{r,f}^{-\alpha}} \end{pmatrix}, \tag{2.28}$$

$$\mathbf{\Psi}_2^{A} = \begin{pmatrix} 1 & \sqrt{\tilde{P}\sigma^2} \\ \sqrt{\tilde{P}\sigma^2} & 1 \end{pmatrix}, \tag{2.29}$$

and $\tilde{P} = (P_{so}d_{so,r}^{-\alpha})/(P_{so}d_{so,r}^{-\alpha}\sigma^2 + N_o)$. The vector of means can be expressed as

$$\mu_{II,2}^{A} = \begin{bmatrix} \sqrt{P_{so}d_{so,f}^{-\alpha}}m & \sqrt{\tilde{P}P_r d_{r,f}^{-\alpha}}m \end{bmatrix}^T. \tag{2.30}$$

Thus, the probability of detection error is given by

$$P_{e,II}^{AWGN} = Q\left(\frac{1}{2}\sqrt{\frac{m^2 N_o(P_{so}d_{so,f}^{-\alpha} + \tilde{P}P_r d_{r,f}^{-\alpha}) + P_{so}P_r d_{so,f}^{-\alpha}d_{r,f}^{-\alpha}m^2(1-\tilde{P}\sigma^2)}{P_{so}P_r d_{so,f}^{-\alpha}d_{r,f}^{-\alpha}\sigma^2(1-\tilde{P}\sigma^2) + N_o(P_{so}d_{so,f}^{-\alpha}\sigma^2 + P_r d_{r,f}^{-\alpha}) + N_o^2}}\right). \tag{2.31}$$

2.6.4 Protocol II - N Nodes Network over AWGN Channels

In this case, the N nodes in the network are split into two sets; $\mathcal{S}_{\mathcal{O}}$ and $\mathcal{R}$ as discussed in Section 2.4.3. However, it should be noted that in this case, the measurements obtained from each of the sensors in the set $\mathcal{S}_{\mathcal{O}}$ can be correlated. For example, for $(N = |\mathcal{R}| + |\mathcal{S}_{\mathcal{O}}| = 4)$, the observations from sensors S_1 and S_3 (paired

with relays R_2 and R_4, respectively) are correlated by $\rho_{1,3}$ that is a function of the distance $d_{s_{1,3}}$ between them.

For a network with arbitrary N nodes under Protocol II, the N-dimensional vector of received observations is $\mathbf{y}_{II,N}^{A} = \begin{bmatrix} y_{s_1,f} & y_{r_2,f} & \cdots & y_{s_{N-1},f} & y_{r_N,f} \end{bmatrix}^T$. In addition, every pair of sensors in $\mathcal{S}_{\mathcal{O}}$ can be correlated depending on their inter-sensor separation. In general, it can be easily shown that for $(N \geq 4)$, the matrix $\boldsymbol{\Upsilon}_N^A$ has the following recursive form

$$\boldsymbol{\Upsilon}_N^A = \begin{pmatrix} \boldsymbol{\Upsilon}_{N/2}^A & \mathbf{0}_{(N/2)\times(N/2)} \\ \mathbf{0}_{(N/2)\times(N/2)} & \boldsymbol{\Upsilon}_{N/2}^A \end{pmatrix}, \tag{2.32}$$

while $\boldsymbol{\Psi}_N^A$ has the general form

$$\boldsymbol{\Psi}_N^A = \begin{pmatrix} \boldsymbol{\Psi}_2^A & \rho_{1,3}\boldsymbol{\Lambda}_2 & \rho_{1,5}\boldsymbol{\Lambda}_2 & \cdots & \rho_{1,N/2-1}\boldsymbol{\Lambda_2} \\ \rho_{1,3}\boldsymbol{\Lambda}_2^T & \boldsymbol{\Psi}_2^A & \rho_{3,5}\boldsymbol{\Lambda}_2^T & \cdots & \rho_{3,N/2-1}\boldsymbol{\Lambda}_2 \\ \rho_{1,5}\boldsymbol{\Lambda}_2^T & \rho_{3,5}\boldsymbol{\Lambda}_2^T & \boldsymbol{\Psi}_2^A & \cdots & \rho_{5,N/2-1}\boldsymbol{\Lambda}_2 \\ \vdots & \vdots & \vdots & \ddots & \vdots \\ \rho_{1,N/2-1}\boldsymbol{\Lambda}_2^T & \rho_{3,N/2-1}\boldsymbol{\Lambda}_2^T & \rho_{5,N/2-1}\boldsymbol{\Lambda}_2^T & \cdots & \boldsymbol{\Psi}_2^A \end{pmatrix}, \tag{2.33}$$

where

$$\boldsymbol{\Lambda}_2 = \begin{pmatrix} 1 & \sqrt{\tilde{P}\sigma^2} \\ \sqrt{\tilde{P}\sigma^2} & \tilde{P}\sigma^2 \end{pmatrix}. \tag{2.34}$$

As in Protocol I, the vector of means for $N \geq 4$ can be shown to have the recursive form

$$\mu_{II,N}^A = \begin{bmatrix} \mu_{II,(N/2)}^A & \mu_{II,(N/2)}^A \end{bmatrix}^T. \tag{2.35}$$

Therefore, the covariance matrix of a network with N nodes can be expressed in matrix form as $\boldsymbol{\Sigma}_{II,N}^A = (\boldsymbol{\Upsilon}_N^A)^T \boldsymbol{\Psi}_N^A \boldsymbol{\Upsilon}_N^A + N_o\mathbf{I}$. As before, under the Equally-Correlated

Scenario, the probability of detection error is determined using

$$P_{e,II}^{AWGN} = Q\left(\frac{1}{2}\sqrt{(\mu_{II,N}^{A})^{T}(\mathbf{\Sigma}_{II,N}^{A})^{-1}\mu_{II,N}^{A}}\right), \tag{2.36}$$

while under the Mutually-Independent Scenario, the probability of detection is given by

$$P_{e,II}^{AWGN} = Q\left(\frac{1}{2}\sqrt{\frac{N}{2}\left(\frac{m^2 N_o(P_{so}d_{so,f}^{-\alpha} + \tilde{P}P_r d_{r,f}^{-\alpha}) + P_{so}P_r d_{so,f}^{-\alpha}d_{r,f}^{-\alpha}m^2(1-\tilde{P}\sigma^2)}{P_{so}P_r d_{so,f}^{-\alpha}d_{r,f}^{-\alpha}\sigma^2(1-\tilde{P}\sigma^2) + N_o(P_{so}d_{so,f}^{-\alpha}\sigma^2 + P_r d_{r,f}^{-\alpha}) + N_o^2}\right)}\right). \tag{2.37}$$

2.7 Theoretical Analysis: Rayleigh Fading Channels

In the following sections, the theoretical analysis of Protocol I and Protocol II over Rayleigh flat-fading channels are presented.

2.7.1 Protocol I - A Two Sensors Network over Rayleigh Fading Channels

In this case, the probability of error detection P_e of the $N = 2$ sensors network in the Rayleigh fading channel is analyzed in a similar manner to the AWGN channel. The received observation vector is defined as $\mathbf{y}_{I,2}^{\mathbf{R}} = [y_{s_1,f} \quad y_{s_2,f}]^T$ where it is straightforward to show that the data model under hypothesis $\mathcal{H}_0$ is written as $\mathbf{y}_{I,2}^{\mathbf{R}} = \mathcal{CN}(\mathbf{0}, \mathbf{\Sigma}_{\mathbf{I,2}}^{\mathbf{R}})$ while under $\mathcal{H}_1$ is given by $\mathbf{y}_{I,2}^{\mathbf{R}} = \mathcal{CN}(\mu_{\mathbf{I},(\mathbf{1,2})}^{\mathbf{R}}, \mathbf{\Sigma}_{\mathbf{I,2}}^{\mathbf{R}})$. The vector of means can be shown to be

$$\mu_{\mathbf{I},(\mathbf{1,2})}^{\mathbf{R}} = \left[\sqrt{P_{so}d_{so,f}^{-\alpha}}h_{s_1,f}m \quad \sqrt{P_{se}d_{se,f}^{-\alpha}}h_{s_2,f}m\right]^T, \tag{2.38}$$

where $h_{s_1,f}$ and $h_{s_2,f}$ are the channel coefficients between sensor nodes S_1 and S_2 and the fusion center, respectively. Furthermore, the $\mathbf{\Sigma}_{I,2}^R$ can be shown to be

$$\mathbf{\Sigma}_{I,2}^R = \begin{pmatrix} P_{so}d_{so,f}^{-\alpha}|h_{s_1,f}|^2\sigma^2 + N_o & \sqrt{P_{so}P_{se}d_{so,f}^{-\alpha}d_{se,f}^{-\alpha}}h_{s_1,f}h_{s_2,f}^*\sigma^2\rho_{1,2} \\ \sqrt{P_{so}P_{se}d_{so,f}^{-\alpha}d_{se,f}^{-\alpha}}h_{s_1,f}^*h_{s_2,f}\sigma^2\rho_{1,2} & P_{se}d_{se,f}^{-\alpha}|h_{s_2,f}|^2\sigma^2 + N_o \end{pmatrix}, \tag{2.39}$$

which can be expressed in the matrix form as $\mathbf{\Sigma}_{I,2}^R = (\mathbf{\Gamma}_{(1,2)}^R)^H\mathbf{\Omega}_2\mathbf{\Gamma}_{(1,2)}^R + N_o\mathbf{I}$ where $(.)^H$ is the hermitian of the parameter matrix. The matrix $\mathbf{\Gamma}_{(1,2)}^R$ is defined as

$$\mathbf{\Gamma}_{(1,2)}^R = \begin{pmatrix} \sqrt{P_{so}d_{so,f}^{-\alpha}\sigma^2}h_{s_1,f}^* & 0 \\ 0 & \sqrt{P_{se}d_{se,f}^{-\alpha}\sigma^2}h_{s_2,f}^* \end{pmatrix}. \tag{2.40}$$

Thus, the probability of detection error can be expressed as

$$P_{e,I}^{Ray} = E\left\{Q\left(\frac{1}{2}\sqrt{(\mu_{I,(1,2)}^R)^H(\mathbf{\Sigma}_{I,2}^R)^{-1}\mu_{I,(1,2)}^R}\right)\right\}, \tag{2.41}$$

which can be written as

$$P_{e,I}^{Ray} = E\left\{Q\left(\frac{1}{2}\sqrt{\frac{2P_{so}P_{se}|h_{s_1,f}|^2|h_{s_2,f}|^2(d_{so,f}^{-\alpha}d_{se,f}^{-\alpha})m^2\sigma^2(1-\rho_{1,2}) + N_om^2(P_{so}|h_{s_1,f}|^2d_{so,f}^{-\alpha} + P_{se}|h_{s_2,f}|^2d_{se,f}^{-\alpha})}{P_{so}P_{se}|h_{s_1,f}|^2|h_{s_2,f}|^2(d_{so,f}^{-\alpha}d_{se,f}^{-\alpha})\sigma^4(1-\rho_{1,2}^2) + N_o\sigma^2(P_{so}|h_{s_1,f}|^2d_{so,f}^{-\alpha} + P_{se}|h_{s_2,f}|^2d_{se,f}^{-\alpha}) + N_o^2}}\right)\right\}. \tag{2.42}$$

For the case of independent observations (i.e. $\rho_{1,2} = 0$), the probability of detection error can be expressed as

$$P_{e,I}^{Ray} = E\left\{Q\left(\frac{1}{2}\sqrt{\frac{P_{so}|h_{s_1,f}|^2d_{so,f}^{-\alpha}m^2}{P_{so}|h_{s_1,f}|^2d_{so,f}^{-\alpha}\sigma^2 + N_o} + \frac{P_{se}|h_{s_2,f}|^2d_{se,f}^{-\alpha}m^2}{P_{se}|h_{s_2,f}|^2d_{se,f}^{-\alpha}\sigma^2 + N_o}}\right)\right\}. \tag{2.43}$$

2.7.2 Protocol I - N Sensors Network over Rayleigh Fading Channels

As in the case of the AWGN channel, the analysis is easily extended to the case of arbitrary large N number of sensors in the network. The $N-dimensional$ vector

of received observations is $\mathbf{y}_{I,N}^{R} = \begin{bmatrix} y_{s_1,f} & y_{s_2,f} & \cdots & y_{s_{N-1},f} & y_{s_N,f} \end{bmatrix}^T$ for which the covariance matrix $\mathbf{\Sigma}_{I,N}^{R}$ can be expressed as $\mathbf{\Sigma}_{I,N}^{R} = (\mathbf{\Gamma}_{I,N}^{R})^H \mathbf{\Omega}_N \mathbf{\Gamma}_{I,N}^{R} + N_o \mathbf{I}$ and the matrix $\mathbf{\Gamma}_{I,N}^{R}$ is given by

$$\mathbf{\Gamma}_{I,N}^{R} = \begin{pmatrix} \mathbf{\Gamma}_{(1,2)}^{R} & 0 & \cdots & 0 \\ 0 & \mathbf{\Gamma}_{(3,4)}^{R} & \cdots & 0 \\ \vdots & \vdots & \ddots & \vdots \\ 0 & 0 & \cdots & \mathbf{\Gamma}_{(N-1,N)}^{R} \end{pmatrix}, \tag{2.44}$$

respectively; where in general

$$\mathbf{\Gamma}_{(i,j)}^{R} = \begin{pmatrix} \sqrt{P_{so} d_{so,f}^{-\alpha} \sigma^2} h_{s_i,f}^{*} & 0 \\ 0 & \sqrt{P_{se} d_{se,f}^{-\alpha} \sigma^2} h_{s_j,f}^{*} \end{pmatrix}. \tag{2.45}$$

Furthermore, the vector of means $\mu_{I,N}^{R}$ can be expressed as

$$\mu_{I,N}^{R} = \begin{bmatrix} \mu_{I,(1,2)}^{R} & \mu_{I,(3,4)}^{R} & \cdots & \mu_{I,(N-1,N)}^{R} \end{bmatrix}^T, \tag{2.46}$$

where

$$\mu_{I,(i,j)}^{R} = \begin{bmatrix} \sqrt{P_{so} d_{so,f}^{-\alpha}} h_{s_i,f} m & \sqrt{P_{se} d_{se,f}^{-\alpha}} h_{s_j,f} m \end{bmatrix}^T. \tag{2.47}$$

Therefore, the probability of detection error is given by

$$P_{e,I}^{Ray} = E\left\{ Q\left(\frac{1}{2} \sqrt{(\mu_{I,N}^{R})^H (\mathbf{\Sigma}_{I,N}^{R})^{-1} \mu_{I,N}^{R}} \right) \right\}. \tag{2.48}$$

Under the Equally-Correlated Scenario, the probability of detection error is evaluated by (2.48). On the other hand, under the Mutually-Independent Scenario, it can be easily shown that the probability of detection error is expressed as

$$P_{e,I}^{Ray} = E\left\{ Q\left(\frac{1}{2} \sqrt{\sum_{i \in \mathcal{S}_{\mathcal{O}}} \frac{P_{so} |h_{s_i,f}|^2 d_{so,f}^{-\alpha} m^2}{P_{so} |h_{s_i,f}|^2 d_{so,f}^{-\alpha} \sigma^2 + N_o} + \sum_{j \in \mathcal{S}_{\mathcal{E}}} \frac{P_{se} |h_{s_j,f}|^2 d_{se,f}^{-\alpha} m^2}{P_{se} |h_{s_j,f}|^2 d_{se,f}^{-\alpha} \sigma^2 + N_o}} \right) \right\}. \tag{2.49}$$

2.7.3 Protocol II - A Sensor with a Relay Network over Rayleigh Fading Channels

Similar to the derivation of Protocol II under the AWGN channel, the received signal vector under the Rayleigh fading channel is obtained as $\mathbf{y}^R_{II,2} = [y_{s_1,f} \quad y_{r_2,f}]^T$ and the data model under hypotheses $\mathcal{H}_0$ and $\mathcal{H}_1$ are given by $\mathbf{y}^R_{II,2} = \mathcal{CN}(\mathbf{0}, \mathbf{\Sigma}^R_{II,2})$ and $\mathbf{y}^R_{II,2} = \mathcal{CN}(\mu^R_{II,(1,2)}, \mathbf{\Sigma}^R_{II,2})$, respectively. The covariance matrix $\mathbf{\Sigma}^R_{II,2}$ is shown to be

$$\mathbf{\Sigma}^R_{II,2} = \begin{pmatrix} P_{so}d^{-\alpha}_{so,f}|h_{s_1,f}|^2\sigma^2 + N_o & \sqrt{\tilde{P}_{(1,2)}P_{so}P_r d^{-\alpha}_{so,f}d^{-\alpha}_{r,f}}h_{s_1,f}h^*_{r_2,f}h^*_{s_1,r_2}\sigma^2 \\ \sqrt{\tilde{P}_{(1,2)}P_{so}P_r d^{-\alpha}_{so,f}d^{-\alpha}_{r,f}}h^*_{s_1,f}h_{r_2,f}h_{s_1,r_2}\sigma^2 & P_r d^{-\alpha}_{r,f}|h_{s_2,f}|^2 + N_o \end{pmatrix}, \tag{2.50}$$

which can be expressed in matrix form as $\mathbf{\Sigma}^R_{II,2} = (\mathbf{\Upsilon}^R_{(1,2)})^H \mathbf{\Omega}_{(1,2)} \mathbf{\Upsilon}^R_{(1,2)} + N_o\mathbf{I}$ where

$$\mathbf{\Upsilon}^R_{(1,2)} = \begin{pmatrix} \sqrt{P_{so}d^{-\alpha}_{so,f}\sigma^2}h^*_{s_1,f} & 0 \\ 0 & \sqrt{P_r d^{-\alpha}_{r,f}}h^*_{r_2,f} \end{pmatrix}, \tag{2.51}$$

$$\mathbf{\Omega}^R_{(1,2)} = \begin{pmatrix} 1 & \sqrt{\hat{P}_{(1,2)}\sigma^2}h^*_{s_1,r_2} \\ \sqrt{\hat{P}_{(1,2)}\sigma^2}h_{s_1,r_2} & 1 \end{pmatrix}, \tag{2.52}$$

and $\hat{P}_{(1,2)} = (P_{so}d^{-\alpha}_{so,r})/(P_{so}d^{-\alpha}_{so,r}|h_{s_1,r_2}|^2\sigma^2 + N_o)$. The vector of means can be expressed as

$$\mu^R_{II,(1,2)} = \left[\sqrt{P_{so}d^{-\alpha}_{so,f}}h_{s_1,f}m \quad \sqrt{\hat{P}_{(1,2)}P_r d^{-\alpha}_{r,f}}h_{r_2,f}h_{s_1,r_2}m\right]^T. \tag{2.53}$$

In this case, the probability of detection error can be written as

$$P^{Ray}_{e,II} = E\left\{Q\left(\frac{1}{2}\sqrt{\frac{m^2N_o(P_{so}d^{-\alpha}_{so,f}|h_{s_1,f}|^2 + \hat{P}_{(1,2)}P_r d^{-\alpha}_{r,f}|h_{r_2,f}|^2|h_{s_1,r_2}|^2) + P_{so}P_r|h_{s_1,f}|^2|h_{r_2,f}|^2 d^{-\alpha}_{so,f}d^{-\alpha}_{r,f}m^2(1-\hat{P}_{(1,2)}\sigma^2)}{P_{so}P_r|h_{s_1,f}|^2|h_{r_2,f}|^2 d^{-\alpha}_{so,f}d^{-\alpha}_{r,f}\sigma^2(1-\hat{P}_{(1,2)}|h_{s_1,r_2}|^2\sigma^2) + N_o(P_{so}d^{-\alpha}_{so,f}|h_{s_1,f}|^2\sigma^2 + P_r d^{-\alpha}_{r,f}|h_{r_2,f}|^2) + N_o^2}}\right)\right\}. \tag{2.54}$$

2.7.4 Protocol II - N Nodes Network over Rayleigh Fading Channels

As in the derivation under the AWGN channel, the $N-$*dimensional* vector of received observations under the Rayleigh fading channel is written as $\mathbf{y}_{II,N}^{R} = \begin{bmatrix} y_{s_1,f} & y_{r_2,f} & \cdots & y_{s_{N-1},f} & y_{r_N,f} \end{bmatrix}^T$ where the covariance matrix can be shown to have the form $\mathbf{\Sigma}_{II,N}^{R} = (\mathbf{\Upsilon}_{N}^{R})^H \mathbf{\Omega}_{N}^{R} \mathbf{\Upsilon}_{N}^{R} + N_o \mathbf{I}$. In addition, every pair of sensors in $\mathcal{S}_{\mathcal{O}}$ can be correlated depending on their inter-sensor separation. In general, it can be easily shown that for $(N \geq 4)$, the matrix $\mathbf{\Upsilon}_N$ can be expressed as

$$\mathbf{\Upsilon}_{N}^{R} = \begin{pmatrix} \mathbf{\Upsilon}_{(1,2)}^{R} & 0 & \cdots & 0 \\ 0 & \mathbf{\Upsilon}_{(3,4)}^{R} & \cdots & 0 \\ \vdots & \vdots & \ddots & \vdots \\ 0 & 0 & \cdots & \mathbf{\Upsilon}_{(N-1,N)}^{R} \end{pmatrix}, \tag{2.55}$$

where

$$\mathbf{\Upsilon}_{(i,k)}^{R} = \begin{pmatrix} \sqrt{P_{so} d_{so,f}^{-\alpha} \sigma^2} h_{s_i,f}^{*} & 0 \\ 0 & \sqrt{P_r d_{r,f}^{-\alpha}} h_{r_k,f}^{*} \end{pmatrix}. \tag{2.56}$$

The matrix $\mathbf{\Omega}_{N}^{R}$ can be shown to have the structure as follows

$$\mathbf{\Omega}_{N}^{R} = \begin{pmatrix} \mathbf{\Omega}_{(1,2)}^{R} & \rho_{1,3} \mathbf{\Theta}_{(1,2),(3,4)} & \cdots & \rho_{1,N/2-1} \mathbf{\Theta}_{(1,2),(N-1,N)} \\ \rho_{1,3} \mathbf{\Theta}_{(3,4),(1,2)} & \mathbf{\Omega}_{(3,4)}^{R} & \cdots & \rho_{3,N/2-1} \mathbf{\Theta}_{(3,4),(N-1,N)} \\ \vdots & \vdots & \ddots & \vdots \\ \rho_{1,N/2-1} \mathbf{\Theta}_{(N-1,N),(1,2)} & \rho_{3,N/2-1} \mathbf{\Theta}_{(N-1,N),(3,4)} & \cdots & \mathbf{\Omega}_{(N-1,N)}^{R} \end{pmatrix}, \tag{2.57}$$

where

$$\mathbf{\Theta}_{(i,j),(k,l)} = \begin{pmatrix} 1 & \sqrt{\hat{P}_{(k,l)} \sigma^2} h_{s_k,r_l}^{*} \\ \sqrt{\hat{P}_{(i,j)} \sigma^2} h_{s_i,r_j} & \sqrt{\hat{P}_{(i,j)} \hat{P}_{(k,l)}} \sigma^2 h_{s_i,r_j} h_{s_k,r_l}^{*} \end{pmatrix}, \tag{2.58}$$

and $\hat{P}_{(i,k)} = P_{so}d_{so,r}^{-\alpha}/(P_{so}d_{so,r}^{-\alpha}|h_{s_i,r_k}|^2\sigma^2 + N_o)$. In addition, the vector of means can be expressed as

$$\mu_{II,N}^{R} = \begin{bmatrix}\mu_{II,(1,2)}^{R} & \mu_{II,(3,4)}^{R} & \cdots & \mu_{II,(N-1,N)}^{R}\end{bmatrix}^{T}, \tag{2.59}$$

where

$$\mu_{II,(i,k)}^{R} = \begin{bmatrix}\sqrt{P_{so}d_{so,f}^{-\alpha}}h_{s_i,f}m & \sqrt{\hat{P}_{(i,k)}P_r d_{r,f}^{-\alpha}}h_{r_k,f}h_{s_i,r_k}m\end{bmatrix}^{T}. \tag{2.60}$$

Under the Equally-Correlated Scenario, the probability of detection error can be determined using

$$P_{e,II}^{Ray} = E\left\{Q\left(\frac{1}{2}\sqrt{(\mu_{II,N}^{R})^{H}(\mathbf{\Sigma}_{II,N}^{R})^{-1}\mu_{II,N}^{R}}\right)\right\}, \tag{2.61}$$

while for the mutually independent scenario, the probability of detection error is given by

$$P_{e,II}^{Ray} = E\left\{Q\left(\frac{1}{2}\sqrt{\sum_{(i,k)\in(\mathcal{S}_{\mathcal{O}},\mathcal{R})}\frac{m^2N_o(P_{so}d_{so,f}^{-\alpha}|h_{s_i,f}|^2 + \hat{P}_{(i,k)}P_r d_{r,f}^{-\alpha}|h_{r_k,f}|^2|h_{s_i,r_k}|^2) + P_{so}P_r|h_{s_i,f}|^2|h_{r_k,f}|^2 d_{so,f}^{-\alpha}d_{r,f}^{-\alpha}m^2(1-\hat{P}_{(i,k)}\sigma^2)}{P_{so}P_r|h_{s_i,f}|^2|h_{r_k,f}|^2 d_{so,f}^{-\alpha}d_{r,f}^{-\alpha}\sigma^2(1-\hat{P}_{(i,k)}|h_{s_i,r_k}|^2\sigma^2) + N_o(P_{so}d_{so,f}^{-\alpha}|h_{s_i,f}|^2\sigma^2 + P_r d_{r,f}^{-\alpha}|h_{r_k,f}|^2) + N_o^2}}\right)\right\}. \tag{2.62}$$

2.8 Performance Evaluation of Network Protocols

In this section, performance evaluation of both protocols under consideration in AWGN and Rayleigh flat fading channels are compared in terms of the derived probability of detection error P_e. To allow a fair comparison between the performance of the network protocols, it is assumed that within a particular area $\mathcal{A}$, the total network power constraint P_T of N nodes is equally distributed amongst all nodes. Hence, the power constraint per sensor/relay node can be computed as $P = P_T/N$.

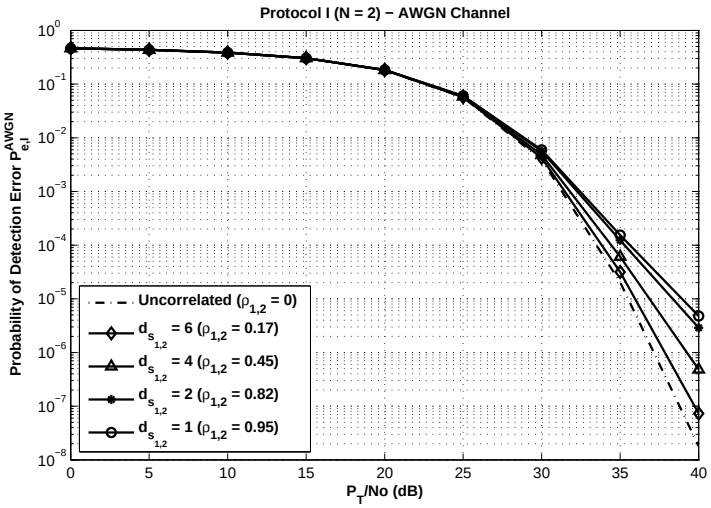

Figure 2.3: Detection error performance of Protocol I for $N = 2$ in the AWGN channel for different ρ values (as a function of the inter-sensor separation $d_{s_{1,2}}$)

This in turn implies that the power allocation to each node decreases linearly with the increase in the total number of nodes in the network area $\mathcal{A}$. The simulation parameters of the network protocols are as follows. The measurement noise variance is $\sigma^2 = 0.01$ while the mean of measurements is $m = 1$. In addition, the path-loss exponent is $\alpha = 3$ and the correlation decay factor is $\lambda = 0.05$. The distance from the sensors in $\mathcal{S}_{\mathcal{O}}$ and $\mathcal{S}_{\mathcal{E}}$ and the relays in $\mathcal{R}$ are $d_{so,f} = 4.5$, $d_{se,f} = 3.5$ and $d_{r,f} = 2.5$, respectively.

Fig. 2.3 illustrates P_e for Protocol I with $N = 2$ under the AWGN channel. As explained in the proposed model for Protocol I, different inter-sensor separations result in different correlation coefficients since $\rho_{1,2} = \exp(-\lambda d_{s_{1,2}}^2)$. Therefore, it is clear that as the inter-sensor separation increases, the correlation coefficient decreases and the error performance improves. This is to be expected since the lower the correlation, the more statistically independent the observations become; hence more

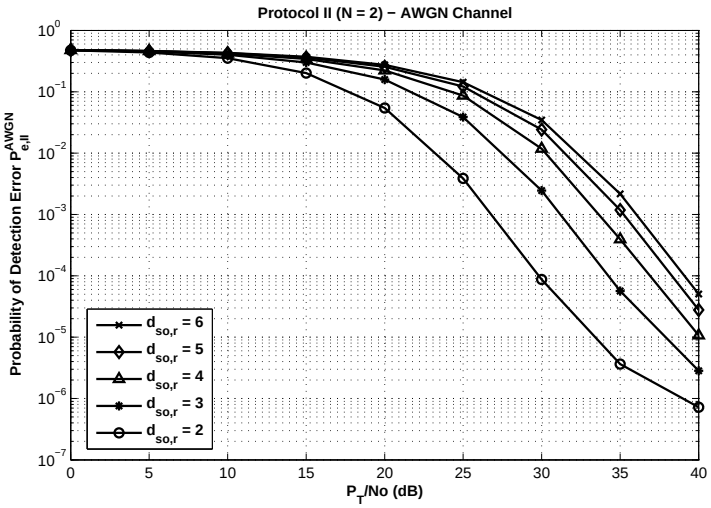

Figure 2.4: Detection error performance of Protocol II for $N = 2$ in the AWGN channel as a function of the inter-sensor/relay separation $d_{so,r}$

information is fed to the fusion center which in turn results in better error detection performance. Also shown, the case where both sensors S_1 and S_2 are far away from each other since that their correlation coefficient $\rho_{1,2} = 0$ (i.e. uncorrelated) and this achieves the optimal *(lower bound)* error performance of Protocol I as a function of $\rho_{1,2}$.

In Fig. 2.4 and under Protocol II for $N = 2$, it can also be seen that as the inter-sensor/relay distance $d_{so,r}$ increases, the error performance degrades. This is due to the fact that farther apart the sensor and the relay become, the weaker the received signal and hence the worse the performance. Hence, the closer the sensor to the cooperating relay, the better the performance, and in this case, the closest the sensor to the cooperating relay node is when $d_{so,r} = 2$ (since $d_{so,f} = 4.5$ and $d_{r,f} = 2.5$ and hence the relay node is on a straight line and in the middle between the sensor and the fusion center). The results obtained under the AWGN channel (presented in

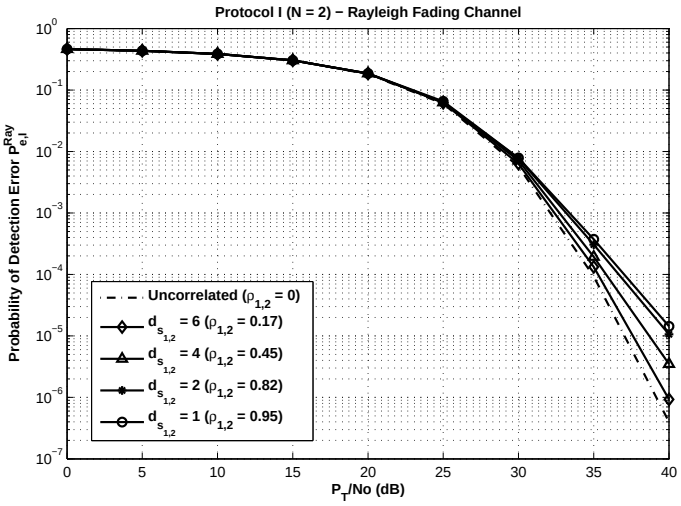

Figure 2.5: Detection error performance of Protocol I for $N = 2$ in the Rayleigh fading channel for different ρ values (as a function of the inter-sensor separation $d_{s_{1,2}}$)

Figs. 2.3 and 2.4) are consistent with the results obtained under the Rayleigh fading channel (see Figs. 2.5 and 2.6).

In order to determine when it is better to use Protocol I (as a function of $d_{s_{1,2}}$) or Protocol II (as a function of $d_{so,r}$) for the simple $N = 2$ network, the error performance at $P_T/N_0 = 40dB$ is plotted in Fig. 2.7 under both the AWGN and the Rayleigh fading channels. It can be seen that under the AWGN (Rayleigh fading) channel for inter-sensor/relay distances less than 2.6 (2.75), Protocol II outperforms Protocol I. In other words, under the AWGN (Rayleigh fading) channel, if two sensors S_1 and S_2 have inter-sensor separation $d_{s_{1,2}} < 2.6$ ($d_{s_{1,2}} < 2.75$), then it would be better not to use S_2 for transmission but instead pair sensor node S_1 with the cooperating relay R_2 (closer to the fusion center) to amplify-and-forward the transmitted observations of S_1 with inter-sensor/relay separation $d_{so,r} < 2.6$ ($d_{so,r} < 2.75$). It should be further noted that the range over which Protocol II outperforms Protocol I is greater

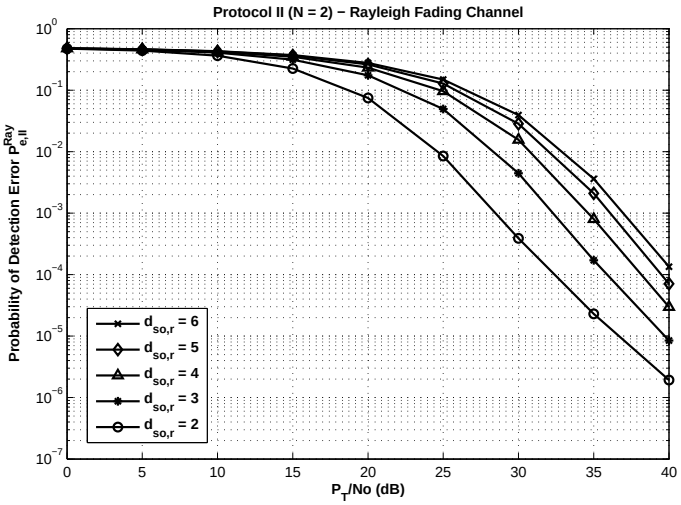

Figure 2.6: Detection error performance of Protocol II for $N = 2$ in Rayleigh fading channel as a function of the inter-sensor/relay separation $d_{so,r}$

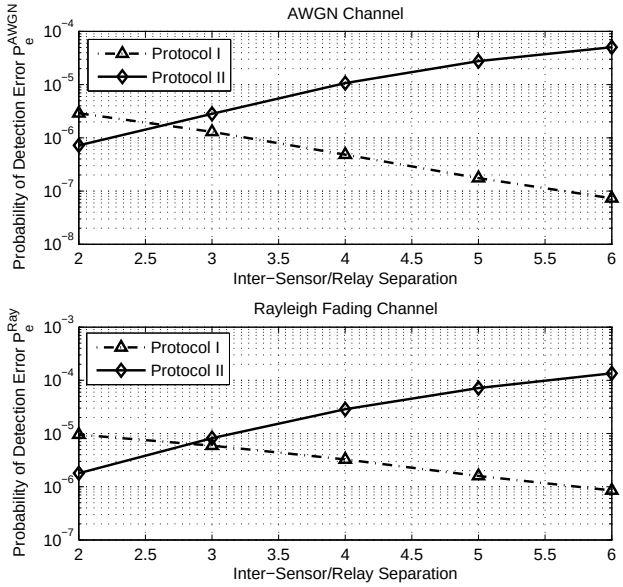

Figure 2.7: Protocol I vs. Protocol II as a function of inter-sensor/relay separation for $N = 2$ in AWGN and Rayleigh fading Channels for $P_T/No = 40dB$

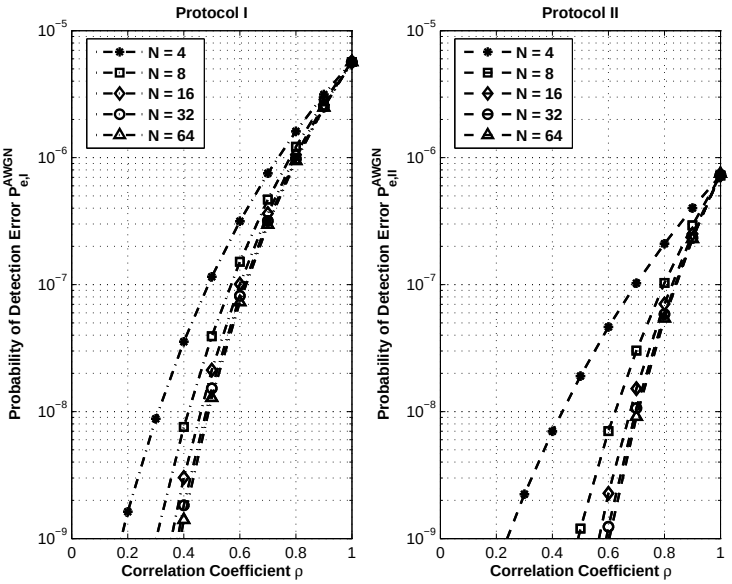

Figure 2.8: Protocol I vs. Protocol II - Equally-Correlated Scenario in the AWGN Channel for $P_T/N_o = 40dB$

under the Rayleigh fading channel and this is attributed to the diversity gain achieved through cooperation. It is also evident from Fig. 2.7, that the sensor/relay separation when $d_{so,r} = 2$ gives the best performance for Protocol II. Thus, it will be assumed in the subsequent simulation results. It would be expected that since the inter-sensor/relay distance of $d_{so,r} = 2$ for Protocol II results in a detection performance that outperforms that of the Protocol I, then for a larger number of nodes (i.e. for $N \geq 4$), it is expected that Protocol II would still outperform Protocol I.

In Fig. 2.8, the performance of Protocol I and Protocol II for $N \geq 4$ under the Equally-Correlated Scenario (ECS) as a function of ρ is evaluated under the AWGN channel. As noticed earlier, when the correlation amongst the observations increases, the performance of the network degrades. It is also clear that the distributed detection performance of the wireless sensor network even when $\rho \rightarrow 1$ under Protocol

II is still much better than that of Protocol I, as would be expected. In addition, with the increase of the number of nodes N, the fusion center has access to more observations for detection and thus a better performance is achieved under both protocols. However, with the increase in ρ, the gain in the detection performance obtained by using a larger number of sensor nodes decreases. This important result illustrates that by optimally setting the separation for each pair of sensor/relay nodes (i.e. for $N = 2$ under Protocol II), in sensor networks with $N \geq 4$, deploying relay nodes significantly improves the detection error performance. Furthermore, increasing the number of sensor nodes within a wireless sensor network area (i.e. increasing node density) under strict network power constraint does not necessarily result in significant detection gains. Another important observation for the case when $\rho \to 1$ is that all the measurements from the sensor nodes and also the relayed measurements result in the same P_e^{AWGN} despite the difference in the total number of nodes. That is, the performance of a high number of sensor/relay nodes ($N \geq 4$) for high correlation ($\rho \to 1$) collapses to that of using just $N = 4$ nodes. In particular, for $\rho = 1$, the $N = 64$ nodes act as $N = 4$ nodes; which implies that the probability of detection error for the $N = 64$ and the $N = 4$ nodes become statistically equivalent. This observation coincides with results proved in [33].

Similarly, in Fig. 2.9, it is also clear that Protocol II significantly outperforms Protocol I for the different numbers of sensor/relay nodes under the Rayleigh fading channel. In addition, it is noticed that Protocol II with $N = 8$ outperforms that of Protocol I for the different numbers of sensor nodes greater than $N = 4$. This implies that with relays deployment, the network detection error performance is im-

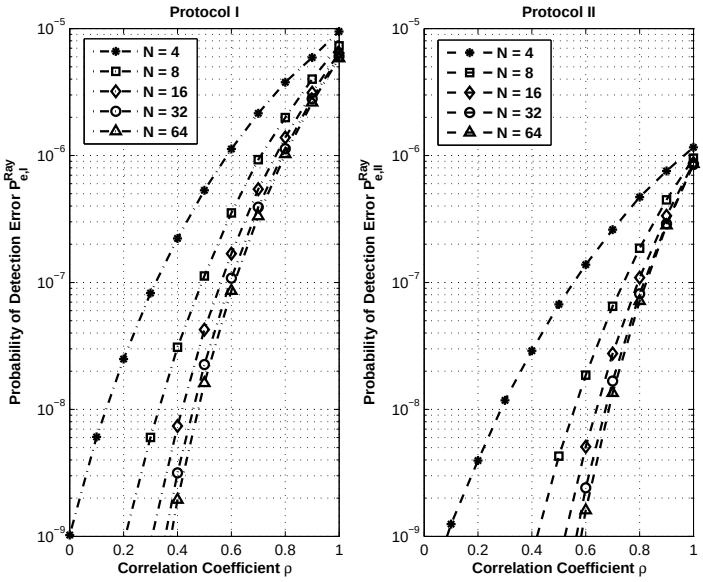

Figure 2.9: Protocol I vs. Protocol II - Equally-Correlated Scenario in the Rayleigh Fading Channel for $P_T/N_o = 40dB$

proved significantly due to the spatial diversity achieved by cooperation. Therefore, sending many observations from sensor nodes does not necessary improve the detection performance significantly. However, by cooperatively relaying a fewer number of observations, greater detection reliability is achieved at the fusion center. On the other hand, as $\rho \to 1$, the P_e^{Ray} for different numbers of sensor/relay nodes N, under both protocols, is different with the best performance achieved with $N = 64$. This is commensurate with the fact that increasing the number of sensor/relay nodes increases the achievable diversity gains. However, this improvement is limited by the total network power constraint P_T.

In Fig. 2.10, Protocols I and II are evaluated under the Mutually-Independent Scenario (MIS) (i.e. independent measurements) in the AWGN channel. It can be seen that Protocol II outperforms Protocol I for different numbers of nodes. It is also

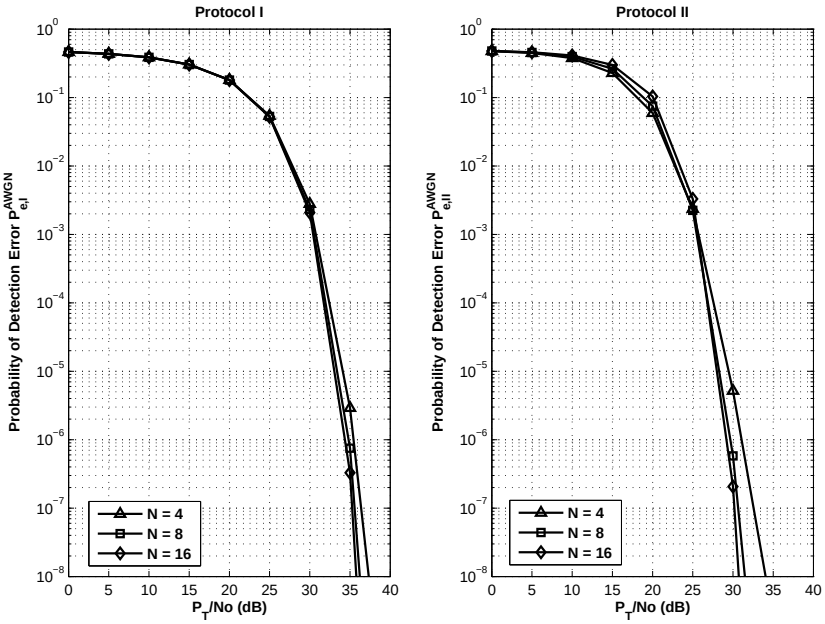

Figure 2.10: Protocol I vs. Protocol II - Mutually Independent Scenario in the AWGN Channel

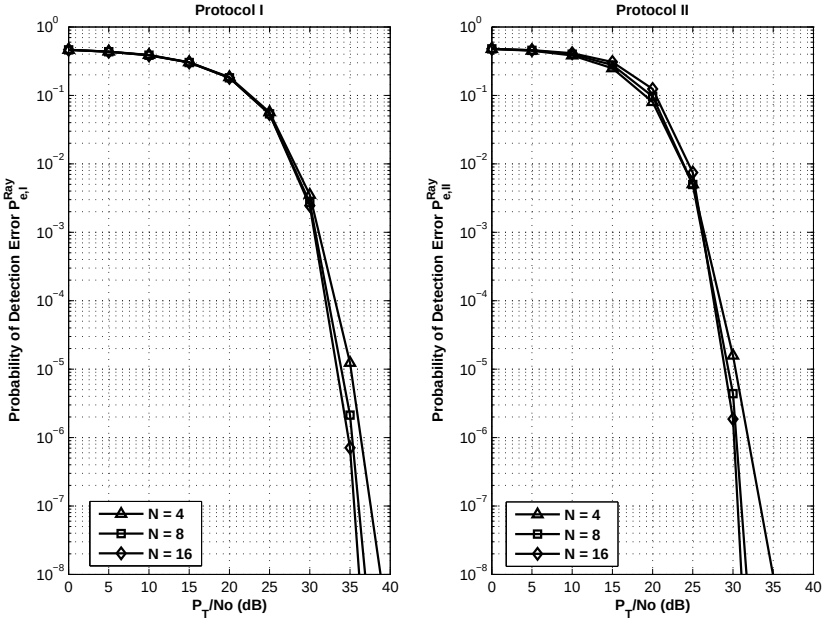

Figure 2.11: Protocol I vs. Protocol II - Mutually Independent Scenario in the Rayleigh fading channel

clear that increasing the number of sensor/relay nodes beyond $N = 8$ does not improve the error performance significantly given the power constraint P_T on the network. In addition, the performance obtained from Protocol II with $N = 4$ sensor/relay nodes is better than the performance obtained from Protocol I with ($N \geq 4$) sensor nodes as was shown earlier. The same observation is noticed under the Rayleigh fading channel (shown in Fig. 2.11). On the other hand, by comparing the detection error performance of Protocols I and II under both channel models, it can be seen that with the increase in the number of sensor/relay nodes N, the performance under the Rayleigh fading channel approaches that of the AWGN channel. For example, consider the detection error performance of Protocol II (as shown in Figs. 2.10 and 2.11). For $N = 4$, under the AWGN channel, about $P_T/N_0 \approx 34dB$ is required to achieve $P_{e,II}^{AWGN} = 10^{-8}$ (see Fig. 2.10); while under the Rayleigh fading channel (see Fig. 2.11), $P_T/N_0 \approx 35dB$ is required for the same probability of error. This in turn implies that under Protocol II, the P_e performance in the Rayleigh fading channel approaches that of the AWGN channel within $1dB$ for $N = 4$, due to the spatial diversity gains. Now, for $N = 16$, under the AWGN channel, $P_T/N_0 \approx 30.5dB$ is required to achieve $P_{e,II}^{AWGN} = 10^{-8}$; while $P_T/N_0 \approx 31dB$ is required to achieve a $P_{e,II}^{Ray} = 10^{-8}$. This implies that with $N = 16$, the detection error performance under the Rayleigh fading channel approaches that of the AWGN channel within $0.5dB$. Hence, as the number of measurements increases (i.e. number of nodes N), $P_e^{Ray} \rightarrow P_e^{AWGN}$ for both protocols.

2.9 Summary and Conclusions

In this chapter, the problem of distributed detection in a correlated wireless sensor network with relays deployment was analyzed and modeled. The detection error performance has been studied as a function of the number of sensor/relay nodes and the degree of correlation of measurements in a wireless sensor network with strict power constraint. Particularly, the performance study was analyzed via two transmission protocols, Protocol I where each sensor node conveys its local measurements directly to the fusion center; while in Protocol II, each sensor node is paired with a cooperative relay node to relay its measurements to the fusion center. Based on a simple two-node network, the detection performance for both protocols has been analyzed and the region over which Protocol II outperforms Protocol I has been determined.

The analysis was then extended to an arbitrary large network with N sensor/relay nodes. It was shown that with the increase in the correlation coefficient, the detection error performance of the network degrades; while, the decrease in the correlation coefficient, improves the detection error performance. This in turn demonstrated that having many correlated sensors increases redundancy at the fusion center but does not necessarily achieve the best detection error performance. In other words, having many highly correlated sensors does not necessarily result in the optimal detection error performance. However, by employing cooperative relay nodes, more reliable measurements are delivered to the fusion center which in turn results in a better detection error performance.

It was also shown that by cooperative relays deployment, measurements can be relayed reliably to the fusion center and thus significant detection error performance

gains can be achieved. Finally, it is concluded that with cooperative distributed detection and exploitation of spatial diversity, a smaller number of sensor/relay nodes is required to achieve the optimal detection error performance under strict network power constraint.

Chapter 3

Energy Efficiency of Cognitive Cooperative Distributed Detection

3.1 Overview

In Chapter 2, the amplify-and-forward cooperative relays deployment has been studied. It was shown that with cooperative detection, significant performance gains can be achieved as well as a reduction in the total number of sensor/relay nodes required for optimal detection performance. However, bandwidth utilization and energy efficiency are important factors of the overall wireless sensor network performance and thus must be analyzed and quantified. This in turn sheds light on the importance of exploiting the merits of the cooperative relays even further to efficiently utilize network bandwidth resources and also to achieve energy efficient distributed detection.

In this chapter, the binary hypothesis distributed detection problem in wireless sensor networks is revisited; however, with *cognitive-cooperative* relays deployment. In energy-constrained wireless sensor networks, the advantages of cooperation can be further exploited by cognitively utilizing wasted channel/time-slots among sensor nodes for optimal data gathering and detection with minimum energy requirements. As in Chapter 2, two transmission protocols are compared; Protocol I in which each

sensor node transmits its measurements directly to the fusion center while in Protocol II, cooperative relay nodes are deployed to cognitively sense empty/under-utilized time-slots and use them to amplify-and-forward (AF) measurements to the fusion center. This chapter also presents a simple example of a binary hypothesis testing distributed detection problem in a spatio-temporally correlated sensor network with two sensor nodes and a relay node to illustrate the merits of cognitive-cooperation. It is concluded that by employing cognitive-cooperative relays, improved transmission reliability, significant detection performance gains and energy savings can be achieved with no bandwidth losses.

3.2 Related Work

Energy efficiency in wireless sensor networks (WSNs) has been a topic of great interest in recent years. Such networks have particularly attracted much attention due to the low-cost low-power of the multi-functional sensor nodes; specially for military, medical and environmental applications [22]. With the introduction of cooperative diversity [15] and cognitive radio [36] for wireless communications, the cooperative and cognitive sharing of transmission channels via relay nodes could provide a significant promise for energy-efficient optimal detection performance.

There has been a plethora of research works in wireless sensor networks, ranging from signal processing techniques, routing, channel access control to energy efficient protocols. From the effect of correlation in wireless sensor networks viewpoint, the authors in [28] analyze the performance of the MAC layer by taking into account the spatio-temporally correlated phenomena when evaluating the distortion

level with minimum energy expenditure. In [37], energy efficient routing for signal detection under the Neyman-Pearson criterion has been considered. In particular, the authors proposed two different metrics to quantify the trade-off between detection performance and energy consumption; the first one aims at identifying a path which achieves the largest possible mean detection-probability-to-energy ratio while the second one reduces to finding a route which minimizes the consumed energy while maintaining a predetermined detection probability. A recent work in [38] considers the lifetime maximization problem in wireless cognitive radio sensor network in which sensor nodes sense the entire spectrum and locate the unutilized set of subcarriers for the transmission of information.

Recently, an interesting paper [39] proposed and analyzed the use of a cognitive-cooperative relay node in multiple-access wireless networks. The authors introduced cognitive communication protocols to utilize periods of silence (when users have no data to transmit) to enable cooperation. It was shown that no extra channel resources are allocated for cooperation (i.e. no bandwidth losses). Also, the analysis revealed that significant gains in terms of the stable throughput region and spectral efficiency are achieved via cognitive cooperation over conventional non-cooperative TDMA systems.

3.3 Motivation and Objectives

In current practical sensor networks, sensor nodes do not operate all the time and do not necessarily fully utilize all their time-slots but instead alternate between sleep/active modes [40]. In active mode, sensor nodes are fully operational, taking

measurements and conveying them to the fusion center; while in sleep mode, sensor nodes are idle. In other words, sensor nodes are configured to operate for a limited time and then be placed in a low-power sleep mode during idle periods [41]. Despite the fact that the sleep/active operation of sensor nodes is an energy-saving technique, it is an unnecessary waste of channel resources, specially within TDMA framework. This in turn suggests that in addition to the energy-saving sleep/active operation, the "empty" time-slots can be cognitively utilized by relay nodes to amplify-and-forward received measurements for optimal energy-efficient detection performance at the fusion center.

The motivation for the research work presented in this chapter is the fact that little research has focused on cognitively utilizing unused channel resources to improve detection performance in energy-constrained correlated wireless sensor networks. Therefore, this chapter addresses two main questions:

1. Can cognitive cooperation within slotted (orthogonal) time-division multiple access (TDMA) framework reduce energy requirements for optimal data detection, compared with conventional non-cooperative networks?

2. Is it better to send many measurements directly from sensor nodes; or can a fewer number of measurements be transmitted reliably with cognitive cooperating relay nodes achieve optimal detection performance with minimum energy requirements?

In the remainder of this chapter, the binary hypothesis testing problem is presented in Section 3.4. In Section 3.5, the spatio-temporal correlation model is pre-

sented; while the network model and operation are discussed in Section 3.6. In Section 3.7, the network transmission protocols are presented. The theoretical network detection error performance and energy calculations are derived in Sections 3.8 and 3.9, respectively. The network performance evaluation is presented in Section 3.10. Finally, conclusions are drawn in Section 3.11.

3.4 Binary Hypothesis Testing Problem

As in chapter 2, the gathering of the correlated spatial data $\mathbf{x}$ is modeled using the *Gaussian Random Field* model [30] which is given by the *N-dimensional* multivariate normal distribution

$$f(\mathbf{x}) = \frac{1}{(2\pi)^{N/2}|\Phi_N|^{1/2}} \exp\left(-\frac{1}{2}(\mathbf{x}-\mathbf{m})^H \Phi_N^{-1}(\mathbf{x}-\mathbf{m})\right), \tag{3.1}$$

where $\mathbf{m} \equiv E[\mathbf{x}]$ represents the means vector of the observations while $\Phi_N \triangleq E[(\mathbf{x}-\mathbf{m})(\mathbf{x}-\mathbf{m})^H]$ is the covariance matrix of $\mathbf{x}$; which is symmetric and positive-definite. The diagonal elements of Φ_N present the measurement noise variances of each sensor node $[\Phi_N]_{ii} = \sigma^2$. Moreover, the remaining coefficients in Φ_N (for $i \neq j$) are expressed as $[\Phi_N]_{i,j} = \sigma^2 \rho_{st}(i,j,\delta)$, where ρ_{st} represents the spatio-temporal correlation coefficient between sensor nodes S_i and S_j, and δ is a time-dependent factor (discussed in the following section).

The distributed detection problem is formulated similarly to chapter 2 as a binary hypothesis testing problem based on the two hypotheses, $\mathcal{H}_1$ and $\mathcal{H}_0$, where the measurements are represented as complex correlated Gaussian random variables and under each hypotheses are given by

$$\begin{aligned} \mathcal{H}_0 &: \mathbf{x} \sim \mathcal{CN}(0, \Phi_N) \\ \mathcal{H}_1 &: \mathbf{x} \sim \mathcal{CN}(\mathbf{m}, \Phi_N). \end{aligned} \tag{3.2}$$

3.5 Spatio-Temporal Correlation

Spatio-temporal correlation is an important feature of sensor observation and an important design factor that must be incorporated to realistically model sensor networks. This section presents the exponential spatio-temporal correlation model studied in this chapter [28].

3.5.1 Spatial Correlation

Spatially distributed sensor nodes collect spatially correlated measurements and the degree of correlation is medium-dependent and is also characterized by the inter-sensor-node spatial separation.

The spatial correlation is based on the covariance of the measured samples of sensors S_i and S_j, and can be expressed as [28]

$$cov\{x_i, x_j\} = \sigma^2 \rho_s(d_{s_{i,j}}), \tag{3.3}$$

where $\rho_s(d_{s_{i,j}}) = \exp(-d_{s_{i,j}}\lambda_s)$, $d_{s_{i,j}}$ is the spatial separation between sensors S_i and S_j. Furthermore, λ_s is a medium-dependent spatial correlation decay factor.

3.5.2 Temporal Correlation

This type of correlation particularly characterizes applications in which periodic/frequent measurements are taken and the degree of correlation is dependent on

the temporal variation of the phenomena as well as the frequency at which measurements are taken.

Sensor nodes sense the phenomena within a particular area with a sampling frequency of f_s (and a sample duration of $\tau_s = 1/f_s$) and then report it to the fusion center. The value of the sampled phenomena $x(t)$ from the Gaussian random field is defined as [28]

$$x[n] = x\left(t_o + \frac{n}{f_s}\right). \tag{3.4}$$

where t_o is the time at which the observation starts. Thus, the temporal correlation between discrete time measurements n and m are characterized according to

$$cov\{x[n], x[m]\} = \sigma^2 \rho_t(\delta), \tag{3.5}$$

where $\rho_t(\delta) = \exp(-|\delta|\lambda_t)$, λ_t is the temporal decay factor and $\delta = |m-n|/f_s$. The measurement taken by sensor S_i at time t_n is correlated with the measurement taken by sensor S_j at time t_m defines the spatio-temporal correlation and is expressed as

$$cov\{x_i[n], x_j[m]\} = \sigma^2 \rho_{st}(i, j, \delta) = \sigma^2 \rho_s(d_{s_{i,j}})\rho_t(\delta). \tag{3.6}$$

By specifying the internode separation and the sampling frequency, the spatio-temporal correlation of the measured and transmitted samples can be characterized.

3.6 Network Model and Operation

A wireless sensor network with N sensor nodes belonging to the set $\mathcal{S}$ are used to sense a particular phenomenon and their observations are then communicated to the fusion center for detection and decision-making. In this work, dumb sensor

nodes are assumed (i.e. they do not perform any local decisions due to their limited capabilities). In addition, M relay nodes belonging to the set $\mathcal{R}$ are deployed between the sensor nodes and the fusion center to allow for cognitive cooperation within a wireless network area $\mathcal{A}$.

In this model, it is assumed that the sensors, relays and the fusion center are stationary and each subset of sensor nodes is "possibly" assigned a subset of the cooperating relay nodes, depending on the transmission protocols used. This can be done through information exchange during the initial network setup phase. In addition, the network has a total power constraint of P_T distributed amongst the set of sensor nodes with power $P_{\mathcal{S}}$ while the relay nodes have a total power of $P_{\mathcal{R}}$.

Orthogonal TDMA transmission channels are assumed between the sensors and the fusion center with a TDMA frame of duration T_s. This model ensures no interference to the sensor node to which the channel is currently assigned. In addition, pairwise synchronization among sensor/relay nodes and between each sensor/relay node and the fusion center is assumed. Also, the transmission of all the sensor nodes is assumed to be half-duplex (i.e. a sensor/relay node cannot transmit and receive simultaneously). Furthermore, an analog transmission/modulation system is assumed where observations transmitted from sensor nodes and combined at the fusion center to produce a decision about the observed phenomena. The samples are generated by each sensor node at a given sampling rate f_s (during active period) and then are conveyed to the fusion center either through direct transmission or with possibly the help of cooperating relay nodes as will be discussed in the following section.

In practical wireless sensor networks, the sleep/active cycles are highly depen-

dent on the presence and/or the changes in a particular phenomenon within the sensor network area. Thus, in order to be able to model the sleep/active modes of the sensor nodes and thus the time-slots utilization, the TDMA frame structure of the model under consideration can be described as follows. Assume that each sensor node is assigned a time-slot of duration $\Delta t_s = T_s/N$. Each sensor *always* utilizes the first half of its time slots for the transmission of measurements. However, in the second half of the time-slot, each sensor decides whether it should take more measurements and access its channel to transmit them with probability p_i or whether it should go to sleep with probability $(1-p_i)$. In particular, let B_i be a Bernoulli random variable (i.i.d for $i = 1, \ldots, N$) with $P(B_i = 1) = p_i$ and $P(B_i = 0) = 1 - p_i$ where $0 \leq p_i \leq 1$ for $\forall i \in \{1, \ldots, N\}$. Then, B_i defines the event that sensor node S_i decides whether it should utilize all its assigned time-slot or only the first half of it and then go to sleep mode in the second half (sleep/active operation). That is, the sensing operation of each sensor node in the second-half of its time-slot is modeled as a bernoulli trial with probability p_i that is dependent on the presence/changes in the phenomenon. This can also be thought of as the probability with which sensor node S_i *accesses* its transmission channel to transmit measurements in the second half of its assigned time-slot (i.e. channel access probability).

It should be noted that the total number of samples transmitted during a complete time slot is given by $N_s = \lfloor \Delta t_s f_s \rfloor$. Furthermore, each time-slot is assumed to be longer in duration than the sampling time (i.e. $\Delta t_s > T_{samp}$) where $T_{samp} = N_s \tau_s$ and τ_s is the sample duration. The TDMA frame structure is illustrated in Fig. 3.1; where the shaded section represents the first half of each time-slot used for the trans-

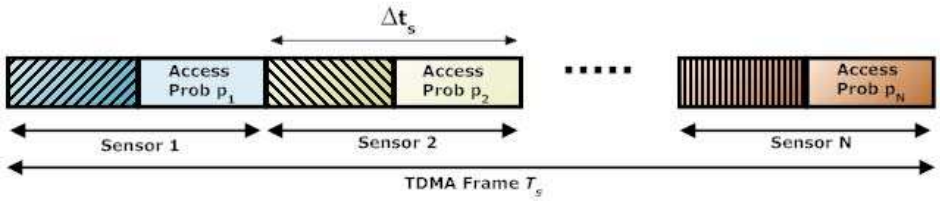

Figure 3.1: TDMA Frame Structure of the Proposed Network Operation

mission of samples while the unshaded section corresponds to the second-half of the time-slot in which each sensor decides to utilize with probability p_i.

It is assumed that the wake-up transient time and the residual time after each transmission/reception are negligible compared to the time duration spent in sampling and transmission.

3.7 Network Protocols

3.7.1 Protocol I - Direct Transmission

In this protocol, no relay deployment is assumed and that each sensor node directly transmits its observations x_i to the fusion center with uncoded analog transmission. The received signal at the fusion center from sensor S_i is expressed as

$$y_{s_i,f}(t) = \sqrt{P_{s_i} d_{s_i,f}^{-\alpha}} h_{s_i,f}(t) x_i(t) + n_{s_i,f}(t), \tag{3.7}$$

where $d_{s_i,f}$ is the distance between sensor S_i and fusion center (α is the path-loss exponent); while $h_{s_i,f}(t)$ is the channel coefficient from sensor S_i to the fusion center and is modeled as zero-mean complex Gaussian random variable with variance $1/2$ per dimension. In addition, P_{s_i} is the transmission power assigned to sensor S_i for $i \in \{1, 2, \ldots, N\}$ and is selected to satisfy a power constraint P at the sensor node and also a total network power constraint P_T. Furthermore, $n_{s_i,f}(t)$ is the additive

white Gaussian noise at the fusion center, modeled as zero-mean circularly symmetric Gaussian random variable with variance $N_o/2$ per dimension. Protocol I operates according to the following rules:

- Sensor node S_i transmits $N_s/2$ samples during the first-half of its assigned time-slot.
- If the sensor node decides to neither take more measurements nor transmit them during the second half of its the time-slot (and thus does not access its channel) – determined by probability $(1 - p_i)$ – it remains idle (sleeps); otherwise, it accesses its channel to transmit more measurements with probability p_i.

It should be noted that under Protocol I, the total power allocated to the set of sensor nodes is $P_{\mathcal{S}} = P_T$, since no relay nodes are deployed in this case.

3.7.2 Protocol II - Cognitive Cooperative Transmission

In Protocol II, a number of sensor nodes are paired with known neighboring cognitive cooperative Amplify-and-Forward (AF) relay node(s) R_k, located at $d_{r_k,f}$ from the fusion center for $k \in \{1, \ldots, M\}$. In the AF relaying, signal transmissions are separated into two phases through orthogonal channels by using TDMA [15]. In Phase 1, sensor node S_i transmits its observation x_i with power P_{s_i} where the received signals at the fusion center $y_{s_i,f}(t)$ and at the relay node $y_{s_i,r_k}(t)$ are

$$y_{s_i,f}(t) = \sqrt{P_{s_i} d_{s_i,f}^{-\alpha}} h_{s_i,f}(t) x_i(t) + n_{s_i,f}(t), \tag{3.8}$$

and

$$y_{s_i,r_k}(t) = \sqrt{P_{s_i} d_{s_i,r_k}^{-\alpha}} h_{s_i,r_k}(t) x_i(t) + n_{s_i,r_k}(t), \tag{3.9}$$

respectively; where $h_{s_i,f}(t)$ and $h_{s_i,r_k}(t)$ are the fading channel coefficients from sensor S_i to the fusion center and to the R_k relay node, respectively; whereas, $d_{s_i,f}$ and d_{s_i,r_k} are the distances from S_i to the fusion center and to R_k relay node, respectively and $n_{s_i,f}(t)$ and $n_{s_i,r_k}(t)$ are the white Gaussian noise. In Phase 2, the relay node amplifies-and-forwards the received signal to the destination with transmit power P_{r_k}. The received signal at the fusion center can be written as

$$\begin{aligned} y_{r_k,f}(t) &= \sqrt{\tilde{P_{r_k}} d_{r_k,f}^{-\alpha}} h_{r_k,f}(t) y_{s_i,r_k}(t) + n_{r_k,f}(t) \\ &= \sqrt{\tilde{P_{r_k}} P_{s_i} d_{s_i,r_k}^{-\alpha} d_{r_k,f}^{-\alpha}} h_{r_k,f}(t) h_{s_i,r_k}(t) x_i(t) + \tilde{n}_{r_k,f}(t), \end{aligned} \tag{3.10}$$

where $\tilde{n}_{r_k,f}(t) = \sqrt{\tilde{P_{r_k}} d_{r_k,f}^{-\alpha}} h_{r_k,f}(t) n_{s_i,r_k}(t) + n_{r_k,f}(t)$. In addition, $\tilde{P_{r_k}}$ represents the normalized transmit power and is chosen to ensure a transmit power at the relay node of P_{r_k} and thus is specified as $\tilde{P_{r_k}} = P_{r_k}/(P_{s_i} d_{s_i,r_k}^{-\alpha} |h_{s_i,r_k}(t)|^2 \sigma^2 + N_o)$. Furthermore, $h_{r_k,f}(t)$ is the channel coefficient between the k^{th} relay node and the fusion center and $n_{r_k,f}(t)$ is the additive Gaussian noise. It should be noted that the noise $n_{s_i,f}(t)$, $n_{s_i,r_k}(t)$ and $n_{r_k,f}(t)$ are modeled as independent complex Gaussian random variables. Protocol II operates according to the following rules:

- Sensor node S_i transmits $N_s/2$ samples during the first-half of its assigned time-slot.
- The cooperating relay node R_k listens to the transmitted samples and stores all the received samples in its queue.
- If the sensor node decides to neither take more measurements nor transmit them during the second half of its the time-slot – determined by probability $(1 - p_i)$

– the relay node cognitively senses that the second half of the sensor node's time-slot is empty and amplifies-and forwards *all* the samples in its queue.

- If the sensor node accesses its channel in the second half of its time-slot to transmit more measurements (with probability p_i), the relay node empties its queue and then remains idle.

Under Protocol II, the total network power constraint P_T is shared by the set of sensor and relay nodes (i.e. $P_T = P_{\mathcal{S}} + P_{\mathcal{R}}$); where $P_{\mathcal{R}}$ is the total power assigned to the relay nodes.

3.8 Probability of Detection Error Performance

Given the foregoing hypothesis testing problem formulation and sensor network operation, the theoretical analysis of the wireless sensor network performance is presented in terms of the probability of detection error P_e. As in Chapter 2, the optimal likelihood decision rule is is based on the assumption of equal prior probabilities under each hypothesis (i.e. $\pi_0 = \pi_1 = 1/2$). Also, the power P_{s_i} at each sensor node S_i is selected such that the average power of each sensor node equals a power constraint P [35]. Therefore, $P = \pi_0 P_{s_i}\sigma^2 + \pi_1 P_{s_i}(m^2 + \sigma^2)$ and thus the sensor transmission power is written as $P_{s_i} = P/(\sigma^2 + \frac{1}{2}m^2)$.

As in Section 2.5, the probability of detection error can be easily shown to be

$$P_e = E\left\{Q\left(\frac{1}{2}\sqrt{\mu_N^H \Sigma_N^{-1} \mu_N}\right)\right\}, \tag{3.11}$$

where $Q(u) \triangleq \frac{1}{\sqrt{2\pi}}\int_u^\infty \exp\left(-\frac{z^2}{2}\right) dz$ is the Gaussian Q-function and the expectation is taken with respect to the channel statistics.

3.9 Energy Calculation

This section presents a simple energy consumption calculation per transmitted sample in each time-slot for a target probability of detection error $\bar{P}_e$ for the transmission protocols under consideration. It is assumed that the receiving energy consumption of the fusion center is not taken into account since the main concern here is the energy consumed by the sensor/relay nodes. For simplicity, the energy calculation neglects the link budget relationship.

3.9.1 Energy Calculation for Protocol I

Under Protocol I, the total energy per transmitted sample per sensor node S_i in each time-slot must take into account the circuit energy consumption as well as the energy per transmitted sample to achieve a target probability of detection error $\bar{P}_e$. Here, two possibilities must be considered, when $B_i = 1$ and when $B_i = 0$. First, when $B_i = 1$, the sensor node S_i utilizes all its assigned time-slot, thus the *conditional* total energy per sample is given by

$$E^1_{Total} = E^1_{S_i,c} + E^1_{S_i,t}, \tag{3.12}$$

where $E^1_{S_i,c} = (\Delta t_s/N_s) \times P_{ct}$ and $E^1_{S_i,t} = (\Delta t_s/N_s) \times \bar{P}_{s_i}$ are the transmitting circuit energy consumption per sample and the transmission energy per sample of sensor S_i for the whole time-slot, respectively. Also, P_{ct} is the circuit power in the state of transmitting and $\bar{P}_{s_i}$ is the sensor transmission power to achieve $\bar{P}_e$. Hence, the conditional total energy per sample is expressed as

$$E^1_{Total} = \frac{\Delta t_s}{N_s}\left(P_{ct} + \bar{P}_{s_i}\right). \tag{3.13}$$

For the case when $B_i = 0$, the sensor node utilizes only the first half of its time-slot and is sleeping (idle) in the second half. Thus, the conditional total energy per sample in this case

$$E^0_{Total} = E^0_{S_i,c} + E^0_{S_i,t} + E^0_{S_{idle},c}, \tag{3.14}$$

where $E^0_{S_i,c} = (\Delta t_s/2N_s) \times P_{ct}$ and $E^0_{S_i,t} = (\Delta t_s/2N_s) \times \bar{P}_{s_i}$ is the transmitting circuit energy consumption per sample and the transmission energy per sample of sensor S_i for the half of time-slot duration, respectively. Furthermore, $E^0_{S_{idle,c}} = (\Delta t_s/2N_s) \times P_{ci}$ is the circuit energy for idle sensor for half of the time-slot duration and P_{ci} is the circuit power in state of idle [42]. Therefore, in this case the conditional total energy can be written as

$$E^0_{Total} = \frac{\Delta t_s}{2N_s} \left(P_{ct} + P_{ci} + \bar{P}_{s_i} \right). \tag{3.15}$$

The general expression for the *conditional* total energy consumption per transmitted samples conditioned on B_i can be written as

$$\tilde{E}^I_{Total} = \frac{\Delta t_s}{N_s} \left(P_{ct} + \bar{P}_{s_i} - (1 - B_i) \left(\frac{P_{ct} + \bar{P}_{s_i} - P_{ci}}{2} \right) \right). \tag{3.16}$$

Therefore, the *average* energy per transmitted sample is given by

$$E^I_{Total} = \frac{\Delta t_s}{N_s} \left(P_{ct} + \bar{P}_{s_i} - (1 - p_i) \left(\frac{P_{ct} + \bar{P}_{s_i} - P_{ci}}{2} \right) \right). \tag{3.17}$$

3.9.2 Energy Calculation for Protocol II

As before, two cases must be considered, i.e. when $B_i = 1$ and when $B_i = 0$. First, when $B_i = 1$, the R_k relay node cannot help because the sensor node S_i utilizes all its time-slot. The important observation under this protocol is that the relay node consumes energy when receiving samples from the pairing sensor node during the first-half of the time-slot. However, after sensing the occupied second-half of the time-slot,

the relay drops the samples in its queue and goes to sleep (idle). For simplicity, it is assumed that the circuit consumption power for transmitting, receiving and idle states for relay nodes are assumed to be identical to sensor nodes. It is straightforward to show that the total conditional energy consumption per sample to be

$$E^1_{Total} = E^1_{S_i,c} + E^1_{S_i,t} + E^1_{R_k,c} + E^1_{R_k,sensing}, \tag{3.18}$$

where $E^1_{R_k,c} = (\Delta t_s/2N_s) \times P_{cr}$ is the energy consumed by the R_k relay's circuit on reception, while $(E^1_{R_k,sensing} = P_{sns} \times t_{sns})$ is the energy spent by the relay for sensing the channel, P_{sns} and t_{sns} are the power and time spent in sensing the channel (such that $t_{sns} \ll \Delta t_s$ and $t_{sns} < \tau_s$), respectively. Thus, the total conditional energy in this case is given by

$$E^1_{Total} = (\Delta t_s/N_s)\left(P_{ct} + \bar{P}_{s_i}\right) + (\Delta t_s/2N_s)\left(P_{cr} + P_{ci}\right) + P_{sns}t_{sns}. \tag{3.19}$$

Now, when $B_i = 0$, the relay node is employed during the second half of the time-slot for transmission (assuming it can sense and transmit with negligible delay) and the consumed conditional energy per sample is given by

$$E^0_{Total} = \frac{\Delta t_s}{2N_s}\left(P_{ct} + P_{cr} + P_{ci} + \bar{P}_{s_i} + \bar{P}_{r_k}\right) + P_{sns}t_{sns}, \tag{3.20}$$

where $\bar{P}_{r_k}$ is the power assigned for the relay node to achieve $\bar{P}_e$. The general expression of the average energy consumption can be easily written as

$$E^{II}_{Total} = \frac{\Delta t_s}{N_s}\left(P_{ct} + \bar{P}_{s_i} + \frac{P_{cr} + P_{ci}}{2} + (1 - p_i)\left(\frac{\bar{P}_{r_k} - (P_{ct} + \bar{P}_{s_i})}{2}\right)\right) + P_{sns}t_{sns}. \tag{3.21}$$

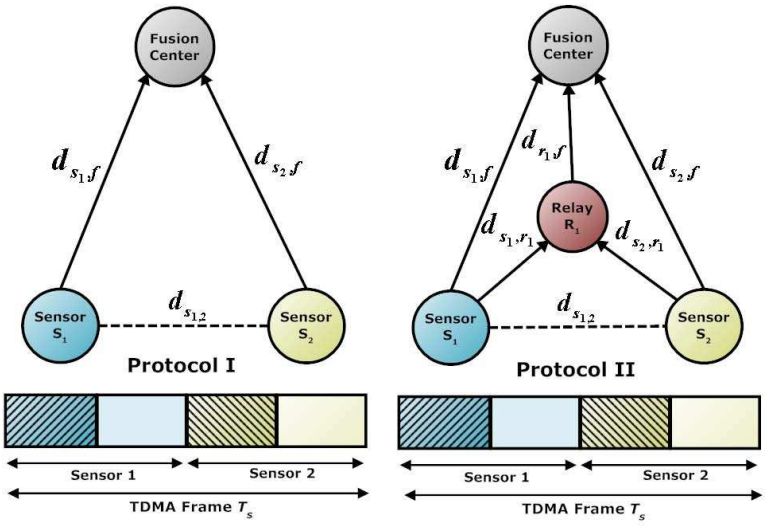

Figure 3.2: Wireless Sensor Network Under Protocols I and II

3.10 Performance Evaluation of Network Protocols

3.10.1 Description

In this section, a simple $N = 2$ sensor nodes wireless network example is presented. For convenience, the direct transmission Protocol I is denoted by P-I; while the cognitive cooperative Protocol II is denoted by P-II. The simple two sensor nodes networks under P-I and P-II (with $M = 1$ relay node) are illustrated in Fig. 3.2.

The aim is to study the trade-off between reliability/redudency of samples as a function of the probability of detection error P_e and energy requirements. Therefore, the performance of protocols P-I and P-II will be evaluated to show the effect of different channel access probability p_i on the detection performance. Also, the performance will be evaluated as a function of the sampling frequency f_s in order to analyze the effect of increasing the number of transmitted samples on the detection performance and energy requirements.

To allow a fair comparison between the transmission protocols and for simplicity, the total wireless sensor network power constraint P_T in each time-slot under P-I is equally distributed amongst the two sensor nodes S_1 and S_2 (i.e. $P_T = P_{\mathcal{S}}$) such that the individual sensor power constraint is satisfied (that is, $P = P_T/2$). Therefore, under P-I, $P_{s_1} = P_{s_2}$. Similarly, under P-II (since $P_T = P_{\mathcal{S}} + P_{\mathcal{R}}$), the relay node R_1 is also assumed to be assigned a power equal to that of each of the sensor nodes. Therefore, in the first time-slot (Sensor S_1) $P_{s_1} = P_{r_1} = P_T/2$; while in the second time-slot (Sensor S_2) $P_{s_2} = P_{r_1} = P_T/2$. This ensures fairness under both transmission protocols in any time-slot and that the total network power P_T is equally distributed amongst the sensor/relay nodes. For a network with arbitrary N sensors and M relays, a power allocation scheme and coordination between sensor/relay nodes is required (beyond the scope of this work).

Without loss of generality and for simplicity, it is assumed that both sensors have equal probability of accessing their second half of each time slot (i.e. $p_1 = p_2 = p$). Moreover, it is assumed that $m_1 = m_2 = m$ in the means vector $\mathbf{m}$ of the measured data. That is, under $\mathcal{H}_1$, both sensor nodes measure the same phenomenon with the same *real* mean within network area $\mathcal{A}$.

To properly model the effect of time-variation on the network performance, the channel fading coefficients should evolve with time from one sample to another. Thus, a flat slow time-varying Rayleigh fading channel is assumed where the channel coefficients are generated according to Jakes Model [43] with a maximum Doppler frequency of $f_m = 1Hz$. Moreover, the transmission channels between the sensors/relays and the fusion center are assumed to be independent and identically distributed.

The simulation parameters[1] are summarized in Table 1.

Parameters	Specifications
Distance From Sensors S_1 and S_2 to Fusion Center	$d_{s_1,f} = d_{s_2,f} = 2$
Distance From Sensors S_1 and S_2 to Relay R_1	$d_{s_1,r_1} = d_{s_2,r_1} = 1.6$
Distance From Relay R_1 to Fusion Center	$d_{r_1,f} = 1$
Inter-sensor Separation	$d_{s_{1,2}} = 2$
Spatial Correlation Decay Factor	$\lambda_s = 0.8$
Temporal Correlation Decay Factor	$\lambda_t = 0.1$
Mean of Measurements	$m = 1$
Measurement Noise Variance	$\sigma^2 = 0.05$
TDMA Frame Duration	$T_s = 5$ ms
Time-slot Duration Assigned to Each Sensor	$\Delta t_s = 2.5$ ms
Carrier Frequency	$f_c = 2.5$ GHz
Channel Bandwidth	$B = 10$ KHz
Channel Model	Rayleigh (Jakes Model)
Circuit Power - Transmission State	$P_{ct} = 30.7mW$
Circuit Power - Receiving State	$P_{cr} = 35.3mW$
Circuit Power - Idle State	$P_{ci} = 712\mu W$
Circuit Power - Sensing	$P_{sns} = 25mW$
Sensing Duration	$t_{sns} = 5\mu s$

Table 3.1: Simulation Parameters

3.10.2 Discussion of Results

In Fig. 3.3, the performance of P-I and P-II is compared as a function of the access probability p (or time-slot utilization) for a sampling frequency of $f_s = 4096Hz$. It is clear that under P-I, the increase in the access probability p, results in an improvement in the probability of detection error P_e. This is due to the fact that as each sensor node more often utilizes all its time-slot, more samples are transmitted and thus the fusion center receives more samples for detection. On the other hand, for P-II, it is evident that as the probability of channel access decreases, the performance

[1]Refer to data sheet of CC2420 [44], for circuit power values (compliant to IEEE802.15.4 standard).

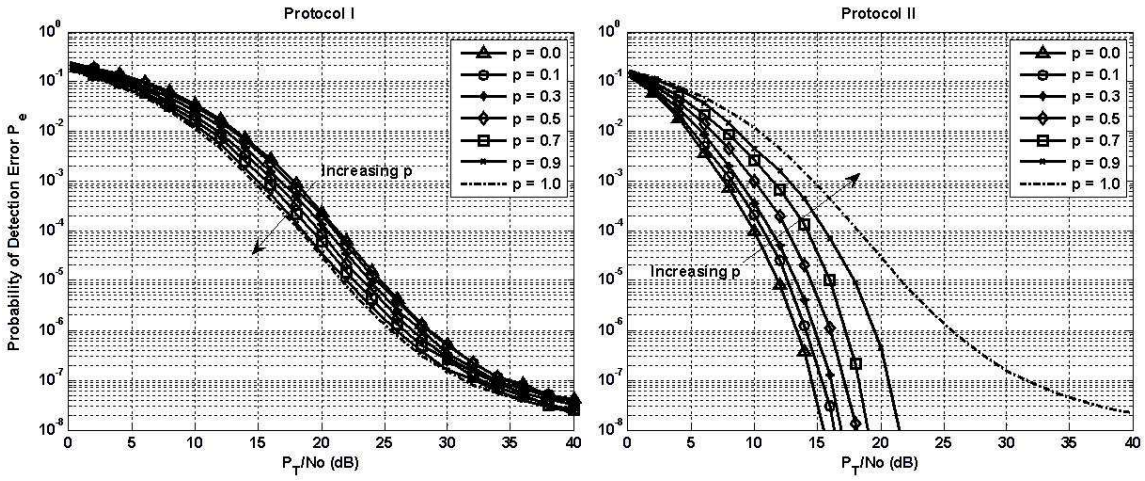

Figure 3.3: Detection Error Performance of Protocols I and II - $f_s = 4096$ Hz

improves and this is obvious since the relay has more chance to utilize the channel to amplify-and-forward the received samples. It should also be clear to see that the P_e for both protocols is *equal* when $p = 1.0$ (dotted-curves); since in this case, both sensors utilize all their time-slots under P-I and the relay node does not get to cooperate with any sensor node under P-II. It can also be seen that P-II does not suffer from any error floor when the relay node cooperates. In addition the performance of P-II has a significantly better detection performance than P-I for channel access probabilities ($0 \leq p < 1$). In this case, the best performance for P-II is achieved when $p = 0$ since in this case the sensor never utilizes the second-half of its time-slot which means that the relay node always helps in relaying measurements to the fusion center.

In Fig. 3.4, the performance of the protocols is compared as a function of the sampling frequency f_s when $p = 0.7$. It is evident that with the increase in the sampling frequency, better performance is achieved under both protocols. This is expected since the higher the sampling frequency the more samples are transmitted to the fusion center which is reflected in a significantly improved detection performance.

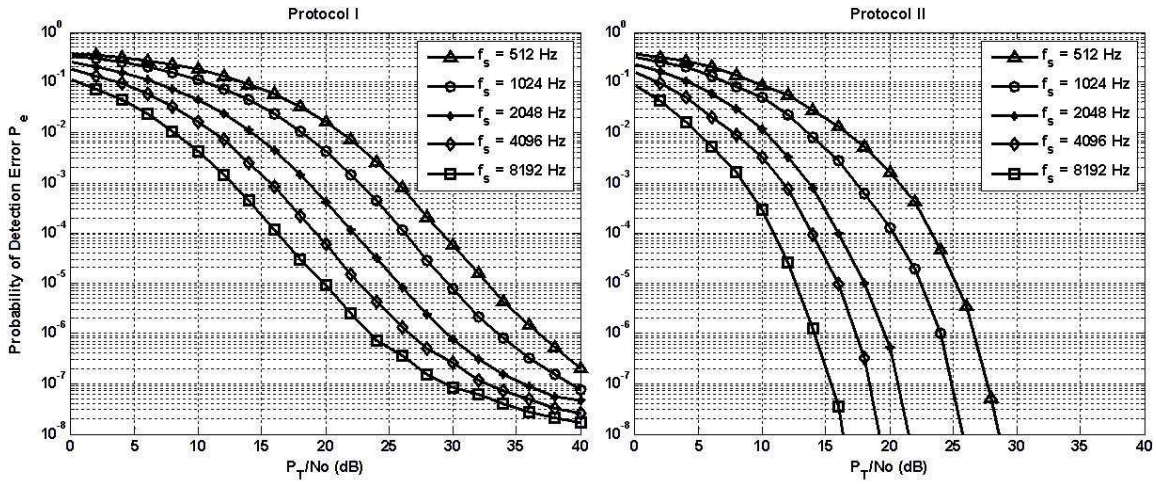

Figure 3.4: Detection Error Performance of Protocols I and II - $p = 0.7$

Moreover, under P-II, the detection performance at $P_e = 10^{-6}$ with $f_s = 2048Hz$ outperforms that of P-I for all the sampling frequencies.

The energy per sample for a target probability of detection error $\bar{P}_e = 10^{-4}$ as a function of channel access probability for $f_s = 4096Hz$ is illustrated in Fig. 3.5. It can be seen that as the probability of access increases, the energy consumption per sample for P-I decreases. This is easily interpreted by the fact that as p increases, more samples are transmitted and thus better performance is achieved. Despite the fact that more energy is required for increasing p, the gain in the detection performance show that less power (and hence less energy) is required to achieve the target $\bar{P}_e$. For P-II, it is evident that with the increase in p, more energy is required. The explanation is intuitive since the relay helps less and thus less reliable samples are received by the fusion. This in turn implies that higher transmission power (and thus more energy) is required by the transmitting sensor nodes in order to achieve the target probability of detection error.

It is also noticed in Fig. 3.5 that when $p = 1$, the energy for P-II is slightly

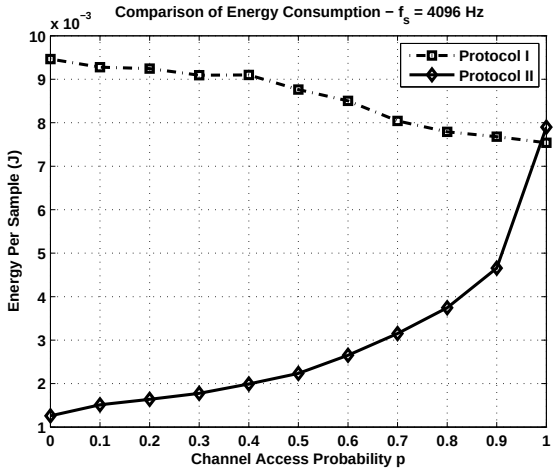

Figure 3.5: Energy Comparison for Protocols I and II for $\bar{P}_e = 10^{-4}$ - $f_s = 4096$ Hz

higher that of P-I despite the fact that both result in the same $\bar{P}_e$ (see Fig. 3.3 - dotted curves). This is due to the fact that some energy is spent in sensing the channel as well as the relay node's circuitry spent in receiving samples from the sensor nodes and also in being idle. In general, P-II is significantly more energy-efficient than P-I for channel access probabilities ($0 \leq p < 1$).

On the other hand, Fig. 3.6 illustrates the energy consumption per transmitted sample as a function of the sampling frequency for P-I and P-II. It is clear that P-II is significantly more energy-efficient than P-I. The performance gain achieved with the larger number of samples transmitted is reflected into a reduction in the energy per sample required to achieve the target $\bar{P}_e$. Furthermore, the energy consumption per sample for P-II with $f_s = 512Hz$ (and $f_s = 1024Hz$) is almost equal to the energy requirement of P-I with $f_s = 1024Hz$ (and $f_s = 2048Hz$). This implies that with cooperative cooperation, a reduced number of transmitted samples is required to achieve the target probability of detection error compared with case of non-cooperative transmission.

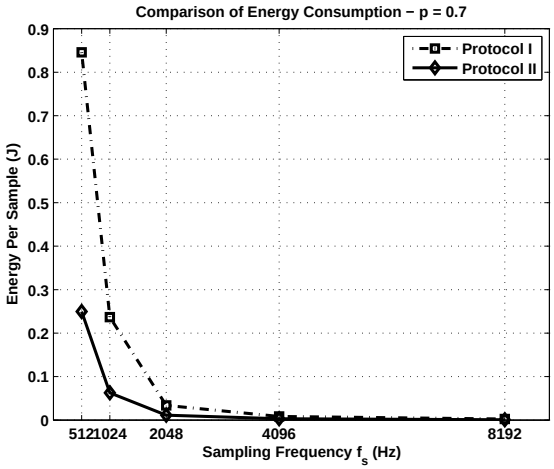

Figure 3.6: Energy Comparison for Protocols I and II for $\bar{P}_e = 10^{-4}$ - $p = 0.7$

3.11 Conclusions

In this chapter, energy-efficiency through cognitive-cooperative communication for distributed detection in correlated wireless sensor network has been modeled and analyzed. In particular, it was shown that by deploying cognitive-cooperative relay nodes, the empty time-slots not utilized by their sensor nodes are exploited. It was illustrated via a a simple two-node sensor network with a single relay, that significant detection performance gains are achievable as well as energy efficiency in transmitted measurements without any bandwidth losses. It was concluded that it is better to transmit less number of samples *reliably* via cooperation than to transmit a larger number of samples without cooperation. Finally, utilizing empty time-slots by cognitive relays deployment directly improves the network detection error performance and also achieves energy-efficiency.

Chapter 4

Many-to-Many Communications via Space-Time Network Coding

4.1 Overview

So far, the work presented in Chapters 2 and 3 has been mainly focused on cooperative distributed detection in wireless sensor networks under the classical source-relay-destination scenario, where a source "sensor node" communicates with a destination "fusion center" through an amplify-and-forward relay for an improved energy-efficient detection performance. However, the potentials of cooperative communications can be further leveraged to allow simultaneous cooperative transmissions from multiple nodes acting as sources, relays and destinations in an alternating fashion.

In this chapter, the mutual cooperative communication between multiple Decode-and-Forward (DF) nodes in a wireless network is efficiently achieved through the utilization of the novel concept of Space-Time Network Coding (STNC). Unlike the conventional point-to-point multinode cooperative communications between two nodes with N relay nodes deployed in between, simultaneous transmissions from the different N nodes acting as source/relay nodes are performed within $2N$ time-slots and achieving a full-diversity order of $(N-1)$ per node. In particular, the communication is split into two phases: 1) Broadcasting Phase and 2) Cooperation Phase. In the

Broadcasting Phase, each node broadcasts its data symbol to the other nodes in the network in its own time-slot, alternatively; while in the Cooperation Phase, in each time-slot, a set of $(N-1)$ nodes transmit while a single destination node receives the other nodes' transmissions. Specifically, in each time-slot, each node performs a linear combination of the other nodes' data symbols and a set of $(N-1)$ nodes simultaneously transmit their signals to a single receiving node; which then performs joint multiuser detection to separate the different nodes' symbols. Exact symbol-error-rate (SER) expressions for arbitrary order M-ary Phase Shift Keying (M-PSK) modulation are derived. In addition, an asymptotic SER approximation is also provided which is shown to be tight at high signal-to-noise ratio (SNR) and the analytical results confirm that for a network of N nodes, a full diversity order of $(N-1)$ per node is achieved by the proposed STNC communication scheme. Finally, a theoretical SER performance analysis of the timing synchronization errors is also provided as a wireless network design guideline for an arbitrary number N of cooperating nodes employing the STNC scheme.

4.2 Introduction

In conventional relay networks, a set of N relay nodes are deployed between the source and destination nodes and the available network bandwidth is split into $N+1$ orthogonal channels using TDMA. However, with the increase in the number of relay nodes, the traditional multinode relay networks become excessively bandwidth inefficient. Moreover, the traditional cooperative communication protocols are not well suited for distributing information from one or more source nodes to possibly many

destination nodes, simultaneously. However, *Network Coding* has recently emerged as an effective approach for efficiently distributing data across multiple nodes and increasing network throughput [45] [46]. This in turn sheds light on the importance of exploiting of the concept of wireless network coding for exchanging data symbols among multiple cooperative nodes over wireless networks.

Recently, there have been several research works that aim at employing wireless network coding in cooperative relay networks. In [47], location-aware cooperative wireless network coding through the novel concept of Wireless Network Cocast (WNC) was proposed. In particular, the authors illustrated that with WNC, a reduction in aggregate transmission power and delay can be achieved along with incremental diversity, for different relaying schemes. In [48], an algebraic superposition of channel codes over a finite field is proposed to allow two nodes to cooperate in transmitting information to a single destination. Bi-directional relaying between two source nodes through a single relay node employing wireless network coding has been introduced in [49]. An outage analysis of network coded communication of multiple users with a single destination node through a set of *dedicated* relay nodes has been analyzed in [50]. In [51], complex field network coding (CFNC) is employed which was shown to achieve full diversity gain and a throughput as high as 1/2 symbol per user per channel use. However, the authors considered the communication between N_S users and a *common* destination through a single relay as well as N_R relay nodes but not for multiple sources between each other. Moreover, a relatively high complexity Maximum-Likelihood (ML) multiuser demodulation was required to separate the different users' data.

In this chapter, the merits of Network Coding and Cooperative Diversity are exploited to allow N nodes "users" to exchange data between each other with the novel concept of *Space-Time Network Coding* (STNC). In this work, the Decode-and-Forward (DF) relaying protocol [15] is studied within the concept of STNC. In particular, the STNC cooperative scheme is based on linear wireless network coding over Decode-and-Forward (DF) nodes and the communication is split into two phases: 1) Broadcasting Phase and 2) Cooperation Phase. In the former phase, each node broadcasts its data to the other nodes, in its dedicated time slot; while in the latter phase, a single node receives simultaneous transmissions from the other $N-1$ nodes of linearly-coded symbols of previously received data symbols. A *simple* multiuser detection [52] is then applied at each node to separate the different data symbols received from the different nodes. It is illustrated that with the STNC scheme, N information symbols of all the N nodes can be exchanged over a total of $2N$ time-slots (i.e. $1/2$ symbol per node per channel use) as well as achieving a *full diversity* order of $(N-1)$ per node.

Exact analytical derivations of the symbol error rate (SER) performance of the STNC scheme and comparative simulation results are provided in this chapter. Moreover, tight asymptotic approximations at high signal-to-noise ratio are also derived and the cooperative diversity order achievable with the STNC scheme is verified. The exact theoretical SER performance under timing synchronization errors is also derived for $N = 3$ nodes while a lower-bound SER performance is provided for $N \geqslant 4$ nodes.

In the remainder of this chapter, the system model and communication phases are presented in Section 4.3. The multi-source signal detection and the exact SER

analysis are presented in Sections 4.4 and 4.5, respectively. In Section 4.6, the asymptotic upper-bound SER expression is derived. In Section 4.7, the synchronization analysis for the STNC scheme, along with the theoretical exact and lower-bound derivations are provided. The SER performance evaluation under both perfect and imperfect timing synchronization is presented in Section 4.8. Finally, the conclusions are drawn in Section 4.9.

4.3 System Model

Consider a wireless network consisting of N nodes ($N \geq 3$) denoted as S_1, S_2, ..., S_N. In this model, each node is equipped with only one antenna and can act as a source as well as a destination. Without loss of generality, the Decode-and-Forward (DF) cooperation protocol is considered. The N nodes are assumed to have own information symbols as $x_1, x_2, \ldots, x_N$, respectively.

The communication between all the source nodes is split into two main phases, namely the Broadcasting Phase (BP) and the Cooperation Phase (CP), over a total of $2N$ time-slots, N time-slots each. During the Broadcasting Phase, source node S_j is assigned a time-slot T_j in which it broadcasts its own data symbol to the other nodes S_i for $i \in \{1, 2, \ldots, N\}$ for $i \neq j$. That is, the Broadcasting Phase is an information exchange phase, which upon completion, each node S_i will have received a set of $(N-1)$ symbols $x_1, \ldots, x_j, \ldots, x_N$ for $j \neq i$ from the other nodes. With respect to the Cooperation Phase, each node acts as a relay for the other nodes with one node being the destination in each time-slot. In particular, each node, except a single receiving node, forms a linearly-coded signal from the overhead symbols and transmits it to the

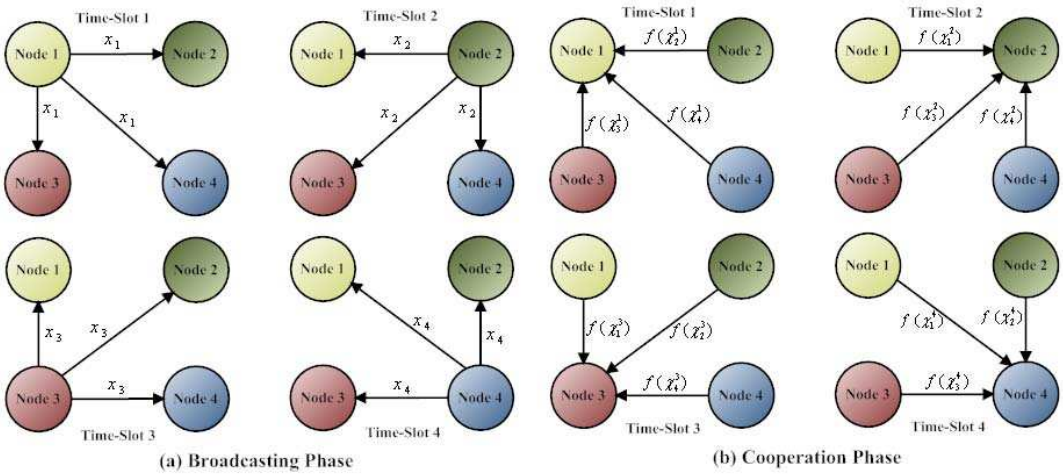

Figure 4.1: Space-Time Network Coding Scheme - Broadcasting and Cooperation Phases - $N = 4$ Nodes

that receiving node which upon receiving the $(N-1)$ linearly-coded signals, performs a multi-source signal separation to extract the desired symbol from each node. To allow for joint detection/source separation for each of the linearly-coded transmitted symbols of the different nodes at each receiving node, each symbol x_j is spread using a signature waveform $s_j(t)$. The cross-correlation between waveforms $s_j(t)$ and $s_i(t)$ over a symbol duration T_s is given by $p_{j,i} = \langle s_j(t), s_i(t) \rangle \triangleq (1/T_s) \int_0^{T_s} s_j(t) s_i^*(t) dt$, where it is assumed that $p_{j,j} = ||s_j(t)||^2 = 1$. It is further assumed that each node knows the signature waveform of the other nodes in the network which is required for multi-source detection. The cooperative communication over the Space-Time Network Coding (STNC) scheme is illustrated in Fig. 4.1.

4.3.1 Broadcasting Phase

In this subsection, the signal model for an arbitrary symbol x_j, $j \in \{1, 2, \ldots, N\}$, transmitted during the Broadcasting Phase from node S_j to the other nodes is pre-

sented. Node S_j broadcasts it own data symbol x_j to the other nodes in its dedicated j^{th} time-slot. Thus, the signal received at each node S_i for $i \neq j$ is given by

$$y_{j,i}(t) = \sqrt{P_{s_j}} h_{j,i} x_j s_j(t) + n_{j,i}(t), \tag{4.1}$$

where P_{s_j} is the transmitted power by node S_j, $s_j(t)$ is the signature waveform of node S_j, and $n_{j,i}(t)$ is the additive white Gaussian noise sample at node S_i due to the signal transmitted by node S_j and is modeled as a zero-mean Complex Gaussian random variable with variance N_0. Moreover, $h_{j,i}$ is the flat fading channel coefficient between nodes S_j and S_i that is distributed as a zero-mean complex Gaussian random variable $h_{j,i} \sim \mathcal{CN}(0, \sigma_{j,i}^2)$, where $\sigma_{j,i}^2$ is the channel gain. In addition, $h_{j,i}$ can be expressed as $h_{j,i} = |h_{j,i}| e^{j\phi_{j,i}}$, where $|h_{j,i}| = \alpha_{j,i}$ is the Rayleigh distributed magnitude as

$$f_{\alpha_{j,i}}(\alpha) = \frac{2\alpha}{\sigma_{j,i}^2} \exp\left(-\frac{\alpha^2}{\sigma_{j,i}^2}\right), \quad \alpha \geq 0, \tag{4.2}$$

where $\phi_{j,i}$ is the phase response, uniformly distributed over the interval $[-\pi, \pi)$. Moreover, it is assumed that the receiving node S_i can perfectly estimate the channel coefficient $h_{j,i}$ from the received signal $y_{j,i}$. Also, the channels are assumed to be reciprocal (i.e. $h_{i,j} = h_{j,i}$) as in Time Division Duplexing (TDD) systems.

The Broadcasting Phase can be put in matrix form as follows

$$\begin{array}{c} \\ T_1 \\ \vdots \\ T_j \\ \vdots \\ T_N \end{array} \begin{array}{c} \begin{array}{ccccc} S_1 & \cdots & S_j & \cdots & S_N \end{array} \\ \left[\begin{array}{ccccc} \sqrt{P_{s_1}} x_1 & \cdots & 0 & \cdots & 0 \\ \vdots & \ddots & \vdots & \cdots & \vdots \\ 0 & \cdots & \sqrt{P_{s_j}} x_j & \cdots & 0 \\ \vdots & \cdots & \vdots & \ddots & \vdots \\ 0 & \cdots & 0 & \cdots & \sqrt{P_{s_N}} x_N \end{array}\right] \end{array}. \tag{4.3}$$

The detection of the data symbol x_j at the node S_i can be achieved by cross-correlating the received signal $y_{j,i}(t)$ in (4.1) with the signature waveform $s_j(t)$ as

$$y_{j,i} = \langle y_{j,i}(t), s_j(t) \rangle = \sqrt{P_{s_j}} h_{j,i} x_j + n_{j,i}, \tag{4.4}$$

where $n_{j,i} \sim \mathcal{CN}(0, N_0)$. Upon the completion of Broadcasting Phase (i.e. after N time-slots), each node S_i will have received a set of $(N-1)$ symbols $\{y_{j,i}\}_{j=1,j\neq i}^{N}$ from all the other nodes in the network. With the knowledge of the channel coefficients at the i^{th} node, a matched filtering operation is applied on each of the received signals $y_{j,i}$, in the form of $\left(\sqrt{P_{s_j}} h_{j,i}^* / N_0\right) y_{j,i}$. Therefore, the SNR at the output of the matched-filter is expressed as

$$\gamma_{j,i} = \frac{P_{s_j} |h_{j,i}|^2}{N_0}. \tag{4.5}$$

After each source has decoded its $(N-1)$ received symbols $\{y_{j,i}\}_{j=1,j\neq i}^{N}$, the set of available decoded data symbols at each node in the network is given by the matrix

$$\mathbf{X} = \left[\begin{array}{ccccc|c} * & x_2\mathcal{I}_{2,1} & \cdots & x_{N-1}\mathcal{I}_{N-1,1} & x_N\mathcal{I}_{N,1} & S_1 \\ x_1\mathcal{I}_{1,2} & * & \cdots & x_{N-1}\mathcal{I}_{N-1,2} & x_N\mathcal{I}_{N,2} & S_2 \\ \vdots & \vdots & \ddots & \vdots & \vdots & \vdots \\ x_1\mathcal{I}_{1,N-1} & x_2\mathcal{I}_{2,N-1} & \cdots & * & x_N\mathcal{I}_{N,N-1} & S_{N-1} \\ x_1\mathcal{I}_{1,N} & x_2\mathcal{I}_{2,N} & \cdots & x_{N-1}\mathcal{I}_{N-1,N} & * & S_N \end{array}\right], \tag{4.6}$$

where $\mathcal{I}_{j,i}$ acts as a binary indicator function as follows

$$\mathcal{I}_{j,i} = \begin{cases} 1, & \text{if node } S_i \text{ decodes } x_j \text{ correctly} \\ 0, & \text{otherwise} \end{cases}. \tag{4.7}$$

4.3.2 Cooperation Phase

The analysis of the Cooperation Phase is considered in this subsection, with the assumption that the nodes are perfectly synchronized by a distributed algorithm. In the Cooperation Phase, each node S_i in its assigned time-slot receives a signal of the $N-1$ source nodes. In particular, each node S_j other than the destination node S_i forms a linearly-coded signal of the other source nodes' received symbols and transmits it to node S_i during the i^{th} time-slot, simultaneously. At each node S_j, each linearly-coded signal contains at most the received data symbols from $(N-2)$, since each node aims at relaying the remaining $(N-2)$ nodes' symbols to node S_i. Specifically, the signal transmitted to node S_i from node S_j is composed from the received data symbols of the j^{th} row in the matrix $\mathbf{X}$ excluding the data symbol $x_i\mathcal{I}_{i,j}$ (since that the symbol x_i was originally generated at node S_i) as follows

$$\mathcal{X}_j^i = \{x_k\mathcal{I}_{k,j}\}_{k=1,k\neq j}^{N} \setminus x_i\mathcal{I}_{i,j}. \tag{4.8}$$

Based on equation (4.6), during the i^{th} time-slot, the signal transmitted from the j^{th} node is given by

$$f(\mathcal{X}_j^i)(t) = \frac{h_{j,i}^*}{|h_{j,i}|} \sum_{\substack{k=1 \\ k\neq i,k\neq j}}^{N} \sqrt{P_{k,j}} x_k\mathcal{I}_{k,j}s_k(t), \tag{4.9}$$

where $s_k(t)$ is the signature waveform of the k^{th} node and $P_{k,j}$ is the power at the j^{th} node used to transmit the symbol x_k. Moreover, $h_{j,i}$ is the channel coefficient between source nodes S_j and S_i; which has already been estimated in the Broadcasting Phase during the j^{th} time-slot. Clearly, the functions $f(\mathcal{X}_j^i)$ at each node are linear combinations of symbols received from other nodes. The operation of the Cooperation Phase can be expressed in matrix form as follows

$$
\begin{array}{c} \\ T_1 \\ \vdots \\ T_i \\ \vdots \\ T_N \end{array}
\begin{array}{c}
\begin{array}{ccccccc} S_1 & & \cdots & & S_i & & \cdots & & S_N \end{array} \\
\left[\begin{array}{ccccc}
0 & \cdots & f(\mathcal{X}_i^1) & \cdots & f(\mathcal{X}_N^1) \\
\vdots & \ddots & \vdots & \cdots & \vdots \\
f(\mathcal{X}_1^i) & \cdots & 0 & \cdots & f(\mathcal{X}_N^i) \\
\vdots & \cdots & \vdots & \ddots & \vdots \\
f(\mathcal{X}_1^N) & \cdots & f(\mathcal{X}_i^N) & \cdots & 0
\end{array}\right]
\end{array}. \tag{4.10}
$$

The received signal at the i^{th} node during the i^{th} time-slot from the $(N-1)$ other nodes is given by

$$\mathcal{Y}_i(t) = \sum_{\substack{m=1 \\ m\neq i}}^{N} h_{m,i} f(\mathcal{X}_m^i)(t) + w_i(t) = \sum_{\substack{m=1 \\ m\neq i}}^{N} x_m a_{i,m} s_m(t) + w_i(t), \tag{4.11}$$

where $w_i(t)$ is the additive white Gaussian noise at node S_i and

$$a_{i,m} = \sum_{\substack{k=1 \\ k\neq i, k\neq m}}^{N} |h_{k,i}| \sqrt{P_{m,k}} \mathcal{I}_{m,k}, \tag{4.12}$$

where the summation in (4.12) contains at most $(N-2)$ terms, depending on how many data symbols have been decoded correctly.

4.4 Multi-source Signal Detection

Based on the received signal $\mathcal{Y}_i(t)$, node S_i performs a multi-source detection operation to extract the $(N-1)$ symbols of the other nodes. Each soft symbol $x_j,\ j \in \{1, 2, \ldots, N\}_{i\neq j}$ is detected by passing the received signal $\mathcal{Y}_i(t)$ through a Matched Filter Bank (MFB) of $(N-1)$ branches, matched to the corresponding set of the nodes' signature waveforms $s_j(t)$ for $j \in \{1, 2, \ldots, N\}_{i\neq j}$ and sampling it at the end of the symbol duration to obtain

$$\mathcal{Y}_{i,j} = \langle \mathcal{Y}_i(t), s_j(t) \rangle = \sum_{\substack{m=1 \\ m \neq i}}^{N} x_m a_{i,m} \rho_{m,j} + w_{i,j}, \tag{4.13}$$

where $\rho_{m,j}$ is the correlation coefficient between the signature waveforms $s_m(t)$ and $s_j(t)$. The matched-filtered signal forms an $(N-1) \times 1$ vector comprising all the $\mathcal{Y}_{i,j}$'s signals as

$$\boldsymbol{\mathcal{Y}}_i = \boldsymbol{R}_i \boldsymbol{A}_i \boldsymbol{x}_i + \boldsymbol{w}_i, \tag{4.14}$$

where

$$\boldsymbol{\mathcal{Y}}_i = \left[\mathcal{Y}_{i,1}, \ldots, \mathcal{Y}_{i,i-1}, \mathcal{Y}_{i,i+1}, \ldots, \mathcal{Y}_{i,N} \right]^T, \tag{4.15}$$

$$\boldsymbol{x}_i = \left[x_1, \ldots, x_{i-1}, x_{i+1}, \ldots, x_N \right]^T, \tag{4.16}$$

$\boldsymbol{w}_i = \left[w_{i,1}, \ldots, w_{i,i-1}, w_{i,i+1}, \ldots, w_{i,N} \right]^T \sim \mathcal{CN}(\boldsymbol{0}, N_0 \boldsymbol{R}_i)$, with

$$\boldsymbol{R}_i = \begin{bmatrix} 1 & \cdots & \rho_{1,(i-1)} & \rho_{1,(i+1)} & \cdots & \rho_{1,N} \\ \vdots & \ddots & \vdots & \vdots & \cdots & \vdots \\ \rho_{(i-1),1} & \cdots & 1 & \rho_{(i-1),(i+1)} & \cdots & \rho_{(i-1),N} \\ \rho_{(i+1),1} & \cdots & \rho_{(i+1),(i-1)} & 1 & \cdots & \rho_{(i+1),N} \\ \vdots & \cdots & \vdots & \vdots & \ddots & \vdots \\ \rho_{N,1} & \cdots & \rho_{N,(i-1)} & \rho_{N,(i+1)} & \cdots & 1 \end{bmatrix}, \tag{4.17}$$

and

$$\boldsymbol{A}_i = \begin{bmatrix} a_{i,1} & \cdots & 0 & 0 & \cdots & 0 \\ \vdots & \ddots & \vdots & \vdots & \cdots & \vdots \\ 0 & \cdots & a_{i,(i-1)} & 0 & \cdots & 0 \\ 0 & \cdots & 0 & a_{i,(i+1)} & \cdots & 0 \\ \vdots & \cdots & \vdots & \vdots & \ddots & \vdots \\ 0 & \cdots & 0 & 0 & \cdots & a_{i,N} \end{bmatrix}, \tag{4.18}$$

where both matrices $\boldsymbol{R}_i$ and $\boldsymbol{A}_i$ have dimensions $(N-1)\times(N-1)$. The signal vector $\boldsymbol{\mathcal{Y}}_i$ can then be decorrelated with the assumption that matrix $\boldsymbol{R}_i$ is invertible with the inverse matrix $\boldsymbol{R}_i^{-1}$ which yields

$$\tilde{\boldsymbol{\mathcal{Y}}}_i = \boldsymbol{R}_i^{-1}\boldsymbol{\mathcal{Y}}_i = \boldsymbol{A}_i\boldsymbol{x}_i + \tilde{\boldsymbol{w}}_i, \tag{4.19}$$

where $\tilde{\boldsymbol{w}}_i \sim \mathcal{CN}(\boldsymbol{0}, N_0\boldsymbol{R}_i^{-1})$. Therefore, the soft symbol of x_j can be obtained from detected signal vector $\tilde{\boldsymbol{\mathcal{Y}}}_i$ at node S_i at the output of the j^{th} branch of the MFB and is expressed as

$$\tilde{\mathcal{Y}}_{i,j} = a_{i,j}x_j + \tilde{w}_{i,j}, \tag{4.20}$$

where $\tilde{w}_{i,j} \sim \mathcal{CN}(0, N_0 r_{i,j})$ with $r_{i,j}$ being the j^{th} diagonal element of the inverse matrix R_i^{-1} associated with the data symbol x_j and $a_{i,j}$ is given by (4.12). Without loss of generality, let $\rho_{j,i} = \rho$ for all $j \neq i$. Thus, it can be easily verified that

$$r_{i,j} = \frac{1+(N-3)\rho}{1+(N-3)\rho-(N-2)\rho^2} \triangleq r_{N-1}. \tag{4.21}$$

It should be noted that upon the completion of the Broadcasting Cooperation Phases, the j^{th} data symbol x_j, $j \in \{1,2,\ldots,N\}_{i\neq j}$ is relayed at most $(N-2)$ times before reaching node S_i. In addition, since in the Broadcasting Phase, the source node S_j has already broadcasted its data symbol x_j to all the other nodes including S_i, this implies that node S_i received a total of $(N-1)$ signals containing the symbol x_j. This fact will be used later to prove that a full diversity order of $(N-1)$ per source node is achieved at a high signal-to-noise ratio.

On the other hand, since $\mathcal{I}_{j,i} \in \{0,1\}$ for $i \neq j$, represents the detection state at S_i of the data symbol x_j; then, in general, node S_k for $k \in \{1,2,\ldots,N\}_{k\neq i,k\neq j}$,

forwards the symbol x_j to node S_i only if it has successfully detected it. Therefore, at node S_i, all the $\mathcal{I}_{j,k}$'s form a binary (base-2) number

$$\mathcal{I}_j^i = [\mathcal{I}_{j,N} \ \ldots \ \mathcal{I}_{j,k=(i+1)} \ \mathcal{I}_{j,k=(i-1)} \ \ldots \ \mathcal{I}_{j,1}]_2 \setminus \mathcal{I}_{j,j}, \tag{4.22}$$

that represents one of the $2^{(N-2)}$ detection states of the $(N-2)$ nodes S_j's acting as relay nodes. In other words, $|\mathcal{I}_j^i|$ contains at most $(N-2)$ 1's (i.e. the hamming weight of $\mathcal{I}_j^i$). For example, for $N = 4$, the detection state of x_1 at node S_2 is given by $\mathcal{I}_1^2 = [\mathcal{I}_{1,4} \ \mathcal{I}_{1,3}]_2$ with $|\mathcal{I}_1^2|$ taking decimal values in $\{0, 1, 2, 3\}$ in the form of $\mathcal{I}_1^2 = [0 \ 0]_2$, $[0 \ 1]_2$, $[1 \ 0]_2$, or $[1 \ 1]_2$, respectively.

The detection of data symbol x_j at the node S_i can be achieved through combining the signals received in the Broadcasting and Cooperation Phases. However, it should be noted that during the Cooperation Phase, it might occur that $a_{i,j} = 0$ (i.e. the receiving node might not receive any linear combination for some symbol x_j and this occurs when all the other nodes decode x_j incorrectly, simultaneously). This in turn implies that the detection state for symbol x_j at node S_i is $|\mathcal{I}_j^i| = 0$. Thus, the j^{th} branch of the MFB is not added into the combined $\tilde{x}_j^i$ to prevent adding the noise term $\tilde{w}_{i,j}$ to it. In other words, for $|\mathcal{I}_j^i| = 0$, a simple phase correction is applied to the received signal $y_{j,i}$ during the j^{th} time-slot in the Broadcasting Phase by multiplying it with the deterministic conjugate of the known channel phase response (i.e. $\tilde{x}_j^i = e^{-j\phi_{j,i}} y_{j,i}$). However, for $|\mathcal{I}_j^i| > 0$ (i.e. $a_{i,j} \neq 0$), the phase-corrected signal is also combined with $\tilde{\mathcal{Y}}_{i,j}$, yielding the combined signal

$$\tilde{x}_j^i = e^{-j\phi_{j,i}} y_{j,i} + \tilde{\mathcal{Y}}_{i,j}, \tag{4.23}$$

where $y_{j,i} = \sqrt{P_{s_j}} h_{j,i} x_j + n_{j,i}$. Upon substitution of $y_{j,i}$, (4.12) and (4.20) into (4.23),

the combined symbol $\tilde{x}_j$ at node S_i becomes

$$\tilde{x}_j^i = \left(|h_{j,i}|\sqrt{P_{s_j}} + \sum_{\substack{k=1 \\ k\neq i, k\neq j}}^{N} |h_{k,i}|\sqrt{P_{j,k}}\mathcal{I}_{j,k} \right) x_j + \eta_{i,j}, \tag{4.24}$$

where $\eta_{i,j} = e^{-j\phi_{j,i}} n_{j,i} + \tilde{w}_{i,j}$ is the zero-mean equivalent noise with variance $(1 + r_{N-1})N_0$, with the assumption that $n_{j,i}$ and $\tilde{w}_{i,j}$ are statistically independent. Hence, the conditional signal-to-noise ratio given the detection state $\mathcal{I}_j^i$ of the combined data symbol $\tilde{x}_j^i$ at node S_i can be expressed as

$$\gamma_{j|\mathcal{I}_j^i}^i = \begin{cases} \frac{|h_{j,i}|^2 P_{s_j}}{N_0}, & \text{if } |\mathcal{I}_j^i| = 0 \\ \frac{\left(|h_{j,i}|\sqrt{P_{s_j}} + \sum_{\substack{k=1 \\ k\neq i, k\neq j}}^{N} |h_{k,i}|\sqrt{P_{j,k}}\mathcal{I}_{j,k} \right)^2}{(1+r_{N-1})N_0}, & \text{if } |\mathcal{I}_j^i| > 0 \end{cases}. \tag{4.25}$$

The total transmit power P_j associated with transmitting symbol x_j is distributed among the $(N-1)$ transmissions. In particular, $P_j = P_{s_j} + \sum_{\substack{k=1 \\ k\neq i, k\neq j}}^{N} P_{j,k}$, where P_{s_j} is the transmit power at node S_j; while the $P_{j,k}$'s are the power allocations for the remaining transmissions at the other nodes.

4.5 Symbol Error Rate (SER) Performance Analysis

In this section, the exact SER expression for the M-ary Phase Shift Keying (M-PSK) modulation for the DF protocol of the symbol x_j detected at node S_i is derived. Since the detection at each node is statistically independent from the others, $\mathcal{I}_{j,k}$'s for $k \in \{1, 2, \ldots, N\}_{k\neq i, k\neq j}$ are defined as independent Bernoulli random variables with a distribution expressed as [1]

$$\Upsilon(\mathcal{I}_{j,k}) = \begin{cases} 1 - \mathcal{P}_{j,k}, & \text{if } \mathcal{I}_{j,k} = 1 \\ \mathcal{P}_{j,k}, & \text{if } \mathcal{I}_{j,k} = 0 \end{cases}, \tag{4.26}$$

where $\mathcal{P}_{j,k}$ is the SER of detecting x_j at the S_k node. Thus, the probability of x_j detection in state $\mathcal{I}_j^i$ at node S_i is written as

$$\Pr(|\mathcal{I}_j^i|) = \prod_{\substack{k=1 \\ k\neq i, k\neq j}}^{N} \Upsilon(\mathcal{I}_{j,k}), \tag{4.27}$$

where in the example of $N = 4$, for $|\mathcal{I}_1^2| = 1$ (i.e. $\mathcal{I}_1^2 = [0\ 1]_2$), $\Pr(|\mathcal{I}_1^2| = 1) = \mathcal{P}_{1,4}(1 - \mathcal{P}_{1,3})$. In general, the conditional SER of M-PSK systems with the instantaneous signal-to-noise ratio (SNR) γ given a generic set of channel coefficients $\{h\}$ is expressed as [53]

$$\Psi_{|\{h\}}(\gamma) \triangleq \frac{1}{\pi} \int_0^{(M-1)\pi/M} \exp\left(-\frac{b_{PSK}\gamma}{\sin^2\theta}\right) d\theta, \tag{4.28}$$

where $b_{PSK} = \sin^2(\pi/M)$. Based on (4.4 - 4.5), the SNR in detecting the symbol x_j at node S_k given the channel gain is $\gamma_{j,k} = P_{s_j}|h_{j,k}|^2/N_0$. In general, the magnitude squared of a circularly symmetric Gaussian random variable $h_{j,k}$ is modeled as an exponential random variable with rate $1/\sigma_{j,k}^2$ (i.e. $|h_{j,k}|^2 \sim \mathcal{E}xp(1/\sigma_{j,k}^2)$), where $\sigma_{j,k}^2$ is the channel gain. Thus, by averaging the expression in (4.28) with respect to $|h_{j,k}|^2$, the SER of detecting x_j at S_k is obtained as

$$\mathcal{P}_{j,k} = \frac{1}{\pi} \int_0^{(M-1)\pi/M} G\left(\frac{b_{PSK}P_{s_j}}{N_0 \sin^2\theta}, \sigma_{j,k}^2\right)\ d\theta, \tag{4.29}$$

where $G(w(\theta), \sigma^2)$ is defined in (4.94) in Appendix I. On the other hand, based on the conditional SNR $\gamma_{j|\mathcal{I}_j^i}^i$ expression in (4.24), the conditional SER of symbol x_j at node S_i can be shown to be

$$\Psi_{|\{h_{k,i}\}_{k=1,k\neq i}^N}(\gamma_{j|\mathcal{I}_j^i}^i) = \frac{1}{\pi} \int_0^{(M-1)\pi/M} \exp\left(-\frac{b_{PSK}\gamma_{j|\mathcal{I}_j^i}^i}{\sin^2\theta}\right) d\theta, \tag{4.30}$$

which reduces to the following two cases:

1. $|\mathcal{I}_j^i| = 0$: After averaging over the exponential random variable $|h_{j,i}|^2$, the conditional SER can be expressed as

$$\Psi(\gamma^i_{j||\mathcal{I}_j^i|=0}) = \frac{1}{\pi}\int_0^{(M-1)\pi/M} G\left(\frac{b_{PSK}P_{s_j}}{N_0\sin^2\theta}, \sigma^2_{j,i}\right)\, d\theta. \tag{4.31}$$

2. $|\mathcal{I}_j^i| > 0$: Similarly, the conditional SER can be obtained as

$$\Psi_{|\{h_{k,i}\}_{k=1,k\neq i}^N}(\gamma^i_{j||\mathcal{I}_j^i|>0}) = \frac{1}{\pi}\int_0^{(M-1)\pi/M} \exp\left(-\frac{C^2_{PSK}}{2\sin^2\theta}\mathcal{H}^2_{i,j}\right) d\theta, \tag{4.32}$$

where

$$\mathcal{H}^2_{i,j} = \left(\sqrt{P_{s_j}}|h_{j,i}| + \sum_{\substack{k=1\\k\neq i,k\neq j}}^{N} |h_{k,i}|\sqrt{P_{j,k}}\mathcal{I}_{j,k}\right)^2, \tag{4.33}$$

and

$$C_{PSK} = \sqrt{\frac{2b_{PSK}}{(1+r_{N-1})N_0}}. \tag{4.34}$$

Clearly, $\mathcal{H}^2_{i,j}$ is a sum of $1+|\mathcal{I}_j^i|$ Rayleigh random variables. The analysis for the conditional SER is analogous to that of the equal gain combining in [54], using the Gauss-Hermite formula [55, p. 890, eq.(25.4.46)]. Thus, after averaging over the channel statistics, the conditional SER is given by [54]

$$\Psi(\gamma^i_{j||\mathcal{I}_j^i|>0}) = \frac{1}{2\pi^2}\int_0^{(M-1)\pi/M} \frac{1}{\sqrt{{}_i\eta_j(\theta)}}\sum_{n=1}^{N_p} w_{ni}\mathcal{F}_j\left(\frac{\kappa_n}{\sqrt{{}_i\eta_j(\theta)}}, \theta\right)\, d\theta, \tag{4.35}$$

where κ_n, w_n are the zeros and weight factors as given in [55, p. 924, table (25.10)] and N_p is the order of the Hermite polynomial $H_{N_p}(\cdot)$, respectively. It was verified that $N_p = 20$ results in excellent accuracy. In addition [54]

$${}_i\eta_j(\theta) = \frac{\sin^2(\theta)}{2C^2_{PSK}} + \frac{1}{4}\left(P_{s_j}\sigma^2_{j,i} + \sum_{\substack{k=1\\k\neq i,k\neq j}}^{N} P_{j,k}\sigma^2_{j,k}\mathcal{I}_{j,k}\right), \tag{4.36}$$

and ${}_i\mathcal{F}_j(\nu,\theta) = {}_iR_j(\nu,\theta)\cos\left({}_i\Theta_j(\nu,\theta)\right)$, with

$$ {}_iR_j(\nu,\theta) = \sqrt{X^2(\theta)+Y^2(\nu,\theta)}D_{j,i}\prod_{\substack{k=1\\k\neq i,k\neq j}}^{N}\sqrt{A^2(\nu,P_{j,k}\sigma_{j,k}^2\mathcal{I}_{j,k})+B^2(\nu,P_{j,k}\sigma_{j,k}^2\mathcal{I}_{j,k})}, \tag{4.37}$$

and ${}_i\Theta_j(\nu,\theta)$ is defined as [54]

$$\begin{aligned} &{}_i\Theta_j(\nu,\theta) = \\ &\arctan\left(\frac{Y(\nu,\theta)}{X(\theta)}\right)+\arctan\left(\frac{B(\nu,P_{s_j}\sigma_{j,i}^2)}{A(\nu,P_{s_j}\sigma_{j,i}^2)}\right)+\sum_{\substack{k=1\\k\neq i,k\neq j}}^{N}\arctan\left(\frac{B(\nu,P_{j,k}\sigma_{j,k}^2\mathcal{I}_{j,k})}{A(\nu,P_{j,k}\sigma_{j,k}^2\mathcal{I}_{j,k})}\right) \\ &+\frac{\pi}{2}\left(N-\operatorname{sgn}\left(Y(\nu,\theta)\right)-\operatorname{sgn}\left(B(\nu,P_{s_j}\sigma_{j,i}^2)\right)-\sum_{\substack{k=1\\k\neq i,k\neq j}}^{N}\operatorname{sgn}\left(B(\nu,P_{j,k}\sigma_{j,k}^2\mathcal{I}_{j,k})\right)\right). \end{aligned} \tag{4.38}$$

On the other hand, $X(\theta)$, $Y(\nu,\theta)$ are defined as

$$X(\theta) = \sqrt{\frac{\pi}{2}}\frac{\sin(\theta)}{C_{PSK}},\ \text{and}\ Y(\nu,\theta) = \frac{\nu\sin^2(\theta)}{C_{PSK}^2}{}_1F_1\left(\frac{1}{2};\frac{3}{2};\frac{\nu^2\sin^2(\theta)}{2C_{PSK}}\right), \tag{4.39}$$

respectively, where $sgn(\cdot)$ is the sign function and ${}_1F_1\left(\cdot;\cdot;\cdot\right)$ is the Kummer confluent hypergeometric function [55]. Moreover, $A(\nu,\tau)$ and $B(\nu,\tau)$ are defined as

$$A(\nu,\tau) = {}_1F_1\left(-\frac{1}{2};\frac{1}{2};\frac{\nu^2\tau}{4}\right),\ \text{and}\ B(\nu,\tau) = \Gamma\left(\frac{3}{2}\right)\sqrt{\tau}\nu, \tag{4.40}$$

respectively; with $\Gamma(\cdot)$ being the gamma function [55]. Also, $D_{j,i}$ is defined as

$$D_{j,i} = \sqrt{A^2(\nu,P_{s_j}\sigma_{j,i}^2)+B^2(\nu,P_{s_j}\sigma_{j,i}^2)}. \tag{4.41}$$

Given the detection state $\mathcal{I}_j^i$, which can take $2^{(N-2)}$ values, the SER for detecting the data symbol x_j at the i^{th} node can be calculated using the law of total probability as

$$
\begin{aligned}
P^j_{SER} &= \sum_{\ell=0}^{2^{(N-2)}-1} \Pr(\tilde{x}^i_j \neq x_j || \mathcal{I}^i_j| = \ell) \cdot \Pr(|\mathcal{I}^i_j| = \ell) \\
&= \Psi(\gamma^i_{j||\mathcal{I}^i_j|=0}) \cdot \Pr(|\mathcal{I}^i_j| = 0) + \sum_{\ell=1}^{2^{(N-2)}-1} \Psi(\gamma^i_{j||\mathcal{I}^i_j|=\ell}) \cdot \Pr(|\mathcal{I}^i_j| = \ell)
\end{aligned}
\tag{4.42}
$$

where $\Pr(\tilde{x}^i_j \neq x_j||\mathcal{I}^i_j|)$ is the probability of making a symbol error for a particular detection state, and $\Pr(|\mathcal{I}^i_j|)$ is as defined (4.27).

4.6 Asymptotic Upper Bound SER Analysis

The asymptotic upper-bound SER performance is obtained at a high SNR by performing a series of approximations to the term $\Psi(\gamma^i_{j||\mathcal{I}^i_j|=\ell})$, for $\ell \in \{0, 1, \ldots, 2^{(N-2)}-1\}$ and also the term $\Pr(|\mathcal{I}^i_j|)$. It should be noted that finding the distribution of the sum of independent but not identical Rayleigh random variables as given by $\mathcal{H}^2_{i,j}$ in (4.33) is extremely difficult [54] and no exact closed form solutions exist in the literature [57]. However, by introducing symmetry to the wireless network model, an upper-bound can be determined and the diversity order can be verified. Therefore, in this section, the upper-bound for a symmetric network is derived by assuming that the channel gains are identical (i.e. $\sigma^2_{j,i} = \sigma^2_{k,i} = \sigma^2_i$, $\forall k \in \{1, 2, \ldots, N\}_{k\neq i}$) and also that the transmission power of each node is identical (i.e. $P_s = P_{s_j} = P_{j,k} = \mu P$, $\forall k \in \{1, 2, \ldots, N\}_{k\neq i, k\neq j}$ and $\mu = 1/(N-1)$). This implies that the same average SNR/symbol/path is assumed between the nodes in the network and that as the number of nodes increase, the power allocation per node decreases. As will be shown in the simulations section, the upper-bound for the symmetric network also acts as an upper-bound for a network with arbitrary power allocations/channel gains (i.e. asymmetric network).

At high SNR, it is expected that the SER $\mathcal{P}_{j,k}$ of detecting x_j at node S_k for $k \in \{1, 2, \ldots, N\}_{k\neq i, k\neq j}$, becomes sufficiently small such that $1 - \mathcal{P}_{j,k} \approx 1$. Thus, only the terms in the quantity $\Pr(|\mathcal{I}_j^i|) = \prod_{\substack{k=1 \\ k\neq i, k\neq j}}^{N} \Upsilon(\mathcal{I}_{j,k})$ that will count are those corresponding to the nodes that have decoded their received x_j symbol incorrectly [58]. Hence, let ${}_0\Phi_j$ and ${}_1\Phi_j$ denote the subsets of the indices of the nodes that decode x_j erroneously and correctly, respectively. That is, ${}_0\Phi_j = \{k : \mathcal{I}_{j,k} = 0\}$ and ${}_1\Phi_j = \{k : \mathcal{I}_{j,k} = 1\}$, for $k \in \{1, 2, \ldots, N\}_{k\neq i, k\neq j}$. Moreover, $|{}_0\Phi_j|$ and $|{}_1\Phi_j|$ $\in \{0, 1, \ldots, N-2\}$. In addition, it should be noted that $|{}_0\Phi_j| + |{}_1\Phi_j| = (N-2)$ for any detection state $\mathcal{I}_j^i$. Thus, the expression for $\Pr(|\mathcal{I}_j^i|)$ given in (4.27) can then be expressed as

$$\Pr(|\mathcal{I}_j^i|) \simeq \prod_{k\in {}_0\Phi_j}^{N} \Upsilon(\mathcal{I}_{j,k}) = \left(\frac{N_0}{P}\right)^{|{}_0\Phi_j|} \left(\frac{\Theta}{\mu b_{PSK}\sigma_i^2}\right)^{|{}_0\Phi_j|}, \tag{4.43}$$

where

$$\Theta = \frac{1}{\pi}\int_0^{(M-1)\pi/M} \sin^2(\theta)\, d\theta = \frac{2\pi(M-1) + M\sin\left(\frac{2\pi}{M}\right)}{4\pi M}. \tag{4.44}$$

With respect to $\Psi(\gamma^i_{j|\mathcal{I}_j^i=0})$, the upper-bound approximation at high SNR can be expressed with the aid of (4.95) as (see Appendix I)

$$\bar{\Psi}(\gamma^i_{j|\mathcal{I}_j^i=0}) = \tilde{F}\left(\frac{b_{PSK}P_s}{N_0\sin^2\theta}, \sigma_i^2\right) \lesssim \left(\frac{N_0}{P}\right)\frac{\Theta}{\mu b_{PSK}\sigma_i^2}. \tag{4.45}$$

In order to find an upper-bound approximation for $\bar{\Psi}(\gamma^i_{j||\mathcal{I}_j^i|=\ell})$, the expression (4.34) must be approximated. Based on (4.25), the conditional SNR for $|\mathcal{I}_j^i| = \ell$ is given by

$$\gamma^i_{j||\mathcal{I}_j^i|=\ell} = \frac{P_s}{(1+r_{N-1})N_0}\left(|h_{j,i}| + \sum_{\substack{k=1 \\ k\neq i, k\neq j}}^{N} |h_{j,i}|\mathcal{I}_{j,k}\right)^2. \tag{4.46}$$

Thus, the average SNR conditioned on the network detection state can be shown to

be [54]

$$\gamma_{av,(\ell+1)} = \gamma_{s_i}\left(1+\frac{\pi}{4}\ell\right), \tag{4.47}$$

where $\gamma_{s_i} = P_s\sigma_i^2/(1+r_{N-1})N_0$. An accurate approximation to the conditional SER has been determined in [54] and is expressed as

$$\bar{\Psi}(\gamma^i_{j||\mathcal{I}^i_j|=\ell}) = I_{(\ell+1)}\left(b_{PSK}\gamma_{av,(\ell+1)}, \frac{(M-1)\pi}{M}\right). \tag{4.48}$$

In general

$$I_L\left(\zeta,\phi\right) = \frac{1}{\pi}\int_0^{\phi}\left(\frac{\sin^2\phi}{\sin^2\phi+\zeta}\right)^L d\phi. \tag{4.49}$$

Therefore, $\bar{\Psi}(\gamma^i_{j||\mathcal{I}^i_j|=\ell})$ with the aid of (4.96) in Appendix II, can be shown to be

$$\begin{aligned}\bar{\Psi}(\gamma^i_{j||\mathcal{I}^i_j|=\ell}) \approx \left(\frac{N_0}{P}\right)^{\ell+1}\left(\frac{(1+r_{N-1})}{\mu b_{PSK}\sigma_i^2\left(1+\frac{\pi}{4}\ell\right)}\right)^{\ell+1}\left(\sin\left(\frac{(M-1)\pi}{M}\right)\right)^{2\ell+3}\times \\ \frac{F_1\left(\ell+\frac{3}{2},\frac{1}{2},\ell+1,\ell+\frac{5}{2},\sin^2\left(\frac{(M-1)\pi}{M}\right),-\frac{(1+r_{N-1})N_0}{\mu P b_{PSK}\sigma_i^2\left(1+\frac{\pi}{4}\ell\right)}\sin^2\left(\frac{(M-1)\pi}{M}\right)\right)}{\pi(2\ell+3)}.\end{aligned} \tag{4.50}$$

Hence, the asymptotic SER expression, after a series of manipulations, can be written as

$$\begin{aligned}P^j_{SER} \lesssim \left(\frac{N_0}{P}\right)^{N-1}\times \\ \left(\left(\frac{\Theta}{\mu b_{PSK}\sigma_i^2}\right)^{N-1} + \right. \\ \left.\sum_{\ell=1}^{2^{(N-2)}-1}\left(\frac{1+r_{N-1}}{1+\frac{\pi}{4}|_1\Phi_j|}\right)^{|_1\Phi_j|+1}\frac{{}_2F_1\left(|_1\Phi_j|+\frac{3}{2},\frac{1}{2},|_1\Phi_j|+\frac{5}{2},\sin^2\left(\frac{(M-1)\pi}{M}\right)\right)}{\pi(\mu b_{PSK}\sigma_i^2)^{N-1}(2|_1\Phi_j|+3)}\left(\sin\left(\frac{(M-1)\pi}{M}\right)\right)^{2|_1\Phi_j|+3}(\Theta)^{|_0\Phi_j|}\right),\end{aligned} \tag{4.51}$$

where it should be noted that $1+|_0\Phi_j|+|_1\Phi_j| = (N-1)$.

The cooperative diversity order of a wireless system is identified from the SER expression as follows [1]

$$P^j_{SER} \sim (SNR\cdot\Delta)^{-d}, \tag{4.52}$$

where $SNR \triangleq P/N_0$ is the signal-to-noise ratio term, the exponent d denotes the diversity order and Δ defines the cooperation gain. Thus, it is clear that $d = N - 1$ and the STNC scheme achieves full cooperative diversity order.

4.7 Synchronization Analysis

It is well-known that due to the diagonal structure of the Broadcasting Phase, as shown in (4.3), the problem of perfect synchronization is alleviated since that within the TDMA framework, only one source node is allowed to transmit at any one time [59]. Moreover, the analysis so far assumed perfect synchronization among the transmitting nodes in the Cooperation Phase. In other words, perfect simultaneous "in-phase" synchronized transmissions of the different source nodes were assumed. However, the simultaneous transmissions of the different nodes during the Cooperation Phase impose a major practical challenge for a large number of the transmitting nodes distributed over wide areas in the network. In other words, mismatches in clocks of the geographically distributed nodes result in different transmission times. Also, the lack of tracking at the receiving node for all the other cooperative nodes and lack of compensation for propagation delays can have detrimental effects on the network performance. In fact, if the transmitting nodes try to synchronize toward one receiving node, they may increase asynchronism toward other receiving nodes in different time-slots because of the different transmission distances. Therefore, in this section, the aim is to analyze the degradation in the SER system performance due to the synchronization errors between the nodes in the Cooperation Phase.

4.7.1 Synchronization Model

Consider the scenario where node S_i is the receiving node while the remaining distributed nodes S_m for $m \in \{1, 2, \ldots, N\}_{m \neq i}$, are assumed to transmit asynchronously. Also, let $\tau_{i,m}$ be the time-jitter for each transmitting node S_m during the i^{th} time-slot (i.e. with node S_i being the receiving node); where $\tau_{i,m} \in [0, T_s)$. Moreover, assume that each distributed node initiates and terminates it transmissions within T_s time units of each other within each TDMA time-slot. As in (4.11), the received signal at node S_i during the i^{th} time-slot is expressed as [60] [61]

$$\begin{aligned} \hat{\mathcal{Y}}_i(t) &= \sum_{\substack{m=1 \\ m \neq i}}^{N} \sum_{n=-\infty}^{\infty} h_{m,i} f(\mathcal{X}_m^i)\,(t - nT_s - \tau_{i,m}) + w_i(t) \\ &= \sum_{\substack{m=1 \\ m \neq i}}^{N} \sum_{n=-\infty}^{\infty} a_{i,m}(n) x_m(n) s_m\,(t - nT_s - \tau_{i,m}) + w_i(t), \end{aligned} \tag{4.53}$$

where $a_{i,m}(n)$ is as defined in (4.12). Clearly, due to the fractional-symbol delay between the linearly-coded symbols transmitted from the different nodes, the channels can become extremely dispersive even for flat-fading channels. Moreover, the effect of the different propagation delays is manifested in the form of superposition of pulses from each node S_m for $m \in \{1, 2, \ldots, N\}_{m \neq i}$ that are shifted by $\tau_{i,m}$. This in turn implies that neighboring symbols will introduce Intersymbol Interference (ISI) to the desired symbol.

In this work, only the ISI contribution from the neighboring symbols to the desired symbol is considered; while the higher-order terms are neglected due to their smaller effect [63]. Therefore, (4.53) can be written as

$$\hat{\mathcal{Y}}_i(t) = \sum_{\substack{m=1 \\ m \neq i}}^{N} \sum_{n=-1}^{1} a_{i,m}(n) x_m(n) s_m\,(t - nT_s - \tau_{i,m}) + w_i(t). \tag{4.54}$$

As before, the received signal is then fed into a bank of $(N-1)$ filters, matched to the nodes' spreading waveforms and is sampled at $t = nT_s + \Delta_i$ for $n \in \{-1, 0, 1\}$, where Δ_i is the timing-shift chosen by the receiving node S_i to compensate for the average delay of the transmitting nodes. Thus, the received signal is given by [62]

$$\hat{\mathcal{Y}}_{i,j}(n) = \langle \hat{\mathcal{Y}}_i(t), s_j(t) \rangle = \int_{nT_s+\Delta_i}^{nT_s+T_s+\Delta_i} \hat{\mathcal{Y}}_i(t) s_j^*(t - nT_s - \Delta_i)\, dt, \tag{4.55}$$

with $s_j(t)$ being zero outside the duration of T_s time units.

Define the $(N-1) \times (N-1)$ cross-correlation matrix $\boldsymbol{R}_i(n)$ whose entries are in general defined and modeled as [52] [64]

$$\tilde{\rho}_{m,j}^{(-1)} = \begin{cases} \frac{1}{T_s} \int_{\Delta_i}^{\tau_{i,m}} s_m(t - \tau_{i,m}) s_j^*(t - \Delta_i)\, dt = \rho_{m,j} \left(\frac{\tau_{i,m} - \Delta_i}{T_s} \right), & \tau_{i,m} > \Delta_i \\ 0, & \text{otherwise} \end{cases}, \tag{4.56}$$

$$\bar{\rho}_{m,j}^{(0)} = \frac{1}{T_s} \int_{\max(\tau_{i,m}, \Delta_i)}^{\min(\tau_{i,m}, \Delta_i)+T_s} s_m(t - \tau_{i,m}) s_j^*(t - \Delta_i)\, dt = \rho_{m,j} \left(1 - \frac{|\Delta_i - \tau_{i,m}|}{T_s} \right), \tag{4.57}$$

and

$$\tilde{\rho}_{m,j}^{(1)} = \begin{cases} \frac{1}{T_s} \int_{\tau_{i,m}}^{\Delta_i} s_m(t - \tau_{i,m}) s_j^*(t - \Delta_i)\, dt = \rho_{m,j} \left(\frac{\Delta_i - \tau_{i,m}}{T_s} \right), & \tau_{i,m} < \Delta_i \\ 0, & \text{otherwise} \end{cases}, \tag{4.58}$$

where $\rho_{m,j} = (1/T_s) \int_0^{T_s} s_m(t) s_j^*(t) dt$, $\boldsymbol{R}_i(n) = 0, \forall |n| > 1$ and $\boldsymbol{R}_i(n) = \boldsymbol{R}_i^T(-n)$. As before, it is assumed that $\rho_{m,j} = \rho$ for $m \neq i$. Furthermore, the time-shifts are assumed to be uniformly distributed $|\Delta_i - \tau_{i,m}| \sim U[0, \Delta T_s]$ around the reference clock Δ_i, $\forall m \in \{1, 2, \ldots, N\}_{m \neq i}$; where $\Delta T_s \in [0, T_s)$ is the maximum time-shift value. Moreover, it is clear that if $|\Delta_i - \tau_{i,m}| \approx 0$, then $\bar{\rho}_{m,j}^{(0)} \approx \rho_{m,j}$ and also $\tilde{\rho}_{m,j}^{(-1)} = \tilde{\rho}_{m,j}^{(1)} \approx 0$. Intuitively, the smaller are the time-shifts, the less severe are timing synchronization errors. Also, in the special case where all the time-jitters are equal

(i.e. $\tau_{i,1} = \ldots = \tau_{i,i-1} = \tau_{i,i+1} = \ldots = \tau_{i,N}$), and are compensated for by setting $\Delta_i = \tau_{i,m}$, then all transmitting nodes are synchronous and ISI is absent.

For convenience, let $\boldsymbol{R}_i(0) = \bar{\boldsymbol{R}}_i$ be defined as

$$\bar{\boldsymbol{R}}_i = \begin{bmatrix} 1 & \cdots & \bar{\rho}^{(0)}_{1,(i-1)} & \bar{\rho}^{(0)}_{1,(i+1)} & \cdots & \bar{\rho}^{(0)}_{1,N} \\ \vdots & \ddots & \vdots & \vdots & \cdots & \vdots \\ \bar{\rho}^{(0)}_{(i-1),1} & \cdots & 1 & \bar{\rho}^{(0)}_{(i-1),(i+1)} & \cdots & \bar{\rho}^{(0)}_{(i-1),N} \\ \bar{\rho}^{(0)}_{(i+1),1} & \cdots & \bar{\rho}^{(0)}_{(i+1),(i-1)} & 1 & \cdots & \bar{\rho}^{(0)}_{(i+1),N} \\ \vdots & \cdots & \vdots & \vdots & \ddots & \vdots \\ \bar{\rho}^{(0)}_{N,1} & \cdots & \bar{\rho}^{(0)}_{N,(i-1)} & \bar{\rho}^{(0)}_{N,(i+1)} & \cdots & 1 \end{bmatrix}, \tag{4.59}$$

and $\boldsymbol{R}_i(1) = \boldsymbol{R}_i^T(-1) = \tilde{\boldsymbol{R}}_i$, where $\tilde{\boldsymbol{R}}_i$ is an upper triangular matrix having a zero diagonal and is defined as follows [52]

$$\tilde{\boldsymbol{R}}_i = \begin{bmatrix} 0 & \cdots & \tilde{\rho}^{(-1)}_{1,(i-1)} & \tilde{\rho}^{(-1)}_{1,(i+1)} & \cdots & \tilde{\rho}^{(-1)}_{1,N} \\ \vdots & \ddots & \vdots & \vdots & \cdots & \vdots \\ 0 & \cdots & 0 & \tilde{\rho}^{(-1)}_{(i-1),(i+1)} & \cdots & \tilde{\rho}^{(-1)}_{(i-1),N} \\ 0 & \cdots & 0 & 0 & \cdots & \tilde{\rho}^{(-1)}_{(i+1),N} \\ \vdots & \cdots & \vdots & \vdots & \ddots & \vdots \\ 0 & \cdots & 0 & 0 & \cdots & 0 \end{bmatrix}. \tag{4.60}$$

Thus, the output of the matched filter bank can be expressed as [52] [62]

$$\hat{\boldsymbol{\mathcal{Y}}}_i(n) = \underbrace{\bar{\boldsymbol{R}}_i \boldsymbol{A}_i(n)\boldsymbol{x}_i(n)}_{\text{Desired Signal}} + \underbrace{\tilde{\boldsymbol{R}}_i^T \boldsymbol{A}_i(n+1)\boldsymbol{x}_i(n+1) + \tilde{\boldsymbol{R}}_i \boldsymbol{A}_i(n-1)\boldsymbol{x}_i(n-1)}_{\text{ISI Signal}} + \hat{\boldsymbol{w}}_i(n), \tag{4.61}$$

where $\boldsymbol{A}_i(n+l)$ for $l \in \{-1, 0, 1\}$ is defined as in (4.18). Furthermore, $\boldsymbol{x}_i(n+l)$ is defined in general as

$$\boldsymbol{x}_i(n+l) = [x_1(n+l), \ldots, x_{i-1}(n+l), x_{i+1}(n+l), \ldots, x_N(n+l)]^T, \tag{4.62}$$

and the zero-mean Gaussian noise $\hat{\boldsymbol{w}}_i(n)$ is defined as [52]

$$E\left[\hat{\boldsymbol{w}}_i(n)\hat{\boldsymbol{w}}_i^H(n+l)\right] = \begin{cases} N_0\tilde{\boldsymbol{R}}_i^T, & \text{if } l=1 \\ N_0\bar{\boldsymbol{R}}_i, & \text{if } l=0 \\ N_0\tilde{\boldsymbol{R}}_i, & \text{if } l=-1 \\ 0, & \text{otherwise} \end{cases}. \tag{4.63}$$

As before, the vector $\hat{\boldsymbol{\mathcal{Y}}}_i(n)$ can be decorrelated as

$$\bar{\boldsymbol{\mathcal{Y}}}_i(n) = \boldsymbol{R}_i^{-1}\hat{\boldsymbol{\mathcal{Y}}}_i(n) = \bar{\bar{\boldsymbol{R}}}_i\boldsymbol{A}_i(n)\boldsymbol{x}_i(n)+\acute{\boldsymbol{R}}_i\boldsymbol{A}_i(n+1)\boldsymbol{x}_i(n+1)+\grave{\boldsymbol{R}}_i\boldsymbol{A}_i(n-1)\boldsymbol{x}_i(n-1)+\bar{\boldsymbol{w}}_i(n), \tag{4.64}$$

where matrix $\boldsymbol{R}_i$ is as defined in (4.17) with off-diagonal elements equal to ρ, $\bar{\bar{\boldsymbol{R}}}_i = \boldsymbol{R}_i^{-1}\bar{\boldsymbol{R}}_i$, $\acute{\boldsymbol{R}}_i = \boldsymbol{R}_i^{-1}\tilde{\boldsymbol{R}}_i^T$, $\grave{\boldsymbol{R}}_i = \boldsymbol{R}_i^{-1}\tilde{\boldsymbol{R}}_i$ and $\bar{\boldsymbol{w}}_i(n) = \boldsymbol{R}_i^{-1}\hat{\boldsymbol{w}}_i(n)$ is defined as

$$E\left[\bar{\boldsymbol{w}}_i(n)\bar{\boldsymbol{w}}_i^H(n+l)\right] = \begin{cases} N_0\acute{\boldsymbol{R}}_i\boldsymbol{R}_i^{-T}, & \text{if } l=1 \\ N_0\bar{\bar{\boldsymbol{R}}}_i\boldsymbol{R}_i^{-T}, & \text{if } l=0 \\ N_0\grave{\boldsymbol{R}}_i\boldsymbol{R}_i^{-T}, & \text{if } l=-1 \\ 0, & \text{otherwise} \end{cases}. \tag{4.65}$$

Hence, the soft symbol of x_j detected at node S_i at the of output of the j^{th} MFB branch is expressed as

$$\begin{aligned} \hat{\mathcal{Y}}_{i,j}(n) = \sum_{\substack{m=1 \\ m\neq i}}^{N} a_{i,m}(n)\bar{\bar{r}}_{j,m}x_m(n) + \sum_{\substack{m=1 \\ m\neq i}}^{N} a_{i,m}(n+1)\acute{r}_{j,m}x_m(n+1) \\ + \sum_{\substack{m=1 \\ m\neq i}}^{N} a_{i,m}(n-1)\grave{r}_{j,m}x_m(n-1) + \bar{w}_{i,j}(n), \end{aligned} \tag{4.66}$$

where $\bar{\bar{r}}_{j,m}$, $\acute{r}_{j,m}$ and $\grave{r}_{j,m}$ are the $(j,m)^{th}$ elements of the matrices $\bar{\bar{\boldsymbol{R}}}_i$, $\acute{\boldsymbol{R}}_i$ and $\grave{\boldsymbol{R}}_i$, respectively. Moreover, the correlated noise $\bar{w}_{i,j}(n) \sim \mathcal{CN}(0, N_0\bar{r}_{i,j})$ and $\bar{r}_{i,j}$ is the corresponding j^{th} diagonal element of the matrix $\bar{\bar{\boldsymbol{R}}}_i\boldsymbol{R}_i^{-T} = \boldsymbol{R}_i^{-1}\bar{\boldsymbol{R}}_i\boldsymbol{R}_i^{-T}$.

As discussed in Section (4.4), the detected symbol $\hat{x}_j^i(n)$ at node S_i can be obtained based on the detection state of the symbol $x_j^i(n)$. As before, it is assumed that the receiving node knows the decoding correctness (i.e. the detection state) at the other nodes. Thus, if $a_{i,j}(n) = 0$ (i.e. $|\mathcal{I}_j^i(n)| = 0$, then $\hat{x}_j^i(n) = e^{-j\phi_{j,i}} y_{j,i}(n)$). However, for $|\mathcal{I}_j^i(n)| > 0$, then the combined the signals receiving in the Broadcasting and Cooperation Phases is $\hat{x}_j^i(n) = e^{-j\phi_{j,i}} y_{j,i}(n) + \hat{\mathcal{Y}}_{i,j}(n)$, which yields

$$\hat{x}_j^i(n) = \left(|h_{j,i}| \sqrt{P_{s_j}} + a_{i,j}(n) \bar{\bar{r}}_{j,j} \right) x_j(n) + \hat{\eta}_{i,j}(n), \tag{4.67}$$

where

$$\begin{aligned} \hat{\eta}_{i,j}(n) = \sum_{\substack{m=1 \\ m \neq i, m \neq j}}^{N} a_{i,m}(n) \bar{\bar{r}}_{j,m} x_m(n) + \sum_{\substack{m=1 \\ m \neq i}}^{N} a_{i,m}(n+1) \acute{r}_{j,m} x_m(n+1) \\ + \sum_{\substack{m=1 \\ m \neq i}}^{N} a_{i,m}(n-1) \grave{r}_{j,m} x_m(n-1) + e^{-j\phi_{j,i}} n_{j,i}(n) + \bar{w}_{i,j}(n), \end{aligned} \tag{4.68}$$

is the equivalent noise plus interference term. In order to determine the conditional signal-to-noise ratio, the detection state at node S_i for the different intersymbol interference symbols must also be taken into consideration. In particular, the detection states $\mathcal{I}_m^i(n+l)$ for $m \neq i$ and $l \in \{-1, 0, 1\}$ must be considered. Thus, the conditional *instantaneous* signal-to-noise ratio given the detection states $\mathcal{I}_j^i(n)$ and $\mathcal{I}_m^i(n+l)$ of the combined data symbol $\hat{x}_j^i(n)$ at node S_i can be verified to be

$$\begin{aligned} &\gamma_{j|\mathcal{I}^i}^i(n) \\ &= \begin{cases} \frac{|h_{j,i}|^2 P_{s_j}}{N_0}, & \text{if } |\mathcal{I}_j^i(n)| = 0, \\ \frac{\bar{\bar{\mathcal{H}}}_{i,j}^2(n)}{\Xi_j^i(n) + (1 + \bar{\bar{r}}_{i,j}) N_0}, & \text{if } |\mathcal{I}_j^i(n)| > 0,\ |\mathcal{I}_m^i(n+l)| \geq 0, \forall m \in \{1, 2, \ldots, N\}_{m \neq i} \text{ and } l \in \{-1, 0, 1\}, \end{cases} \end{aligned} \tag{4.69}$$

where

$$\bar{\bar{\mathcal{H}}}^2_{i,j}(n) = \left(\sqrt{P_{s_j}}|h_{j,i}| + \bar{\bar{r}}_{j,j} \sum_{\substack{k=1 \\ k\neq i, k\neq j}}^{N} |h_{k,i}|\sqrt{P_{j,k}}\mathcal{I}_{j,k}(n) \right)^2 , \tag{4.70}$$

and

$$\Xi^i_j(n) = \sum_{\substack{m=1 \\ m\neq i, m\neq j}}^{N} \left(a_{i,m}(n)\bar{\bar{r}}_{j,m}\right)^2 + \sum_{\substack{m=1 \\ m\neq i}}^{N} \left(a_{i,m}(n+1)\acute{r}_{j,m}\right)^2 + \sum_{\substack{m=1 \\ m\neq i}}^{N} \left(a_{i,m}(n-1)\grave{r}_{j,m}\right)^2 , \tag{4.71}$$

with the assumption that

$$E\left[x_m(n)x_k(n+l)\right] = \begin{cases} 1, & \text{if } l = 0 \text{ and } m = k \\ 0, & \text{otherwise} \end{cases} . \tag{4.72}$$

That is, the data symbols are statistically independent. It is noteworthy that in the absence of the ISI, the conditional SNR expression in (4.69) reduces to that of (4.25).

4.7.2 SER Performance Analysis with Synchronization Errors

In this subsection, a theoretical analysis of the SER performance with synchronization errors is provided. The following performance analysis is aimed at defining the worst case SER performance that results as a consequence of the imperfect timing synchronization; and thus defines the STNC theoretical performance limits as a guideline for network design. In other words, since perfect synchronization is practically difficult, the effects of the timing synchronization errors on the performance of nodes communicating under the STNC scheme must be analyzed and quantified.

The analysis starts by assuming that $\rho_{i,j} = \rho$ for all $j \neq i$, as before. It is extremely difficult to obtain a closed form SER expression by averaging over all the uniformly distributed time-shifts; so, the SER performance due to timing synchro-

nization errors is analyzed by fixing $|\Delta_i - \tau_{i,m}| = \Delta T_s/2,\ \forall m \in \{1, 2, \ldots, N\}_{i \neq m}$. That is, the time-shift due to each node $m \neq i$ is set at its average value. From (4.56 - 4.58), the correlation coefficients reduce to $\tilde{\rho}_{m,j}^{(-1)} = \tilde{\rho}_{m,j}^{(1)} \triangleq \tilde{\rho}$; while $\bar{\rho}_{m,j}^{(0)} \triangleq \bar{\rho}$. Therefore, the matrices $\bar{\boldsymbol{R}}_i$ and $\tilde{\boldsymbol{R}}_i$ can be written as

$$\bar{\boldsymbol{R}}_i = \begin{bmatrix} 1 & \cdots & \bar{\rho} & \bar{\rho} & \cdots & \bar{\rho} \\ \vdots & \ddots & \vdots & \vdots & \cdots & \vdots \\ \bar{\rho} & \cdots & 1 & \bar{\rho} & \cdots & \bar{\rho} \\ \bar{\rho} & \cdots & \bar{\rho} & 1 & \cdots & \bar{\rho} \\ \vdots & \cdots & \vdots & \vdots & \ddots & \vdots \\ \bar{\rho} & \cdots & \bar{\rho} & \bar{\rho} & \cdots & 1 \end{bmatrix}, \tag{4.73}$$

and

$$\tilde{\boldsymbol{R}}_i = \begin{bmatrix} 0 & \cdots & \tilde{\rho} & \tilde{\rho} & \cdots & \tilde{\rho} \\ \vdots & \ddots & \vdots & \vdots & \cdots & \vdots \\ 0 & \cdots & 0 & \tilde{\rho} & \cdots & \tilde{\rho} \\ 0 & \cdots & 0 & 0 & \cdots & \tilde{\rho} \\ \vdots & \cdots & \vdots & \vdots & \ddots & \vdots \\ 0 & \cdots & 0 & 0 & \cdots & 0 \end{bmatrix}, \tag{4.74}$$

respectively. Due to the symmetry of the matrices $\boldsymbol{R}_i$, $\bar{\boldsymbol{R}}_i$ and $\tilde{\boldsymbol{R}}_i$, the j^{th} diagonal element of the matrix $\boldsymbol{R}_i^{-1}\bar{\boldsymbol{R}}_i\boldsymbol{R}_i^{-T}$ in (4.66) can be defined as $\bar{r}_{i,j} = \bar{r}_{N-1}$ and the $\bar{\bar{r}}_{j,j}$ in (4.70) can also be defined for convenience as $\bar{\bar{r}}_{N-1}$.

In order to evaluate the symbol error rate performance for the STNC scheme with timing synchronization errors, the terms $\bar{\bar{\mathcal{H}}}_{i,j}^2(n)$ and $\Xi_j^i(n)$ in the conditional instantaneous SNR $\gamma_{j|\mathcal{I}^i}^i(n)$ expression given in (4.69), must averaged over the channel

statistics. In particular, the following two cases are considered.

1. $N = 3$: It is straightforward to show that $\bar{\bar{\mathcal{H}}}^2_{i,j}(n)$ can be expanded as

$$\begin{aligned}\bar{\bar{\mathcal{H}}}^2_{i,j}(n) &= \left(\sqrt{P_{s_j}}|h_{j,i}| + \bar{\bar{r}}_{N-1}|h_{k,i}|\sqrt{P_{j,k}}\mathcal{I}_{j,k}(n)\right)^2 \\ &= \underbrace{P_{s_j}|h_{j,i}|^2 + \bar{\bar{r}}^2_{N-1}P_{j,k}|h_{k,i}|^2\mathcal{I}_{j,k}(n)}_{\mathcal{E}^i_j = \text{Exponential Random Variables}} + \underbrace{2\bar{\bar{r}}_{N-1}\sqrt{P_{s_j}P_{j,k}}|h_{j,i}||h_{k,i}|\mathcal{I}_{j,k}(n)}_{\mathcal{R}^i_j = \text{Double-Rayleigh Random Variable}},\end{aligned} \tag{4.75}$$

for $k \neq i$ and $k \neq j$. Note that in the right hand side of (4.75), the first two terms are weighted exponential random variables while the last term is a weighted double Rayleigh random variable. On the other hand, the term $a^2_{i,m}(n+l)$ for $l \in \{-1, 0, 1\}$ in $\Xi^i_j(n)$ (given in (4.71)), reduces to $a^2_{i,m}(n+l) = |h_{k,i}|^2 P_{m,k}\mathcal{I}_{m,k}(n+l)$. Therefore, the denominator of the second case in (4.69) is nothing but a weighted sum of exponential random variables with a shift in the mean of $(1 + \bar{r}_{N-1})N_0$, where $\bar{r}_{N-1}$ is the diagonal element of the matrix $\boldsymbol{R}_i^{-1}\bar{\boldsymbol{R}}_i\boldsymbol{R}_i^{-T}$.

2. $N \geq 4$: The term $\bar{\bar{\mathcal{H}}}^2_{i,j}(n)$ can be expressed as follows

$$\begin{aligned}\bar{\bar{\mathcal{H}}}^2_{i,j}(n) = \underbrace{|h_{j,i}|^2 P_{s_j} + \bar{\bar{r}}^2_{N-1}\sum_{\substack{k=1\\k\neq i,k\neq j}}^{N}|h_{k,i}|^2 P_{j,k}\mathcal{I}_{j,k}(n) +}_{\mathcal{E}^i_j = \text{Exponential Random Variables}} \\ \underbrace{\bar{\bar{r}}^2_{N-1}\sum_{\substack{m=1\\m\neq i,m\neq j}}^{N}\sum_{\substack{k=1,k\neq m\\k\neq i,k\neq j}}^{N}|h_{m,i}||h_{k,i}|\sqrt{P_{j,m}P_{j,k}}\mathcal{I}_{j,m}(n)\mathcal{I}_{j,k}(n) + 2\bar{\bar{r}}_{N-1}\sum_{\substack{k=1\\k\neq i,k\neq j}}^{N}\sqrt{P_{s_j}P_{j,k}}|h_{j,i}||h_{k,i}|\mathcal{I}_{j,k}(n)}_{\mathcal{R}^i_j = \text{Double-Rayleigh Random Variables}}.\end{aligned} \tag{4.76}$$

The terms of the form $a^2_{i,m}(n+l) = \left(\sum^{N}_{\substack{k=1\\k\neq i,k\neq m}}|h_{k,i}|\sqrt{P_{m,k}}\mathcal{I}_{m,k}(n+l)\right)^2$ for $l \in \{-1, 0, 1\}$ in (4.71) can be expanded as

$$a_{i,m}^2(n+l) = \sum_{\substack{k=1 \\ k\neq i,k\neq m}}^{N} |h_{k,i}|^2 P_{m,k}\mathcal{I}_{m,k}(n+l) + \sum_{\substack{p=1 \\ p\neq i,p\neq m}}^{N} \sum_{\substack{q=1,q\neq p \\ q\neq i,q\neq m}}^{N} |h_{p,i}||h_{q,i}|\sqrt{P_{m,p}P_{m,q}}\mathcal{I}_{m,p}(n+l)\mathcal{I}_{m,q}(n+l), \tag{4.77}$$

which is a weighted sum of exponential and double Rayleigh random variables. Finding the distribution for sums of form of $a_{i,m}^2(n+l)$ is extremely difficult. However, using the argument of the mathematical inequality of the arithmetic and geometric means [57], every term in the form of $|h_{m,i}||h_{k,i}|\sqrt{P_{j,m}P_{j,k}} = \sqrt{|h_{m,i}|^2|h_{k,i}|^2 P_{j,m}P_{j,k}}$ can be upper-bounded as

$$P_{j,m}|h_{m,i}|^2 + P_{j,k}|h_{k,i}|^2 \geq \sqrt{|h_{m,i}|^2|h_{k,i}|^2 P_{j,m}P_{j,k}}. \tag{4.78}$$

Thus, the term $a_{i,m}^2(n+l) = \left(\sum_{\substack{k=1 \\ k\neq i,k\neq m}}^{N} |h_{k,i}|\sqrt{P_{m,k}}\mathcal{I}_{m,k}(n+l)\right)^2$ can be expanded and upper-bounded as

$$\begin{aligned} a_{i,m}^2(n+l) &\leq \sum_{\substack{k=1 \\ k\neq i,k\neq m}}^{N} |h_{k,i}|^2 P_{m,k}\mathcal{I}_{m,k}(n+l) + \\ &\qquad \sum_{\substack{p=1 \\ p\neq i,p\neq m}}^{N} \sum_{\substack{q=1,q\neq p \\ q\neq i,q\neq m}}^{N} \left(P_{m,p}|h_{p,i}|^2 + P_{m,q}|h_{q,i}|^2\right)\mathcal{I}_{m,p}(n+l)\mathcal{I}_{m,q}(n+l) \\ &\triangleq \bar{a}_{i,m}^2(n+l), \end{aligned} \tag{4.79}$$

which is a sum of at most $2(N-2)^2$ weighted distinct exponential random variables. This in turn implies that

$$\Xi_j^i(n) \lesssim \sum_{\substack{m=1 \\ m\neq i,m\neq j}}^{N} \left(\bar{a}_{i,m}(n)\bar{\bar{r}}_{j,m}\right)^2 + \sum_{\substack{m=1 \\ m\neq i}}^{N} \left(\bar{a}_{i,m}(n+1)\acute{r}_{j,m}\right)^2 + \sum_{\substack{m=1 \\ m\neq i}}^{N} \left(\bar{a}_{i,m}(n-1)\grave{r}_{j,m}\right)^2, \tag{4.80}$$

is a weighted sum of exponential random variables and upper-bounds the expression of $\Xi_j^i(n)$ given in (4.71) for $N \geq 4$. Therefore, for $N \geq 4$, the derived SER acts as a lower-bound for the performance of the STNC scheme with timing synchronization errors.

It should be noted that for the first case when $|\mathcal{I}^i(n)| = 0$, it is similar to that given in (4.31). However, in order to determine the conditional SER for the the second case, define for convenience the set of detection states $\Lambda_j^i(n)$ as

$$\Lambda_j^i(n) = \{|\mathcal{I}_j^i(n)| > 0, |\mathcal{I}_m^i(n+l)| \geq 0, \forall m \in \{1, 2, \ldots, N\}_{m \neq i} \text{ and } l \in \{-1, 0, 1\}\}. \tag{4.81}$$

From this point onwards, the time index n is dropped to simplify notation. Now, the conditional SER can be expressed as

$$\Psi_{|\{h\}}(\gamma^i_{j||\Lambda_j^i|>0}) = \frac{1}{\pi}\int_0^{(M-1)\pi/M} \exp\left(-\frac{b_{PSK}}{\sin^2\theta}\left(\mathbb{E}_j^i + \mathbb{R}_j^i\right)\right)\, d\theta, \tag{4.82}$$

where

$$\mathbb{E}_j^i = \frac{\mathcal{E}_j^i}{\Xi_j^i + (1+\bar{r}_{N-1})N_0}, \tag{4.83}$$

and

$$\mathbb{R}_j^i = \frac{\mathcal{R}_j^i}{\Xi_j^i + (1+\bar{r}_{N-1})N_0}. \tag{4.84}$$

The term in (4.83) is a ratio of a sum of exponential random variables to a sum of exponential random variables with a shift in the mean of $(1+\bar{r}_{N-1})N_0$; while (4.84) is a ratio of a sum of double Rayleigh random variables to a sum of exponential random variables with a shift in the mean of $(1+\bar{r}_{N-1})N_0$.

Upon averaging the expression in (4.82) over the channel statistics, it can be shown to be

$$\Psi(\gamma^i_{j||\Lambda_j^i|>0}) = \frac{1}{\pi}\int_0^{(M-1)\pi/M} \Psi_{\mathbb{E}^i_{j||\Lambda_j^i|>0}}(\gamma^i_{j||\Lambda_j^i|>0})\Psi_{\mathbb{R}^i_{j||\Lambda_j^i|>0}}(\gamma^i_{j||\Lambda_j^i|>0})\, d\theta, \tag{4.85}$$

where $\Psi_{\mathbb{E}^i_{j||\Lambda^i_j|>0}}(\gamma^i_{j||\Lambda^i_j|>0})$ can be determined with the aid of (4.102) and (4.104) in Appendix III as

$$\Psi_{\mathbb{E}^i_{j||\Lambda^i_j|>0}}(\gamma^i_{j||\Lambda^i_j|>0}) = U\left(\frac{b_{PSK}P_{s_j}}{\sin^2(\theta)}, \sigma^2_{j,i}, \Xi^i_j, |\Lambda^i_j|, (1+\bar{r}_{N-1})N_0\right) \times \prod_{\substack{k=1 \\ k\neq i, k\neq j}}^{N} \bar{U}\left(\frac{\bar{\bar{r}}^2_{N-1}b_{PSK}P_{j,k}}{\sin^2(\theta)}, \sigma^2_{k,i}, \Xi^i_j, |\Lambda^i_j|, (1+\bar{r}_{N-1})N_0, \mathcal{I}_{j,k}\right), \tag{4.86}$$

where

$$\bar{U}\left(\frac{\bar{\bar{r}}^2_{N-1}b_{PSK}P_{j,k}}{\sin^2(\theta)}, \sigma^2_{k,i}, \Xi^i_j, |\Lambda^i_j|, (1+\bar{r}_{N-1})N_0, \mathcal{I}_{j,k}\right) = \begin{cases} U\left(\frac{\bar{\bar{r}}^2_{N-1}b_{PSK}P_{j,k}}{\sin^2(\theta)}, \sigma^2_{k,i}, \Xi^i_j, |\Lambda^i_j|, (1+\bar{r}_{N-1})N_0\right), & \text{if } \mathcal{I}_{j,k}=1 \\ 1, & \text{otherwise} \end{cases}. \tag{4.87}$$

Also,

$$U\left(\frac{\bar{\bar{r}}^2_{N-1}b_{PSK}P_{j,k}}{\sin^2(\theta)}, \sigma^2_{k,i}, \Xi^i_j, |\Lambda^i_j|, (1+\bar{r}_{N-1})N_0\right) = \sum_{u=1}^{|\Lambda^i_j|} \frac{\mu_u}{\lambda_u}\left(\lambda_u - \frac{\bar{\bar{r}}^2_{N-1}\sigma^2_{k,i}b_{PSK}P_{j,k}}{\sin^2(\theta)} \exp\left(\frac{(1+\bar{r}_{N-1})N_0 + \frac{\bar{\bar{r}}^2_{N-1}\sigma^2_{k,i}b_{PSK}P_{j,k}}{\sin^2(\theta)}}{\lambda_u}\right)\Gamma\left(0, \frac{(1+\bar{r}_{N-1})N_0 + \frac{\bar{\bar{r}}^2_{N-1}\sigma^2_{j,i}b_{PSK}P_{j,k}}{\sin^2(\theta)}}{\lambda_h}\right)\right), \tag{4.88}$$

where λ_u for $u \in \{1, 2, \ldots, |\Lambda^i_j|\}$ are the rates of the distinct exponential random variables in the sum term $\bar{\Xi}^i_j$, $\mu_u = \prod_{q=1, q\neq u}^{|\Lambda^i_j|} \frac{\lambda_u}{\lambda_u - \lambda_q}$ and $\Gamma(a, \xi)$ is the incomplete Gamma function and is expressed as [55]

$$\Gamma(a, \xi) = \int_{\xi}^{\infty} t^{a-1}e^{-t}\, dt. \tag{4.89}$$

In addition, the term $\Psi_{\mathbb{R}^i_{j||\Lambda^i_j|>0}}(\gamma^i_{j||\Lambda^i_j|>0})$ can be written with the aid of (4.109 - 4.110) in Appendix III as

$$\Psi_{\mathcal{R}^i_{j||\Lambda^i_j|>0}}(\gamma^i_{j||\Lambda^i_j|>0})$$
$$= \prod_{\substack{m=1\\ m\neq i, m\neq j}}^{N} \prod_{\substack{k=1, k\neq m\\ k\neq i, k\neq j}}^{N} \bar{R}\left(\frac{\bar{\bar{r}}^2_{N-1} b_{PSK}\sqrt{P_{j,m}P_{j,k}}}{\sin^2\theta}, {}_i\Omega^2_{m,k}, \Xi^i_j, N, (1+\bar{r}_{N-1})N_0, \mathcal{I}_{j,m}\mathcal{I}_{j,k}\right) \times$$
$$\left(\prod_{\substack{k=1\\ k\neq i, k\neq j}}^{N} \bar{R}\left(\frac{2\bar{\bar{r}}_{N-1} b_{PSK}\sqrt{P_{s_j}P_{j,k}}}{\sin^2\theta}, {}_i\Omega^2_{j,k}, \Xi^i_j, N, (1+\bar{r}_{N-1})N_0, \mathcal{I}_{j,k}\right)\right), \tag{4.90}$$

where ${}_i\Omega^2_{m,k} = \Omega^2_{m,i}\Omega^2_{k,i} = \sigma^2_{m,i}\sigma^2_{k,i}/4$, ${}_i\Omega^2_{j,k} = \Omega^2_{j,i}\Omega^2_{k,i} = \sigma^2_{j,i}\sigma^2_{k,i}/4$ and in general

$$\bar{R}(w(\theta), \Omega^2, X, N, c, \mathcal{I})$$
$$= \begin{cases} \int_0^\infty \exp(-w(\theta)z)\left(\sum_{i=1}^N \frac{\mu_i}{\lambda_i}\int_0^\infty \exp\left(-\frac{x}{\lambda_i}\right)\frac{(x+c)^2 z}{\Omega^2}K_0\left(\frac{(x+c)z}{\Omega}\right)\,dx\right)\,dz, & \text{if } \mathcal{I}=1 \\ 1, & \text{otherwise} \end{cases}, \tag{4.91}$$

where X is a sum of distinct exponential random variables, c is some constant, Ω^2 represents the channel variances and is the indicator function $\mathcal{I}$.

Given the collective detection states $\mathcal{I}^i_j$ and Λ^i_j, the SER for detecting the data symbol x_j at node S_i with synchronization errors can be calculated using (4.42) as

$$P^j_{SER} \lesssim \Psi(\gamma^i_{j||\mathcal{I}^i_j|=0}) \cdot \Pr(|\mathcal{I}^i_j| = 0) + \sum_{\ell=1}^{|\Lambda^i_j|-1} \Psi(\gamma^i_{j||\Lambda^i_j|>0}) \cdot \Pr(|\Lambda^i_j| = \ell), \tag{4.92}$$

where $\Psi(\gamma^i_{j||\mathcal{I}^i_j|=0})$ and $\Psi(\gamma^i_{j||\Lambda^i_j|>0})$ are defined in (4.31) and (4.85), respectively. As discussed, P^j_{SER} happens to be exact for $N = 3$ and a lower-bound for $N \geqslant 4$.

4.8 Performance Evaluation

4.8.1 SER Performance with Perfect Synchronization

In this subsection, the simulated SER performance and the theoretical exact and upper-bound SER expressions of the STNC scheme with $N = 3$ and $N = 4$

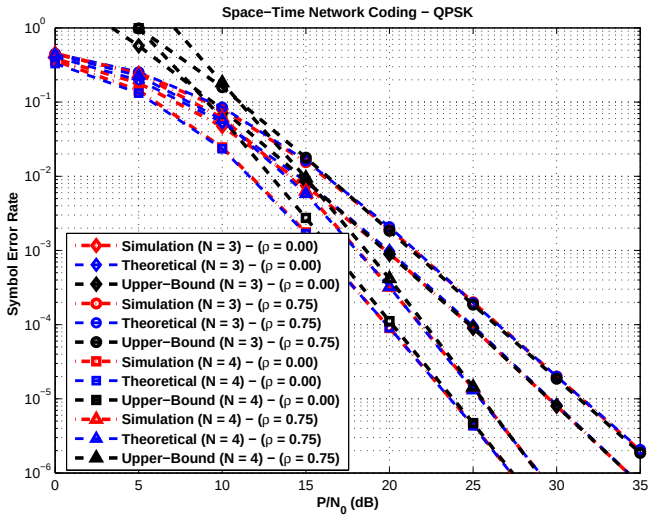

Figure 4.2: QPSK SER Performance of the Space-Time Network Coding Scheme for $N = 3$ and $N = 4$ Nodes - Symmetric Network with Perfect Timing Synchronization

nodes are evaluated. In particular, the SER performance for the symbol x_2 received at node S_1 is evaluated. Perfect synchronization is assumed between the nodes in the network.

In order to validate the derived exact SER and upper-bound expressions, the following two network scenarios are considered.

1. Symmetric Network: In this network scenario, all the channel coefficients are i.i.d. with equal unity gain (i.e. $h_{i,j} \backsim \mathcal{CN}(0,1)$, $\forall i,j \in \{1,2,\ldots,N\}$ and $i \neq j$).

   It is clear from Fig. 4.2, that the simulated SER performance agrees perfectly with derived exact SER performance. It can also be seen that as the number of nodes increases, the performance improves. This is due to the fact that with the increase in N (i.e. the number of nodes), higher diversity gains are

achieved. In addition, it is noticed that the best SER performance is achieved when $\rho = 0$, that is the signature waveforms are perfectly orthogonal and there is no interference between the nodes. However, when $\rho = 0.75$, there is about 2 dB SER performance degradation. This in turn signifies the importance of the STNC scheme as it allows N nodes to communicate simultaneously and achieves $N-1$ diversity order with only a slight degradation for non-orthogonal signature waveforms. It is further observed that the derived upper-bound asymptotically matches the simulated SER performance, at high SNR. This is due to the fact that the channel gains are identical, which is the assumption upon which the upper-bound has been derived.

2. Asymmetric Network: In this network scenario, asymmetric channel gains are assumed in order to verify the derived exact SER and upper-bound expressions. For example, let the channel gains between the odd-indexed nodes in the network be 2; while the channel gains between the even-indexed nodes be 1. Also, the channel gains between the odd- and even-indexed nodes take the value of 1/2. This scenario implies that the even-indexed nodes are placed closer to each other; while the odd-indexed nodes are placed farther apart.

   It is evident from Fig. 4.3 that the derived exact SER expression coincides with the simulated SER performance for the case of $\rho = 0.00$ (i.e. orthogonal signature waveforms). Furthermore, it can be seen that the simulation results for the asymmetric network are upper-bounded by the theoretical derivation of the upper-bound obtained for the symmetric network. The same observation also applies to Fig. 4.4 for the asymmetric network with $\rho = 0.75$.

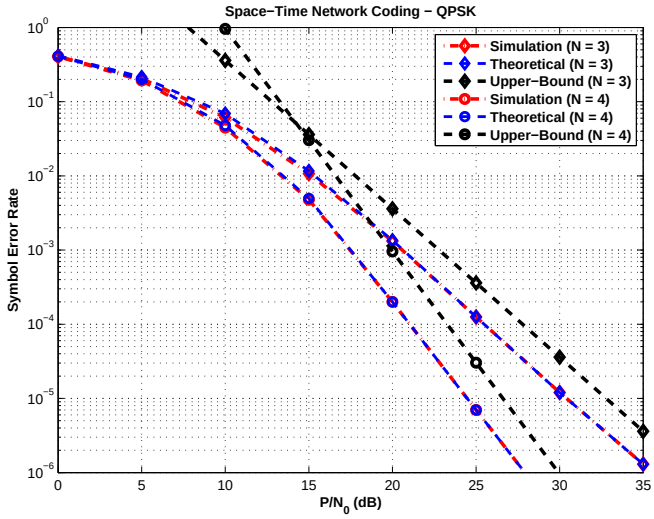

Figure 4.3: QPSK SER Performance of the Space-Time Network Coding Scheme for $N = 3$ and $N = 4$ Nodes - Asymmetric Network with Perfect Timing Synchronization and $\rho = 0.00$

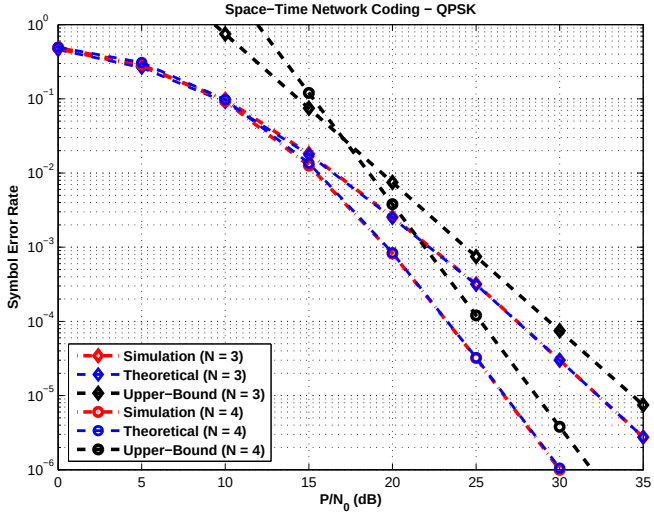

Figure 4.4: QPSK SER Performance of the Space-Time Network Coding Scheme for $N = 3$ and $N = 4$ Nodes - Asymmetric Network with Perfect Timing Synchronization and $\rho = 0.75$

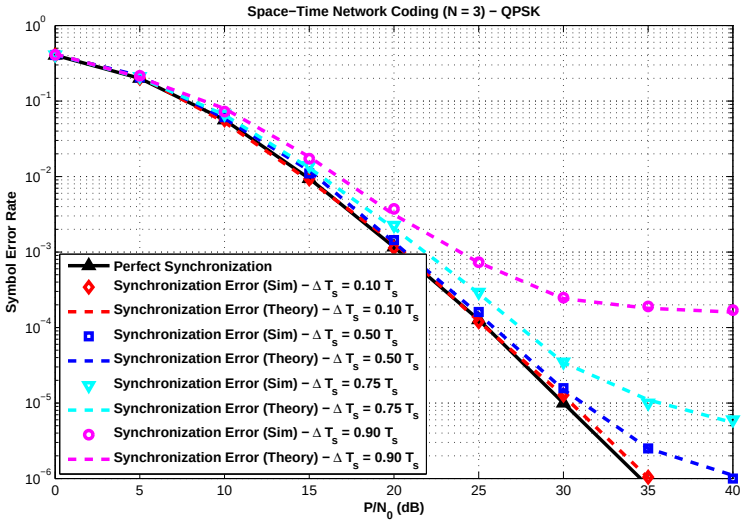

Figure 4.5: QPSK SER Performance of the Space-Time Network Coding Scheme for $N = 3$ Nodes - Symmetric Network with Imperfect Timing Synchronization and $\rho = 0.50$

4.8.2 SER Performance with Timing Synchronization Errors

This subsection presents the SER performance of the STNC scheme for $N = 3$ and $N = 4$ for different timing synchronization errors ΔT_s as well as the derived theoretical expressions. In the following simulations, it is assumed that all the channel coefficients are i.i.d. with equal unity gain (i.e. a symmetric network) and the correlation coefficient of the signature waveforms has a value of $\rho = 0.50$.

It is evident from Fig. 4.5 that the SER performance of the STNC scheme for $N = 3$ degrades as the timing synchronization error ΔT_s increases, as expected. Moreover, for $\Delta T_s = 0.90\ T_s$, the STNC scheme suffers from an irreducible error floor of approximately 1.8×10^{-4}. This illustrates that the STNC scheme is resilient against timing synchronization errors as compared with the conventional cooperative networks [59] [60]. It can also be seen that the derived theoretical SER performance

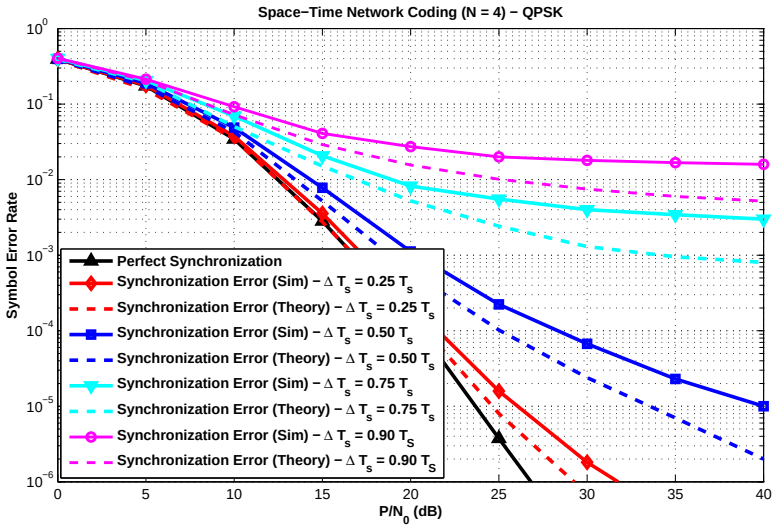

Figure 4.6: QPSK SER Performance of the Space-Time Network Coding Scheme for $N = 4$ Nodes - Symmetric Network with Imperfect Timing Synchronization and $\rho = 0.50$

coincides with the simulation results.

In Fig. 4.6, it is clear that the SER performance of the STNC for $N = 4$ suffers from high irreducible errors floor for $\Delta T_s \geq 0.5\ T_s$ and the performance is severely degraded. This is because the increase in number of nodes results in higher synchronization errors which is reflected in a severe intersymbol interference and thus a severe performance degradation. It can also be seen in Fig. 4.6, that the derived theoretical lower-bound agrees with the the simulated SER performance.

By comparing Figs. 4.5 and 4.6, it is evident that the performance of the STNC for a network with $N = 4$ nodes with $\Delta T_s = 0.25\ T_s$ outperforms that of a network with $N = 3$ nodes and $\Delta T_S = 0.10\ T_s$. Moreover, the SER performance of a network with $N = 3$ nodes and $\Delta T_S = 0.75\ T_s$ is comparable to that of $N = 4$ nodes and $\Delta T_s = 0.50\ T_s$.

Based on the above discussion, it is clear that there is a tradeoff between the number of nodes and the worst-case timing synchronization errors. Thus, the derived analytical exact and lower-bound expressions should serve a network design guideline upon which the performance limits can be determined given the number of nodes N as well as the worst case scenario timing synchronization error ΔT_s.

4.9 Conclusions

In this chapter, the novel Space-Time Network Coding (STNC) scheme that allows N nodes to exchange their data symbols over a total of $2N$ time-slots, was presented. The exact and asymptotic SER expressions for an arbitrary number N of nodes were derived and it was shown that under perfect synchronization, each node achieved a full diversity order of $N-1$. Moreover, it was shown that the theoretical upper-bound derivation for symmetric networks agrees with the SER performance of asymmetric networks. Furthermore, an exact theoretical analysis on the effects of timing synchronization errors has been presented for $N = 3$ nodes and the performance limits due to such errors have been analytically characterized with a lower bound on the SER performance for $N \geq 4$ which serves as a network design guideline. Finally, it is concluded that the STNC serves as a potential many-to-many cooperative communication scheme and its scope goes much further beyond the generic source-relay-destination communications.

4.10 Appendix I

4.10.1 Derivation

Let Y be an exponentially distributed random variable with probability density function

$$f_Y(y) = \frac{1}{\lambda} \exp\left(-\frac{y}{\lambda}\right), \quad y \geq 0, \tag{4.93}$$

where λ is the rate parameter. In general, averaging the function $\exp(-w(\theta)y)$ over the distribution of the exponential random variable Y, yields

$$G(w(\theta), \lambda) = \int_0^\infty \exp\left(-w(\theta)y\right) \left(\frac{1}{\lambda}\right) \exp\left(-\frac{y}{\lambda}\right) \, dy = \frac{1}{1 + w(\theta)\lambda}, \tag{4.94}$$

where $w(\theta)$ is some function of θ.

4.10.2 Upper-Bound Approximation

For large values of $w(\theta)$, denominator of $G(w(\theta), \lambda)$ can be approximated as $1 + w(\theta)\lambda \approx w(\theta)\lambda$; thus

$$\tilde{G}(w(\theta), \lambda) \lesssim \frac{1}{w(\theta)\lambda}. \tag{4.95}$$

4.11 Appendix II

The approximate conditional SNR can be shown to be

$$\begin{aligned} I_L\left(\xi, \phi\right) &= \frac{1}{\pi} \int_0^\phi \left(\frac{\sin^2 \phi}{\sin^2 \phi + \xi}\right)^L \, d\phi \\ &= \frac{(1/\xi)^L (\sin(\phi))^{2L+1}}{\pi(2L+1)} F_1\left(L + \frac{1}{2}, \frac{1}{2}, L, L + \frac{3}{2}, \sin^2(\phi), -\frac{\sin^2(\phi)}{\xi}\right), \end{aligned} \tag{4.96}$$

where

$$F_1\left(\alpha; \beta, \beta'; \zeta; x, y\right) = \sum_{m=0}^{\infty} \sum_{n=0}^{\infty} \frac{(\alpha)_{m+n} (\beta)_m (\beta')_n}{m! n! (\zeta)_{m+n}} x^m y^n, \tag{4.97}$$

is the Appell hypergeometric function of the first kind [56]. It can be shown that for $y \to 0$, the Appell hypergeometric function can be approximated as [56]

$$F_1\left(\alpha;\beta,\beta';\zeta;x,y\right) \approx {}_2F_1\left(\alpha,\beta,\gamma;x\right), \tag{4.98}$$

where ${}_2F_1\left(\alpha,\beta;\gamma;x\right)$ is the hypergeometric function [55].

4.12 Appendix III

4.12.1 Quotient of an Exponential Random Variable to a Weighted Sum of Exponential Random Variables

Let Y be an exponentially distributed random variable as defined in (4.93). Also, let X be a random variable representing a weighted sum of N *distinct* exponential random variables, such that $\lambda_i \neq \lambda_k$ for $i \neq k$, [66]

$$f_X(x) = \sum_{i=1}^{N} \frac{\mu_i}{\lambda_i} \exp\left(-\frac{x}{\lambda_i}\right), \quad x \geq 0, \tag{4.99}$$

where $\mu_i = \prod_{k=1,k\neq i}^{N} \frac{\lambda_i}{\lambda_i - \lambda_k}$. The pdf of the random variable $Z = \frac{Y}{(X+c)}$ for some constant c, is given by [67]

$$f_Z(z) \int_{-\infty}^{\infty} |x+c| f_X(x) f_Y((x+c)z)\ dx, \tag{4.100}$$

where $f_X(x)$ and $f_Y(y)$ are the pdf's of the random variables X and Y, respectively. Therefore, the pdf of Z can be obtained as

$$\begin{aligned} f_Z(z) &= \int_0^{\infty} (x+c) \sum_{i=1}^{N} \frac{\mu_i}{\lambda_i} \exp\left(-\frac{x}{\lambda_i}\right) \frac{1}{\lambda} \exp\left(-\frac{(x+c)z}{\lambda}\right)\ dx \\ &= \sum_{i=1}^{N} \frac{\mu_i e^{-\frac{cz}{\lambda}}}{\left(\lambda + \lambda_i z\right)^2} \left(\lambda(\lambda_i + c) + \lambda_i c z\right), \quad z \geq 0, \end{aligned} \tag{4.101}$$

As before, averaging the function $\exp(-w(\theta)z)$ over the distribution of the random variable Z, yields

$$\begin{aligned} U(w(\theta),\lambda,X,N,c) &= \int_0^\infty \exp\left(-w(\theta)z\right) \sum_{i=1}^{N} \frac{\mu_i e^{-\frac{cz}{\lambda}}}{\left(\lambda+\lambda_i z\right)^2} \left(\lambda(\lambda_i+c)+\lambda_i cz\right) dz \\ &= \sum_{i=1}^{N} \frac{\mu_i}{\lambda_i} \left(\lambda_i - \lambda w(\theta) e^{\frac{c+\lambda w(\theta)}{\lambda_i}} \Gamma\left(0, \frac{c+\lambda w(\theta)}{\lambda_i}\right)\right), \end{aligned} \tag{4.102}$$

where X is the sum of N distinct exponential random variables and $\Gamma(a,\xi)$ is the incomplete Gamma function and is expressed as [55]

$$\Gamma(a,\xi) = \int_\xi^\infty t^{a-1}e^{-t}\, dt. \tag{4.103}$$

Also, the function $U(w(\theta),\lambda,X,N,c)$ can be defined in terms of an indicator function $\mathcal{I}$ as follows

$$\bar{U}(w(\theta),\lambda,X,N,c,I) = \begin{cases} U(w(\theta),\lambda,X,N,c), & \text{if } \mathcal{I}=1 \\ \\ 1, & \text{otherwise} \end{cases}. \tag{4.104}$$

4.12.2 Quotient of a Double-Rayleigh Random Variable to a Weighted Sum of Exponential Random Variables

The product of two Rayleigh distributed random variables Y_1 and Y_2 is given by

$$Y = Y_1 \cdot Y_2, \tag{4.105}$$

where the probability density function of Y_i for $i \in \{1,2\}$ is expressed as

$$f_{Y_i}(y_i) = \frac{y_i}{\Omega_i^2} \exp\left(-\frac{y_i^2}{2\Omega_i^2}\right), \quad y_i \geq 0. \tag{4.106}$$

The distribution of the Double-Rayleigh random variable Y (or cascaded Rayleigh distribution) is obtained as [65]

$$f_Y(y) = \frac{y}{\Omega^2} K_0\left(\frac{y}{\Omega}\right), \quad y \geq 0, \tag{4.107}$$

where $K_0(\cdot)$ is the zeroth order modified Bessel function of the second kind [68] and $\Omega^2 = \prod_{i=1}^{2} \Omega_i^2$. Hence, the pdf of Z for the distinct exponential random variables can be obtained as

$$f_Z(z) = \sum_{i=1}^{N} \frac{\mu_i}{\lambda_i} \int_0^{\infty} \exp\left(-\frac{x}{\lambda_i}\right) \frac{(x+c)^2 z}{\Omega^2} K_0\left(\frac{(x+c)z}{\Omega}\right) \, dx, \quad z \geq 0, \tag{4.108}$$

for which no closed form solution exists. Again, by averaging the function $\exp(-w(\theta)z)$ over the $f_Z(z)$, the following expression is straightforwardly obtained as

$$\begin{aligned} &R(w(\theta), \Omega^2, X, N, c) \\ &= \int_0^{\infty} \exp(-w(\theta)z) \left(\sum_{i=1}^{N} \frac{\mu_i}{\lambda_i} \int_0^{\infty} \exp\left(-\frac{x}{\lambda_i}\right) \frac{(x+c)^2 z}{\Omega^2} K_0\left(\frac{(x+c)z}{\Omega}\right) \, dx \right) \, dz. \end{aligned} \tag{4.109}$$

By incorporating an indicator function $\mathcal{I}$, the term $R(w(\theta), \Omega^2, X, N, c)$ can be defined as

$$\bar{R}(w(\theta), \Omega^2, X, N, c, \mathcal{I}) = \begin{cases} R(w(\theta), \Omega^2, X, N, c), & \text{if } \mathcal{I} = 1 \\ 1, & \text{otherwise} \end{cases}. \tag{4.110}$$

.

Chapter 5

Conclusions and Future Work

5.1 Conclusions

In this thesis, the application of cooperative communications in wireless networks has been studied and analyzed. In particular, relays with the amplify-and-forward cooperative protocol have been applied in wireless sensor networks for cooperative distributed detection and data gathering. In addition, the decode-and-forward cooperative protocol has been applied in wireless networks with the aid of network coding to allow multiple terminals to exchange information between each other. More specifically, the following topics have been addressed.

In Chapter 2, the cooperative relays deployment for distributed detection in wireless sensor network has been studied. In particular, the detection error performance has been studied as function of the number of sensor/relay nodes and the correlation of measurements. It was shown that by exploiting the correlation between the measurements and appropriately deploying relays, significant detection error performance gains are achievable, as compared with the classical wireless sensor networks. In addition, under constrained total sensor network power constraint, a wireless sensor network with a fewer number of sensor nodes paired with cooperative relay nodes outperforms that of a large number of sensor nodes only.

In Chapter 3, the cognitive-cooperative relays deployment has been considered in energy-constrained wireless sensor networks for distributed detection in order to quantify the energy savings achievable by cognitively exploiting the empty/under-utilized time-slots. In particular, it was shown that with cognitive-cooperation, empty time-slots not utilized by their sensor nodes can be utilized with cognitive relays in order to amplify-and-forward measurements received from sensor nodes and thus to improve network reliability, eliminate bandwidth losses and minimize energy requirements. It was concluded that it is better to transmit a fewer number of measurements reliably via cooperation than to transmit a larger number of measurements without cooperation which in turn improves the network detection performance and also achieves energy-efficiency.

In Chapter 4, the novel concept of Space-Time Network Coding (STNC) has been introduced and analyzed. In particular, it was shown that with the STNC cooperative communication scheme, N nodes can exchange N information symbols in a total of $2N$ time-slots (i.e. $1/2$ symbol per node per channel use). Furthermore, a full cooperative diversity order of $N-1$ has been shown to be achievable for each node. Moreover, the impact of the timing synchronization errors on the STNC scheme have been analyzed and analytical expressions were derived in order to provide network designers with a guideline of the number of nodes that can participate in the information exchange and the possible performance limits due to the timing synchronization errors. It is concluded that the STNC scheme serves as a potential many-to-many cooperative communications scheme and its potentials and extensions go much further beyond than the conventional source-relay-destination cooperative communications.

5.2 Future Work

There are several potential research directions that could contribute to the advancement of cooperative communications; among which the following two problems, which are expected to be of great importance.

5.2.1 Network Coding for Data Gathering and Detection in Wireless Sensor Networks

Currently, there is a great push in the wireless research literature for developing bandwidth and energy efficient cooperative communication protocols for distributed detection in wireless sensor networks. As has been shown in this thesis, significant energy savings and detection performance gains can be achieved through the deployment of cooperative relay nodes. However, the work presented in Chapter 2 has focused on the scenario where each sensor node is paired with a neighboring relay node. This setting may not be cost effective or bandwidth efficient since each pair of sensor/relay nodes will require two time-slots to transmit their measurements to the fusion center and also because each relay serves only a single sensor node.

In the future work aimed at in this direction, the following important issues must be addressed and studied. First, what is the optimum number of sensor nodes that must be paired with each relay for optimal detection performance? In other words, the study should be focused on the tradeoff between the number of paired sensor/relay nodes, the degree of correlation, bandwidth efficiency and the detection error performance. Second, if one or more relay nodes are to serve a set of sensor nodes

within a cluster, how can the operation of the sensor/relay nodes be coordinated such that interference levels between the different transmitting nodes is reduced?

The solution to the above raised issues/questions starts be applying linear wireless network coding at each amplify-and-forward relay node with each sensor node being assigned a particular signature waveform. Each relay node then forms an optimal weighted linear combination of the different sensors' measurements, taking into account the effects of path-loss, channel fading and the degree of correlation between each of the sensor nodes. Hierarchal sensor network architectures and clustering could be employed to assign sets of sensor nodes to cooperative relay nodes.

5.2.2 Dynamic Node Selection and Optimal Power Allocation for Space-Time Network Coding

In Chapter 4, it was shown that the theoretical lower-bound performance analysis can be used as a guideline for selecting the number of network-coded nodes to cooperate for information exchange. In other words, for a particular expected timing synchronization error, the number of cooperating nodes can be selected for a target network probability of symbol error. However, in practical wireless networks, fading channels are evolving over time and the geographic locations of the nodes can be changing which in turn implies that perfect distributed timing synchronizations can be practically impossible and the expected propagation delays can be very difficult to determine due to the inaccurate nodes' location estimation.

The research work in this direction is aimed at dynamically switching and se-

lecting potential cooperative nodes for information exchange. In particular, it might be possible and practically less expensive to dynamically synchronize nodes that are in close proximity of each other as time evolves and the locations of the nodes change. This can be achieved by defining an appropriate threshold that is a function of the expected transmission delays and the approximated geographic locations of the neighboring nodes in the network. Furthermore, in Chapter 4, equal power allocation was assumed among the distributed communicating nodes. Optimal power allocation can also be pursued in order to improve the overall network performance and throughput. In addition, the expected timing synchronization errors can be taken into the formulation the dynamic optimal power allocation. Moreover, it is anticipated that with the optimal power allocation, the performance of a fewer number of communicating nodes can outperform that of a larger number of nodes with equal power allocation. Finally, the performance comparison can also be quantified in terms of the achievable data rates of each node in the network.

Bibliography

[1] K. J. Ray Liu, Ahmed K. Sadek, Weifung Su and Andreas Kwasinski, "Cooperative Communications and Networking", *Cambridge University Press*, 2008

[2] E. C. van der Meulen, "Three-Terminal communication channels", *Adv. Appl. Probab.*, 1971

[3] T. Cover and A. E. Gamal, "Capacity theorems for the relay channel", *IEEE Trans. on Information Theory*, vol. 25, no. 5, pp. 572 - 584, Sept. 1979

[4] Brett Schein and Robert G. Gallager, "The Gaussian parallel relay network", *In the Proce. IEEE Int. Symp. Information Theory (ISIT)*, page 22, June 2000.

[5] G. Kramer, M. Gatspar and P. Gupta, "Cooperative strategies and capacity theorems for relay networks", *IEEE Trans. Information Theory*, vol. 51, no. 9, pp. 3037 - 3063, Sept. 2005

[6] L. Sankaranarayanan, G. Kramer, and N. B. Mandayam, "Capacity theorems for the multiple-access relay channel", *42nd Annual Allerton Conference on Communication, Control, and Computing*, Allerton, IL, Sept 2004

[7] Piyush Gupta and P. R. Kumar, "The Capacity of Wireless Netwoks", *IEEE Trans. Inform. Theory*, vol. 46, no. 2, pp. 388 - 404, March 2002

[8] M. Gastpar and M. Vetterli, "On the capacity of wireless networks: The relay case", *In Proc. IEEE INFOCOM*, New York, NY, June 2002

[9] D. Tse and P. Viswanath, "Fundamentals of Wireless Communications", Cambridge University Press, 2005

[10] V. Tarokh, N. Seshadri and A. R. Calderbank, "Space-time codes for high data rate wireless communication: Performance criterion and code construction", *IEEE Trans. Information Theory*, vol. 44, no. 2, pp. 744 - 765, Mar. 1998

[11] S. M. Alamouti, "A simple transmit diversity technique for wireless communications", *IEEE Journal on Selected Areas in Communications*, vol. 16, no. 8, pp. 1451 - 1458, Oct. 1998

[12] G. J. Foschini and M. Gans, "On the limits of wireless communications in a fading environment when using multiple antennas", *Wireless Personal Communications*, vol. 6, pp. 311 - 335, Mar. 1998

[13] A Sendonaris, E. Erkip and B. Aazhang, "User Cooperation Diversity, Part I: System Description", IEEE Transactions on Communications, vol. 51, no. 11, pp. 1927 - 1938, Nov. 2003

[14] A Sendonaris, E. Erkip and B. Aazhang, "User Cooperation Diversity, Part II: Implementation Aspects and Performance Analysis", IEEE Transactions on Communications, vol. 51, no. 11, pp. 1939 - 1948, Nov. 2003

[15] J. N. Laneman, D. N. C. Tse and G. W. Wornell, "Cooperative Diversity in Wireless Networks: Efficient Protocols and Outage Behavior", *IEEE Transactions on Information Theory*, vol. 50, pp. 3062 - 3080, Dec. 2004

[16] J. N. Laneman, and G. W. Wornell, "Distributed Space-time Coded Protocols for Exploiting Cooperative Diversity in Wireless Networks", *IEEE Trans. Inform. Theory*, vol. 49, pp. 2415 - 2525, Oct. 2003

[17] W. Su, A. Sadek and K. J. R. Liu, "Cooperative communications in wireless networks: Performance analysis and optimum power allocation", Wireless Personal Communications, vol. 44, pp. 181 - 217, 2008

[18] Mohammed W. Baidas, Ahmed S. Ibrahim, Karim G. Seddik and K. J. Ray Liu, "On the Impact of Correlation on Distributed Detection in Wireless Sensor Networks with Relays Deployment", *IEEE International Conference on Communcations (ICC2009)*, pp. 1 - 6, Jun. 2009

[19] L. Zhang and L. J. Cimini, "Cooperative network coding in selective decode-and-forward networks with multiple source-destination pairs", *The 42nd IEEE Annual Conference on Information Sciences and Systems 2008 (CISS2008)*, pp. 521 - 526, March 2008

[20] D. H. Woldegebreal and H. Carl, "Network-coding-based adaptive decode-and-forward cooeprative transmission in wireless networks: outage analysis", *Proc. of the 13th European Wireless Conference*, April 2007

[21] Youngchul Sung, Saswat Misra, Lang Tong and Anthony Ephremides, "Cooperative Routing for Distributed Detection in Large Sensor Networks", *IEEE Journal on Selected Areas in Communications*, pp. 471 - 483, Feb. 2007

[22] I. F. Akyildiz, W. Su, Y. Sankarasubramaniam and E. Cayirci, "A Survey on Sensor Networks", *IEEE Comunications Magazine*, pp. 102 - 114, Aug. 2002

[23] Bo Wang, Junshan Zhang and Lizhong Zheng, "Achievable Rates and Scaling Laws of Power-Constrained Wireless Sensory Relay Networks", *IEEE Transactions on Information Theory*, pp. 4084 - 4104, Sept. 2006

[24] S. Cui, A. J. Goldsmith and A. Bahai, "Energy-efficiency of MIMO and Cooperative MIMO Techniques in Sensor Networks", *IEEE Journal on Selected Areas in Communications*, vol. 22, pp. 1089 - 1098, Aug. 2004

[25] Laxminarayana S. Pilluta and Vikram Krishnamurthy, "Minimum Energy Data Gathering in Correlated Sensor Networks with Cooperative Transmission", *IEEE International Conference on Communcations (ICC2007)*, pp. 3623 - 3628, Jun. 2007

[26] Jean-Fracois Chamberland and Venugopal V. Veeravalli, "How Dense Should a Sensor Nework Be for Detection with Correlated Observations", *IEEE Transactions on Information Theory*, vol. 52, pp. 5099 - 5106, Nov. 2006

[27] Jean-Fracois Chamberland and Venugopal V. Veeravalli, "Decentralized Detection in Sensor Networks", *IEEE Transactions on Signal Processing*, vol. 51, pp. 407 - 416, Feb. 2001

[28] Mehmet C. Vuran, Ozgur B. Akan and Ian F. Akyilfiz, "Spatio-temporal Correlation: Theory and Applications for Wireless Sensor Networks", *Elsevier Journal on Computer Networks*, vol. 45, pp. 245 - 259, Jun. 2004

[29] A. Fischione, A. Bonivento, Sangiovanni-Vincentelli, F. Santucci and K. H. Johansson, "Performance Analysis of Collaborative Spatio-Temporal Processing for Wireless Sensor Networks", *IEEE 3rd Consumer Communications and Networking Conference (CCNC2006)*, vol. 1, pp. 325 - 329, Jan. 2006

[30] Razvan Critescu, Baltasar Beferull-Lozano and Martin Vetterli, "On Network Correlated Data Gathering", *IEEE Conference on Computer Communications*, vol. 4, pp. 2571 - 2582, Mar. 2004

[31] H. L. Van Trees, "Detection, Estimation and Modulation Theory - Part I", Wiley and Sons, 1968

[32] H. Vincent Poor, "An Introduction to Signal Detection and Estimation, 2nd Edition", Springer-Verlag, 1994

[33] E. Drakopoulos and C. Lee, "Optimum Multisensor Fusion of Correlated Local Decisions", *IEEE Transactions on Aerospace and Electronic Systems*, pp. 593 - 606, Jul. 1991

[34] S. Boyd and L. Vandenberghe, "Convex Optimization", *Cambridge University Press*, 2004

[35] K. G. Seddik and K. J. R. Liu, "On Relay Nodes Deployment for Distributed Detection in Wireless Sensor Networks", *IEEE GLOBECOM2008*, pp. 1 - 6, Dec. 2008

[36] S. Haykin, "Cognitive Radio: Brain-empowered Wireless Communications", *IEEE JSAC*, vol. 23, pp. 201 - 220, 2005

[37] Yang Yang and Rick S. Blum, "Energy-efficient Routing for Signal Detection under the Neyman-Pearson Criterion in Wireless Sensor Networks", *6th International Symposium on Information Processing in Sensor Networks*, pp. 303 - 312, 2007

[38] Song Gao, Lijun Qian, Dhadesugoor R. Vaman and Qi Qu, "Energy Efficient Adaptive Modulation in Wireless Cognitive Radio Sensor Networks", *IEEE International Conference on Communications and Networks*, vol. 1, pp. 3980 - 3986, Jun. 2007

[39] Ahmed K. Sadek, K. J. Ray Liu and Anthony Ephremides, "Cognitive Multiple Access Via Cooperation: Protocol Design and Performance Analysis", *IEEE Trans. on Information Theory*, vol. 53, pp. 3677 - 3696, 2007

[40] P. Galiotos, "Sleep/Active Schedules as a tunable Characteristic of a Wireless Sensor Network", *Proceedings of the International Conference on Networking and Services*, vol. 1, pp. 51 - 56, 2006

[41] C. F. Chiasserini and M. Garetto, "Modeling the Performance of Wireless Sensor Networks", *IEEE INFOCOM 2004*, vol. 1, pp. 231 - 235, 2004

[42] Zhenzhen Chen and Chenyang Yang, "Energy Efficiency of Cooperative Diversity at PHY Layer in Wireless Sensor Networks", *IEEE* 8^{th} *International Conference on Signal Processing*, vol. 4, 2006

[43] P. Dent, G. E. Bottomly and T. Croft, "Jakes Fading Model Revisited", *IEE Electronics Letters*, vol. 29, pp. 1162 - 1163, 1993

[44] *http://www.chipcon.com/files/CC2420_Data sheet_1_2.pdf*

[45] Rudolf Ahlswede, Ning Cai, Shuo-Yen Li and Raymond W. Yeung, "Network Information Flow", *IEEE Transactions on Information Theory*, vol. 46, pp. 1204 - 1216, July 2000

[46] Shuo-Yen Li, Raymond W. Yeung and Ning Cai, "Linear Network Coding", *IEEE Transactions on Information Theory*, vol. 49, pp. 371 - 381, Feb. 2003

[47] H. Q. Lai, A. S. Ibrahim and K. J. R. Liu, "Wireless Network Cocast: Location-Aware Cooperative Communications using Network Coding", *IEEE Trans. on Wireless Communications*, vol. 8, no. 7, pp. 3844 - 3854, July 2009

[48] Lei Xiao, Thomas E. Fuja, Jorg Kliewer and Daniel J. Costello Jr., "A Network Coding Approach to Cooperative Diversity", *IEEE Transactions on Information Theory*, vol. 53, pp. 3714 - 3722, 2007

[49] Petar Poposki and H. Yomo, "Wireless network coding by amplify-and-forward for bi-directional traffic flows", *IEEE Communications Letters*, vol. 11, pp. 16 - 18, 2007

[50] Yingda Chen, S. Kishore and Jing Li, "Wireless Diversity through Network Coding", *IEEE Wireless Communications and Networking Conference, 2006 (WCNC 2006)*, vol. 3, pp. 1681 - 1686, 2006

[51] Tairan Wang and Georgios B. Giannakis, "Complex Field Network Coding for Multisuer Cooperative Communications", *IEEE Journal on Selected Areas in Communications*, vol. 26, pp. 561 - 571, 2008

[52] S. Verdu, "Multiuser Detection", *Cambridge University Press*, 1998

[53] M. K. Simon and M. S. Alouini, "A unified approach to the performance analysis of digital communications over generalized fading channels", *Proc. IEEE*, vol. 86, no. 9, pp. 1860 - 1877, 1998

[54] Mohamed-Slim Alouini and Marvin K. Simon, "Performance Analysis of Coherent Equal Gain Combiing Over Nakami-m Fading Channels", *IEEE Transactions on Vehicular Technology*, vol. 50, pp. 1449 - 1462, 2001

[55] M. Abramowitz and I. A. Stegun, "Handbook of Mathematical Functions, with Formulas, Graphs and Mathematical Tables", *New York: Dover publications, 9th Edition*, 1970

[56] E. T. Whittaker and G. N. Watson, "A Course in Modern Analysis, 4th Edition", *Cambridge University Press*, 1990

[57] G. K. Karagiannidis, T. A. Tsiftsis and N. C. Sagias, "A closed-form upper-bound for the distribution of the weighted sum of Rayleigh variates", *IEEE Communications Letters*, vol. 9, pp. 589 - 591, 2005

[58] A. K. Sadek, W. Su and K. J. R. Liu, "Multi-node cooperative communications in wireless networks", *IEEE Trans. Signal Processing*, vol. 55, pp. 341 - 355, 2007

[59] Karim G. Seddik, Ahmed K. Sadek, Ahmed S. Ibrahim and K. J. Ray Liu, "Design Criteria and Performance Analysis for Disributed Space-Time Coding", *IEEE Transactions on Vehicular Technology*, vol. 57, pp. 2280 - 2292, July 2008

[60] Xiao Li, Yik-Chung Wu and Erchin Serpedin, "Timing Synchronization in Decode-and-Forward Cooperative Communication Systems", *IEEE Transactions on Signal Processing*, vol. 57, pp. 1444 - 1455, April 2009

[61] S. Jagannathan, H. Aghajan and A. Goldsmith, "The effect of time synchronization errors on the performance of cooperative MISO systems", *IEEE Globecom 2004*, pp. 102 - 107, April 2004

[62] H. Elders-Boll and A. Busboom and H.D. Schotten, "Implementation of linear multiuser detectors for asynchronous CDMA system by linear interference cancellation algorithms", *IEEE Vehicular Technology Conference VTC98*, vol. 3, pp. 1849 - 1853, May 1998

[63] Ahmed S. Ibrhaim and K. J. Ray Liu, "Mitigating Channel Estimation Error and Co-Channel Interference Effects via Cooperative Communications", to appear, *IEEE Transactions on Signal Processing*

[64] K. S. Kim, I. Song, Y. H. Kim, Y. U. Lee and J. Lee, "Analysis of quasi-ML multiuser detection of DS/CDMA systems in asynchronous channels", *IEEE Transactions on Communications*, vol. 47, pp. 1875 - 1883, December 1999

[65] J. Salo and H. M. El-Shallabi and P. Vainikainen, "The distribution of the product of independent Rayleigh random variables", *IEEE Transactions on Antennas and Propagation*, vol. 54, pp. 639 - 634, February 2006

[66] J. G. Proakis, "Digital Communications, 4th Ed.", *McGraw Hill Series in Electrical and Computer Engineering*, 2001

[67] Athanasios Papoulis and S. Unnikrishna Pillai, "Probability, Random Variables and Stochastic Processes, 4th Edition", *McGraw Hill*, 2002

[68] I. S. Gradshteyn and I. M. Ryshik, "Table of Integrals, Series and Products, 7th. Edition", *New York: Academic Press*, 2007